CONTINUOUS-MODE SINGLE-PHOTON STATES: CHARACTERIZATION, PULSE-SHAPING AND FILTERING

ZHIYUAN DONG

Ph.D

The Hong Kong Polytechnic University

2017

The Hong Kong Polytechnic University

Department of Applied Mathematics

Continuous-mode Single-photon States: Characterization, Pulse-shaping and Filtering

Zhiyuan Dong

A thesis submitted in partial fulfilment of the requirements

for the degree of Doctor of Philosophy

September 2016

Certificate of Originality

I hereby declare that this thesis is my own work and that, to the best of my knowledge and belief, it reproduces no material previously published or written, nor material that has been accepted for the award of any other degree or diploma, except where due acknowledgement has been made in the text.

______________________________(Signed)

DONG Zhiyuan (Name of student)

Dedicate to my parents.

Abstract

This thesis is devoted to studying the statistical properties and quantum filtering of continuous-mode single-photon Fock states. Four topics are under consideration:

1. Wigner spectrum of continuous-mode single-photon Fock states.

2. Coherent feedback control of continuous-mode single-photon Fock states.

3. Quantum filtering for multiple measurements of quantum systems driven by fields in continuous-mode single-photon Fock states.

4. Quantum filtering for multiple measurements of quantum systems driven by two continuous-mode single-photon Fock states.

For the first topic, we propose to use Wigner spectrum to analyze continuous-mode single-photon Fock states. Normal ordering (Wick order) is commonly used in the analysis of quantum correlations. Unfortunately, it can only give partial information for correlation analysis. For example, for a continuous-mode single-photon Fock state (whose correlation function consists of two parts, one due to quantum vacuum noise and the other due to photon pulse shape), the normal ordering analysis simply ignores the contribution from the quantum vacuum noise. In this topic, we show Wigner spectrum is able to provide complete quantum correlation in time and frequency domains simultaneously. We demonstrate the effectiveness of the method by means of two examples, namely, optical cavity (a passive system) and

degenerate parametric amplifier (DPA, a non-passive system). Numerical simulations show that Wigner spectra are able to reveal the clear difference between the output states of these two systems driven by the same single-photon state.

For the second topic, we show how various control methods can be used to manipulate the pulse shapes of continuous-mode single-photon Fock states. More specifically, we illustrate that two control methods, direct coupling and coherent feedback control, can be used for pulse-shaping of continuous-mode single-photon Fock states. The effect of control techniques on pulse-shaping is visualized by the Wigner spectrum of the output single-photon states. It can be easily seen that the linear quantum feedback network has much more influence on the detection probability of a single-photon than the directly coupled system. In addition, for a simple quantum feedback network, the changes of the output Wigner spectrum with respect to beamsplitter parameter also have been analyzed.

For the third topic, we extend the existing single-photon filtering framework by taking into account imperfect measurements. The master equations and stochastic master equations for quantum systems driven by a single-photon input state are given explicitly. More specifically, we study the case when the output light field is contaminated by a vacuum noise. We show how to design filters based on multiple measurements to achieve desired estimation performance. Two scenarios are studied: 1) homodyne plus homodyne detection, and 2) homodyne plus photon-counting detection. A numerical study of a two-level system driven by a single-photon state demonstrates the advantage of filtering design based on multiple measurement when the output filed is contaminated by quantum vacuum noise.

For the fourth topic, the problem of quantum filtering with two homodyne detection measurements for a two-level system is considered. The quantum system is driven by two input light field channels, each of which contains a single photon. A quantum filter based on multiple measurements is designed; both the master equations and stochastic master equations are derived. In addition, numerical simulations for master equations with various pulse shape parameters are compared. It seems that the maximum of excitation probability can be achieved when the two photons have the same peak arrival time and the same ratio of bandwidth to the decay rate of the two-level system.

Acknowledgements

The endeavor of carrying out research is a fascinatingly non-isolated activity. I am grateful to the several individuals who have supported me in various ways during my PhD program and would like to hereby acknowledge their assistance.

First and foremost, I am greatly indebted to my supervisor, Dr. Guofeng Zhang, for his enlightening guidance, invaluable discussions and insightful ideas throughout the years. Especially, I would like to show my great appreciation to Dr. Zhang, for his strong encouragement and patience during my study period. What I have benefited most from him is the rigorous and diligent attitude to scientific research.

Then, I will show my gratitude to my co-supervisor Dr. Heung Wing Joseph Lee, who has been a constant source of inspiration at the forefront of my PhD experience. Furthermore, I will give my great thanks to Prof. Hongchen Fu and Dr. Nina Hadis Amini for their support and help during the research process at The Hong Kong Polytechnic University.

Last but not least, I owe much to my beloved parents for their loving considerations and great confidence in me all through these years. My gratitude also extends to my friends for their love, encouragement and support.

Contents

List of Figures

List of Notations

i	the imaginary unit
I	the identity matrix
$\|0\rangle$	the vacuum state of free fields
$\|1_\xi\rangle$	the continuous-mode single-photon Fock state with pulse shape $\xi(t)$
$X^\#$	the adjoint of each element of the vector/matrix X
$\breve{X}$	$:= \begin{bmatrix} X \\ X^\# \end{bmatrix}$
$X^\dagger$	the adjoint operator or complex conjugate transpose of the operator X, $X^\dagger = (X^\#)^T$
J_n	$:= \begin{bmatrix} I_n & 0 \\ 0 & -I_n \end{bmatrix}$
$X^\flat$	$:= J_m X^\dagger J_n$
$[A, B]$	$:= AB - BA$, the commutator of operators A and B
$\Delta(U, V)$	$:= \begin{bmatrix} U & V \\ V^\# & U^\# \end{bmatrix}$
$\otimes$	the tensor product
$\mathfrak{D}_A B$	$:= A^\dagger BA - \frac{1}{2}(A^\dagger AB + BA^\dagger A)$
$\mathfrak{D}_A^\star B$	$:= ABA^\dagger - \frac{1}{2}(A^\dagger AB + BA^\dagger A)$
$\mathfrak{L}_G X$	$:= -i[X, H] + \mathfrak{D}_L X$, the *Lindbladian* operator
$\mathfrak{L}_G^\star \rho$	$:= -i[X, \rho] + \mathfrak{D}_L^\star \rho$, the *Liouvillian* operator

Chapter 1

Introduction

In this chapter, we firstly give the background of the research to be carried out in the thesis, which mainly include single-photon states, Wigner spectrum, photon pulse-shaping and quantum filtering. We also list the contributions and organizations of the thesis.

1.1 Background

1.1.1 Single-photon states

Non-classical states of light are fundamental resources for quantum communication [9], quantum computing [32], quantum metrology [22, 31], and quantum networks [30, 37, 1]. Photon states are typical non-classical states. In contrast to single-mode photon states, continuous-mode photon states are closer to a real experimental environment in quantum information processing [19, 11, 10, 12]. In [21], continuous-mode single- and two-photon wave packets have been studied and the single-photon state is defined in [21, Eq. (3)]. The pulse shape is expressed by a unit norm function $g(\omega)$ in the frequency domain, the master equation of a quantum system driven by a single-photon state is given in [21, Eq. (24)]. A two-photon state is defined in [21, Eq. (58)] and the master equation is presented in [21, Eq. (68)]. Moreover, the issue of generation of continuous-mode single-photon state is discussed in [21, Sections V and VII]. In [5], a theoretical framework is presented which describes the interaction between light wave packets of arbitrary spectral distribution functions and a quantum system. Master equations for the system and output field quantities (e.g., quadratures and photon flux) have also been discussed in this framework. In [40], real-time quadrature measurement of a continuous-mode single-photon wavepacket is studied. To overcome the vacuum fluctuation, filtration of the field is used in this experiment. The optical parametric oscillator (OPO) with a built-in polarization beamsplitter is used to make sure the *signal* photon ejected earlier than the *idler*. Two filter cavities which can remove photons in irrelevant frequencies in the idler line have been added and then the filtration becomes a third-order low-pass filter (LPF). Quantum filters for single-photon states have been derived in [27, 28]. In particular, both the homodyne detection and photon counting measurements are discussed and the filtering equations are explicitly given by a set of stochastic differential equations in those research works. In [14], by applying the stochastic master equations to an optical cavity driven by a continuous-mode single-photon field, the conditional dynamics for the cross phase modulation in a doubly resonant cavity are analyzed. Based on a quantum stochastic model, the phase shift for the doubly resonant cavity which driven by a coherent field in one mode and by a single photon in the other mode is simulated. Furthermore, the formalism proposed in [14] is well suited for measurement-based feedback control [54]. In [62], linear signals and systems theory has been proposed to study single-photon quantum signals, and the response of quantum linear systems driven by multi-channel single-photon input fields are investigated. It is shown that the steady-state output is in a single-photon state for a cavity driven by a single-photon input state, while this is not the case for a degenerate parametric amplifier (DPA). A class of photon-Gaussian states is defined which can describe the steady-state output state of the DPA driven by a single-photon state. It has also been proved that the class of photon-Gaussian states is invariant in regard to quantum linear dynamics. Interestingly, single-photon states are special cases of photon-Gaussian states. In [59], a mathematical framework for analyzing the quantum linear systems' response to multi-photon states is presented, where both the factorizable and unfactorizable wave packtes are treated. Particularly, a more general class of states represented by tensors is defined when the quantum linear system is driven by multi-photon input states.

1.1.2 Wigner spectrum

The Wigner function (also called the Wigner quasiprobability distribution or the Wigner-Ville distribution) is firstly introduced by Eugene Wigner [52], and used to link the wave function to a probability distribution in phase space. In [33], an experiment in which the relative optical phase of the signal and local oscillator varies randomly is presented. The phase-averaged Wigner function and diagonal elements of the density matrix for a single-photon Fock state are reconstructed using the method of homodyne tomography. Due to the exhibition of negative values around the origin of phase space, the reconstructed Wigner function reflects the non-classical property of the single-photon state. In this case, experimental results, such as detection efficiency, minimum of Wigner function, are consistent with the theoretical evaluations. In [58], a continuous-wave (cw) laser was used in the experiment as light source to generate arbitrary superposition of Fock states. Those generated superposition states with wider bandwidth are applicable to the teleportation-based quantum operations. Particularly, a three-photon Fock state $|3\rangle$, superpositions of Fock states $|1\rangle$ and $|3\rangle$, and of $|0\rangle$ and $|3\rangle$ are generated in the experiments. Multiple areas of negativity of the Wigner function are observed which confirm the non-classical property of the generated states. In [43], an experimental technique of polychromatic optical heterodyne tomography is presented and nonvanishing imaginary parts have been added into the temporal mode function (TMF) to demonstrate that the technique can reconstruct photon states with complex temporal modes. Both the real and imaginary components of a single-photon's temporal density matrix are considered by measuring the reduced autocorrelation matrix. In addition, the experimental temporal modes and their theoretical predictions are compared with several phase modulations.

1.1.3 Photon pulse-shaping

The problem of pulse-shaping of single-photon states has been investigated in [36]. The relation between input and output pulse shapes is derived in the frequency domain when the underlying system is an empty cavity. In [6], a solution for interfacing quantum optics and microwaves has been proposed based on a micromechanical resonator (MR). In the presented scheme, the cavity output modes are mixed with the input field on a photon detector, which results in a homodyne current. Upon measurement results, a conditional displacement in the receiving site is made and the resulting state of the output microwave field could be prepared in the same quantum state as the input. In addition, the teleportation protocol can be reversed by exchanging the role of the optical and microwave output fields. In [41], the response of quantum nonlinear systems to single-photon input states is presented. Particularly, the output states and pulse shapes for quantum two-level systems are derived explicitly in time and frequency domains. In [62], the input-output relation of pulse shapes is expressed by transfer functions. The pulse-shaping problem in the case of quantum linear systems has been discussed in [62]. It has also been proved that any two pulse shapes which satisfy some specific conditions can be implemented by an all-pass linear quantum stochastic system. In [55], a memory subsystem within a linear network is proposed. The memory system is decoupled from the optical field during the storage process while coupled to the field in the writing or reading process. The zero-dynamic principle, that is, the output field in a general passive system must be vacuum during the writing or reading process for perfect state transfer, is emphasized for the quantum memory problem. Recently, a complete framework for quantum information science with the temporal modes (TMs) of single-photon states is proposed in [12]. The definition of temporal modes and their application in quantum information encoding are reviewed. Particularly, the quantum pulse gate (QPG), which is equivalent to a TM reshaper, is presented and the reshaping operation is given theoretically.

1.1.4 Quantum filtering

After the interaction between light and a quantum system, e.g., an optical cavity or a two-level atom, partial information of the system could be transferred to the output state. Then, the output light can be measured via homodyne detection or photon-counting measurement. The quantum filtering problem is firstly introduced by Belavkin in [7, 8] within a framework of continuous measurements. To estimate the stochastic evolution of the conditional system state, quantum filters with various Gaussian input fields, such as vacuum state, squeezed state, thermal states, have been presented and investigated in [16, 20, 54, 13, 38]. Non-classical lights have also been considered in connection with quantum networks with the aid of a variety of physical architectures, such as quantum dots in semiconductors [57], cavity quantum electrodynamics (QED) [35], and circuit QED [17]. Particularly, the interaction between a two-level atom and a propagating mode single photon in free space is considered in [51]. The influence of various temporal pulse shapes for both single-photon Fock states and coherent states on the atomic excitation probability has been analyzed in terms of the temporal and spectral features. In [27], the problem of quantum filtering of a quantum system driven by single-photon states and coherent states has been discussed. Both the master equations and quantum filters are presented for an arbitrary quantum system which is probed by a single-photon input field. As for application, the conditional dynamics for the cross phase modulation in a doubly resonant cavity are described in [14]. Homodyne detection and photon-counting measurements are simulated respectively for a cavity driven by single-photon input states.

Due to the existence of vacuum noise, there may exist limitations for single measurement in real quantum physical experiments. In [15], quantum filtering with multiple output fields has been investigated, and quantum trajectory theory with multi-input-multi-output (MIMO) feedback is used to overcome such imperfection. In [45], a closed-loop simulation has been presented with an experimental implementation which has been conducted by using the photon box. In [46], the impacts of experimental parameters, such as the impurity of input states, inefficiency of the detector, mode mismatch, on the Schrödinger kitten's generation have also been analyzed quantitatively. In [2], a finite dimensional Markov system in discrete time with perfect and imperfect measurements have been considered. Quantum filtering equations and general robustness property for the two cases of measurements are presented for state estimation. In [3], the general sufficient and necessary convergence conditions have been derived. The diffusive stochastic master equations for quantum systems with perfect measurements is presented in the discrete-time approximation. Then imperfections and errors of the measurements are modeled by a left stochastic matrix, and quantum filters for systems driven by either Poisson, Wiener processes or both are derived.

1.2 Contributions and organization of the thesis

As the novelty, this thesis mainly considers the Wigner spectrum, coherent feedback control and quantum filtering for systems driven by continuous-mode single-photon states and two single-photon states. In Chapter 3, we characterize continuous-mode single-photon state by means of its Wigner spectrum. In chapter 4, we study how to engineer the pulse shape of a single-photon state via coherent feedback networks. In Chapter 5, we discuss single-photon filtering for a quantum system where the output channel is corrupted by a quantum vacuum noise, and in Chapter 6, we investigate a two-photon filtering problem. Details can be summarized as follows.

- Chapter 2 gives some basic knowledge about quantum systems, quantum filtering, continuous-mode single-photon states, Wigner distribution function and Wigner spectrum.

- Wigner spectra for an optical cavity and a DPA are characterized respectively in Chapter 3. The changes of Wigner spectrum with respect to cavity decay rate and de-tuning are treated in Chapter 3.1. On the other hand, Wigner spectrum for DPA is presented in Chapter 3.2, together with a brief comparison with the case of cavity. The difference between cavity (passive system) and DPA (non-passive system) are revealed by their respective Wigner spectra.

- In Chapter 4, the wave packets of several coupled systems are compared. Photon pulse shape synthesis by means of coherent feedback control and the detection probability have also been analyzed. It has been shown how to use coherent feedback control to engineer photon wave packets and Wigner spectrum of single-photon states.

- Single-photon filtering framework with multiple measurements in [27, 18] is extended in Chapter 5. Particularly, when the output light field is corrupted by a vacuum noise, quantum filters based on multiple measurements have been designed to obtain better estimation performance. By comparison with the ideal case, i.e., quantum filtering with the absence of noise in the output light field, simulation results demonstrate the significant advantage of filtering design based on multiple measurements.

- In contrast to the scenarios given by Chapter 5, we have also considered a more complicated case in Chapter 6. The problem of quantum filtering with two homodyne detection measurements for a two-level atom is investigated. The two-level atom is driven by two input channels and each channel contains a single photon. Numerical simulations for master equations with various pulse shape parameters are also conducted in this chapter.

- Chapter 7 concludes this thesis and point out some future work.

Chapter 2

Preliminaries

This chapter records some preliminary results necessary for the presentation of the thesis. Continuous-mode single-photon Fock states and coherent states are briefly discussed in Section 2.1. Open quantum systems with three basic examples are introduced in Section 2.2. The concatenation and series products are reviewed in Section 2.3. Section 2.4 presents the definition and properties of quantum filtering. Wigner distribution function and Wigner spectrum are discussed in Section 2.5.

2.1 Continuous-mode single-photon states

2.1.1 Continuous-mode single-photon Fock states

Define an operator

$$\mathbf{B}(\xi) \triangleq \int_{-\infty}^{\infty} d\omega \xi^*[\omega] b[\omega],$$

where the Euclidian norm of ξ, $\|\xi\| = 1$ and $b[\omega]$ is the annihilation operator of a free field in the frequency domain. A continuous-mode single-photon Fock state with spectral pulse shape $\xi[\omega]$ is

$$|1_\xi\rangle \triangleq \mathbf{B}^\dagger(\xi)|0\rangle = \int_{-\infty}^{\infty} d\omega \xi[\omega] b^\dagger[\omega] \, |0\rangle \, . \tag{2.1}$$

$b^\dagger[\omega]$, the adjoint of $b[\omega]$, is the creation operator of the light field, $b^\dagger[\omega]\,|0\rangle \equiv |1_\omega\rangle$ can be understood as phton generation at frequency ω, while the probability is given by $|\xi[\omega]|^2$. So, the single-phton Fock state $|1_\xi\rangle$ can be interpreted as a photon coherently superposed over a continumn of frequency modes with probability amplitudes given by the spectral density function $\xi[\omega]$ [47]. Fourier transforming Eq. (2.1) gives the time-domain expresson of the single-photon Fock state, which is

$$|1_\xi\rangle = \int_{-\infty}^{\infty} dt \xi(t) b^\dagger(t)|0\rangle. \tag{2.2}$$

Noticing the commutation relation

$$\left[b[\omega_1], b^\dagger[\omega_2]\right] = \delta(\omega_1 - \omega_2)$$

and $b[\omega]|0\rangle = 0$, it is easy to show that

$$\langle 1_\xi | b[\omega] | 1_\xi \rangle = \left\langle 1_\xi | b^\dagger[\omega] | 1_\xi \right\rangle = 0, \quad \forall \omega \in \mathbb{R},$$

and

$$\left\langle 1_\xi | \mathbf{B}^\dagger(\xi) | 1_\xi \right\rangle = \langle 1_\xi | \mathbf{B}(\xi) | 1_\xi \rangle = 0.$$

Moreover,

$$\begin{aligned}
\mathbf{B}(\xi)\,|1_\xi\rangle &= \int_{-\infty}^{\infty} d\omega_1 \xi^*[\omega_1] b[\omega_1] \int_{-\infty}^{\infty} d\omega_2 \xi[\omega_2] b^\dagger[\omega_2]|0\rangle \\
&= \int_{-\infty}^{\infty} d\omega_1 \int_{-\infty}^{\infty} d\omega_2 \xi^*[\omega_1]\xi[\omega_2]\delta(\omega_1 - \omega_2)|0\rangle \\
&= \int_{-\infty}^{\infty} d\omega_1 |\xi[\omega_1]|^2 |0\rangle \\
&= |0\rangle.
\end{aligned}$$

2.1.2 Continuous-mode single-photon coherent states

A continuous-mode single-photon coherent state ([10, Eq. (3.1)]) can be defined to be

$$\begin{aligned}
|\alpha_\xi\rangle &\triangleq \exp\left(\alpha \mathbf{B}^\dagger(\xi) - \alpha^* \mathbf{B}(\xi)\right)|0\rangle \\
&= \exp\left(\int_{-\infty}^{\infty} d\omega\ \alpha\xi[\omega] b^\dagger[\omega] - \int_{-\infty}^{\infty} d\omega\ (\alpha\xi[\omega])^* b[\omega]\right)|0\rangle,
\end{aligned}$$

where $\alpha = e^{i\theta}$ is a complex number. It can be readily shown that

$$\begin{aligned}
\left[\mathbf{B}(\xi), \mathbf{B}^\dagger(\xi)\right] &= \int_{-\infty}^{\infty} d\omega_1 \int_{-\infty}^{\infty} d\omega_2\ \xi[\omega_1]\xi^*[\omega_2]\left[b[\omega_1, b[\omega_2]^\dagger\right] \\
&= \int_{-\infty}^{\infty} d\omega_1 \int_{-\infty}^{\infty} d\omega_2\ \xi[\omega_1]\xi^*[\omega_2]\delta(\omega_1 - \omega_2) \\
&= \int_{-\infty}^{\infty} d\omega_1 \left|\xi[\omega_1]\right|^2 \\
&= 1.
\end{aligned}$$

Moreover, by the Baker-Hausdorff formula [34],

$$\exp(A+B) = \exp(B)\exp(A)\exp\left(\frac{1}{2}[A,B]\right),$$

we have

$$\begin{aligned}
\mathbf{B}(\xi)|\alpha_\xi\rangle &= \mathbf{B}(\xi)\exp\left(\alpha\mathbf{B}^\dagger(\xi)-\alpha^*\mathbf{B}(\xi)\right)|0\rangle \\
&= \mathbf{B}(\xi)\exp\left(-\alpha^*\mathbf{B}(\xi)\right)\exp\left(\alpha\mathbf{B}^\dagger(\xi)\right)\exp\left(\frac{|\alpha|^2}{2}\right)|0\rangle \\
&= \exp\left(\frac{|\alpha|^2}{2}\right)\exp\left(-\alpha^*\mathbf{B}(\xi)\right)\mathbf{B}(\xi)\sum_{n=0}^{\infty}\left\{\frac{1}{n!}(\alpha\mathbf{B}^\dagger(\xi))^n\right\}|0\rangle \\
&= \exp\left(\frac{|\alpha|^2}{2}\right)\exp\left(-\alpha^*\mathbf{B}(\xi)\right)\alpha\sum_{n=0}^{\infty}\left\{\frac{1}{n!}(\alpha\mathbf{B}^\dagger(\xi))^n\right\}|0\rangle \\
&= \alpha\exp\left(\frac{|\alpha|^2}{2}\right)\exp\left(-\alpha^*\mathbf{B}(\xi)\right)\exp\left(\alpha\mathbf{B}^\dagger(\xi)\right)|0\rangle \\
&= \alpha|\alpha_\xi\rangle.
\end{aligned}$$

Obviously,

$$\langle\alpha_\xi|\mathbf{B}(\xi)|\alpha_\xi\rangle = \alpha.$$

2.2 Open quantum systems

The system model we discuss is an arbitrary quantum system G driven by a single-photon input field. Here, we will describe the system by using the (S, L, H) formalism [23, 48, 61]. The scattering operator S is unitary, which satisfies $S^\dagger S = SS^\dagger = I$. The coupling between the system and field is described by the operator $L = C_-a + C_+a^\#$ with $C_-,\ C_+ \in \mathbb{C}^{m\times n}$. The initial Hamiltonian of the system is $H = \frac{1}{2}\breve{a}^\dagger\Delta(\Omega_-,\Omega_+)\breve{a}$ with $\Omega_-,\ \Omega_+ \in \mathbb{C}^{n\times n}$ satisfying $\Omega_-^\dagger = \Omega_-$ and $\Omega_+^T = \Omega_+$.

The input field is represented by the annihilation operator $b(t)$ and the creation operator $b^\dagger(t)$ on the Fock space H_F [42], which satisfy $[b(t), b^\dagger(s)] = \delta(t-s)$. The integrated annihilation and creation operators, together with the gauge process are given by

$$B(t) = \int_0^t b(s)ds, \quad B^\dagger(t) = \int_0^t b^\dagger(s)ds, \quad \Lambda(t) = \int_0^t b^\dagger(s)b(s)ds.$$

In this thesis, we assume that these quantum stochastic processes are canonical, that is, their products satisfy the following Itō table

$$\begin{array}{c|cccc} \times & dt & dB & d\Lambda & dB^\dagger \\ \hline dt & 0 & 0 & 0 & 0 \\ dB & 0 & 0 & dB & dt \\ d\Lambda & 0 & 0 & d\Lambda & dB^\dagger \\ dB^\dagger & 0 & 0 & 0 & 0 \end{array} . \tag{2.3}$$

The dynamical evolution of the system can be described by a unitary operator $U(t)$ on the tensor product Hilbert space $\mathsf{H}_S \otimes \mathsf{H}_F$, which is given by the following quantum stochastic differential equation (QSDE)

$$dU(t) = \left\{(S - I)d\Lambda(t) + LdB^\dagger(t) - L^\dagger SdB(t) - \left(\frac{1}{2}L^\dagger L + iH\right) dt\right\}U(t), \tag{2.4}$$

where $U(0) = I$ (the identity operator).

In the Heisenberg picture, the system operator X at time $t \geq 0$ is given by $j_t(X) = U^\dagger(t)(X \otimes I_{\text{field}})U(t)$ on $\mathsf{H}_S \otimes \mathsf{H}_F$. By the quantum Itō product rule and table (2.3), the temporal evolution of $j_t(X) \equiv X(t)$ is derived as

$$\begin{aligned} dj_t(X) =& j_t(\mathcal{L}_G X)dt + j_t([L^\dagger, X]S)dB(t) \\ &+ j_t(S^\dagger[X, L])dB^\dagger(t) + j_t(S^\dagger XS - X)d\Lambda(t), \end{aligned} \tag{2.5}$$

where $\mathcal{L}_G X = -i[X, H] + L^\dagger XL - \frac{1}{2}(L^\dagger LX + XL^\dagger L)$.

The output fields are defined by

$$B_{\text{out}}(t) = U^\dagger(t)(I_{\text{system}} \otimes B(t))U(t),$$

$$\Lambda_{\text{out}}(t) = U^\dagger(t)(I_{\text{system}} \otimes \Lambda(t))U(t),$$

and by Itō calculus, we can find the following QSDEs for the evolution of the output field

$$\begin{aligned} dB_{\text{out}}(t) =& S(t)dB(t) + L(t)dt, \\ d\Lambda_{\text{out}}(t) =& S^*(t)d\Lambda(t)S^T(t) + S^*(t)dB^*(t)L^T(t) \\ & + L^*(t)dB^T(t)S^T(t) + L^*(t)L^T(t)dt. \end{aligned} \tag{2.6}$$

2.2.1 Optical cavity

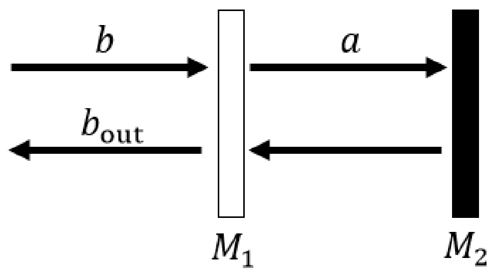

Figure 2.1: A Fabry-Perot cavity.

An optical cavity is a system which consists of totally reflecting and/or partially transmitting mirrors [56], [4, Chapter 5.3], [50, Chapter 7], [39]. A widely used type of optical cavities is the so-called Fabry-Perot cavity, as depicted in Fig. 2.1. Arrows indicate the direction of light in the cavity. The black rectangle (M_2) denotes a fully reflecting mirror, while the white rectangle (M_1) denotes a partially transmitting mirror. In this figure, the electromagnetic filed inside the cavity is mathematically modelled by the bosonic annihilation operator a. The left-hand mirror (M_1) allows the incident light (denoted by its annihilation operator b) to enter into the cavity. After bouncing inside the cavity for a while, the electromagnetic field leaves the cavity from the partially transmitting mirror M_1, and together with the directly reflected light, forms the outgoing electromagnetic field, as represented by b_{out} in Fig. 2.1.

The coupling strength between the cavity and the external electromagnetic field in Fig. 2.1 is denoted by $\kappa > 0$. Moreover, let the de-tuning between the cavity mode and the carrier frequency of the incident light field be ω_0, then the Fabry-Parot cavity can be described by $(I, \sqrt{\kappa}a, \omega_0 a^\dagger a)$. The quantum stochastic differential equations of the Fabry-Parot cavity are, [20, Chapter 5.3], [50, Chapter 7], [56, Section III],

$$\dot{a}(t) = -(\frac{\kappa}{2} + i\omega_0)a(t) - \sqrt{\kappa}b(t), \tag{2.7}$$

$$b_{\text{out}}(t) = \sqrt{\kappa}a(t) + b(t). \tag{2.8}$$

2.2.2 DPA

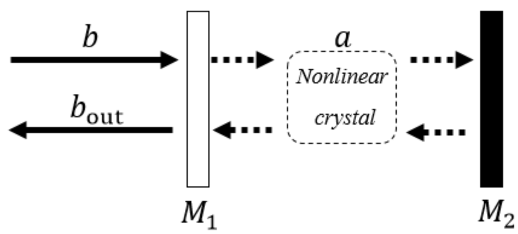

Figure 2.2: A DPA consists of a classically pumped nonlinear crystal in the Fabry-Perot cavity.

A degenerate parametric amplifier (DPA) is an open oscillator that is able to amplify a quadrature of the cavity mode and produce squeezed output fields, see Fig. 2.2, [20, Chapter 6.3], [50, Chapter 7.6], [4, Chapter 6.3], [39]. The black rectangle (M_2) denotes a fully reflecting mirror, while the white rectangle (M_1) denotes a partially transmitting mirror. A nonlinear crystal is placed in the cavity to be a source of additional quanta for amplification. For this open oscillator, $C_- = \sqrt{\kappa}$, $C_+ = 0$ and $\Omega_- = 0$, $\Omega_+ = \frac{i\epsilon}{2}$. The DPA in Fig. 2.2 can be described by the following quantum stochastic differential equations, [20, 62]

$$\begin{aligned}\begin{bmatrix} \dot{a}(t) \\ \dot{a}^\dagger(t) \end{bmatrix} &= -\frac{1}{2}\begin{bmatrix} \kappa & -\epsilon \\ -\epsilon & \kappa \end{bmatrix}\begin{bmatrix} a(t) \\ a^\dagger(t) \end{bmatrix} - \sqrt{\kappa}\begin{bmatrix} b(t) \\ b^\dagger(t) \end{bmatrix}, \\ b_{\text{out}}(t) &= \sqrt{\kappa}a(t) + b(t), \quad (0 < \epsilon < \kappa). \end{aligned} \tag{2.9}$$

2.2.3 Beamsplitter

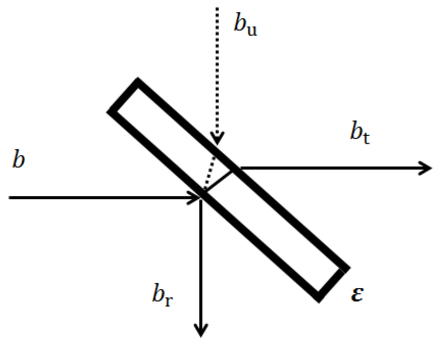

Figure 2.3: A beamsplitter with reflection parameter ϵ in the quantum operator mode.

A beamsplitter can be described by a quantum-mechanical model, see Fig 2.3 [4, Chapter 5.1], [50, Chapter 14.4]. The input light is a travelling beam, which is represented by the operator b. There are two waves leaving the beamsplitter: the reflected light b_{r}, and the transmitted light b_{t}. The reflection parameter is denoted by ϵ. A special case $\epsilon = \frac{1}{2}$ describes the balanced 50/50 beamsplitter. As required by quantum-mechanics, there exists a second input light, i.e., b_{u} in Fig 2.3, two input waves are made to interfere. The beamsplitter can be described by $(S_b, 0, 0)$ in terms of (S, L, H) formalism with

$$S_b = \begin{bmatrix} \sqrt{\epsilon} & \sqrt{1-\epsilon} \\ \sqrt{1-\epsilon} & -\sqrt{\epsilon} \end{bmatrix},$$

and we can obtain

$$\begin{bmatrix} b_{\mathrm{r}} \\ b_{\mathrm{t}} \end{bmatrix} = \begin{bmatrix} \sqrt{\epsilon} & \sqrt{1-\epsilon} \\ \sqrt{1-\epsilon} & -\sqrt{\epsilon} \end{bmatrix} \begin{bmatrix} b \\ b_{\mathrm{u}} \end{bmatrix}. \tag{2.10}$$

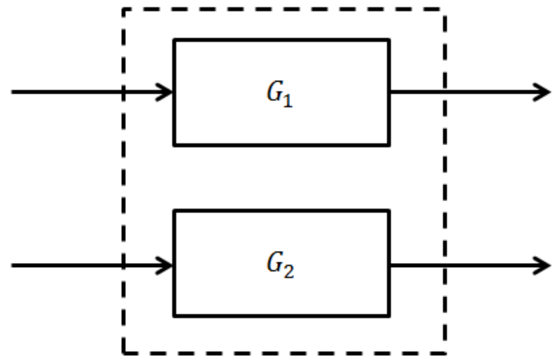

Figure 2.4: Concatenation product.

2.3 The concatenation and series products

Concatenation product [23]

Given two systems $G_1 = (S_1, L_1, H_1)$ and $G_2 = (S_2, L_2, H_2)$, see Fig. 2.4, we define the concatenation product to be the system $G_1 \boxplus G_2$ by

$$G_1 \boxplus G_2 = \left(\begin{bmatrix} S_1 & 0 \\ 0 & S_2 \end{bmatrix}, \begin{bmatrix} L_1 \\ L_2 \end{bmatrix}, H_1 + H_2 \right). \tag{2.11}$$

Series product [23]

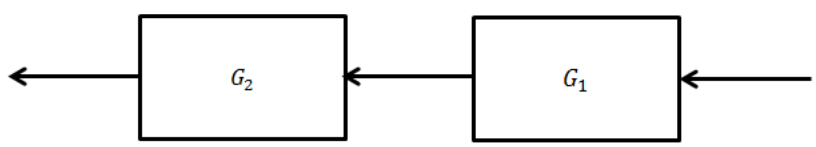

Figure 2.5: Series product.

Given two systems $G_1 = (S_1, L_1, H_1)$ and $G_2 = (S_2, L_2, H_2)$ with the same number of field channels, see Fig. 2.5, we define the series product $G_2 \triangleleft G_1$ by

$$G_2 \triangleleft G_1 = \left(S_2 S_1, L_2 + S_2 L_1, H_1 + H_2 + \frac{1}{2i}(L_2^\dagger S_2 L_1 - L_1^\dagger S_2^\dagger L_2) \right). \tag{2.12}$$

2.4 Quantum filtering

Homodyne and photon-counting detections are the most commonly used measurement methods in quantum filtering [47]. By using homodyne detection, the measurement is given by the quadrature phase

$$Y(t) = U^{\dagger}(t)(I_{\text{system}} \otimes (B(t) + B^{\dagger}(t)))U(t), \tag{2.13}$$

while in the photon-counting case,

$$Y(t) = \Lambda_{\text{out}}(t) = U^{\dagger}(t)(I_{\text{system}} \otimes \Lambda(t))U(t). \tag{2.14}$$

Both of these measurements satisfy the following commutation relations

$$[Y(s), Y(t)] = 0, \quad 0 \le s \le t. \tag{2.15}$$

The quantum conditional expectation is defined by

$$\hat{X}(t) \equiv \pi_t(X) = \mathbb{E}[j_t(X)|\mathcal{Y}_t], \tag{2.16}$$

where $\mathcal{Y}_t$ is generated by the observation processes $\{Y(s) : 0 \le s \le t\}$. Generally speaking, the quantum filtering problem is about minimizing the least mean-squares estimate $\mathbb{E}[\{\hat{X}(t) - j_t(X)\}^2]$ of the system observable $j_t(X)$ based on the past measurement information $\mathcal{Y}_t$. Furthermore, we note that the set of observables $\{Y(s) : 0 \le s \le t\}$ is self-commuting

$$[Y(t), Y(s)] = 0, \quad s \le t. \tag{2.17}$$

Recall $X(t) \equiv j_t(X)$, and the quantum conditional expectation is well-defined since it satisfies the non-demolition property

$$[X(t), Y(s)] = 0, \quad s \le t. \tag{2.18}$$

The quantum filters for an arbitrary quantum system driven by a continuous-mode single-photon Fock state have been derived in [26]. Two approaches are proposed, the non-markovian embedding technique [28] and the markovian embedding technique [27], and the latter discussed how to design a two-level system to generate a desired continuous-mode single-photon Fock state. The study in [26] are extended in [5] to derive the master equations of an arbitrary quantum system driven by continuous-mode multi-photon Fock wave packets. Moreover, based on [28], the quantum filters of an arbitrary quantum system driven by a continuous-mode multi-photon state are derived in [47].

2.5 Wigner distribution function and Wigner spectrum

For the continuous-mode single-photon Fock state $|1_\xi\rangle$ defined in (2.2), we have

$$\langle 1_\xi | b(t) b^\dagger(\tau) | 1_\xi \rangle = \delta(t-\tau) + \xi(t)\xi^*(\tau), \tag{2.19}$$

which shows the non-stationarity of the single-photon state $|1_\xi\rangle$. The presence of the Dirac delta function is cumbersome for the statistical analysis of the single-photon state $|1_\xi\rangle$. Because of this, time ordering is commonly used in quantum optics, see e.g., [20]. The *normal ordering* of $b(t)b^\dagger(\tau)$ is defined as

$$: b(t) b^\dagger(\tau) : \triangleq b^\dagger(\tau) b(t). \tag{2.20}$$

Notice that in this case,

$$\langle 1_\xi | : b(t) b^\dagger(\tau) : | 1_\xi \rangle = \xi(t)\xi^*(\tau). \tag{2.21}$$

That is, the impulse function $\delta(t-\tau)$ has been thrown away. In this thesis, instead of the partial information of the normal ordering term $: b(t)b^\dagger(\tau) :$, we adopt an alternative method for analyzing the statistical properties of input and output quantum signals. We aim to present a direct analysis on $b(t)b^\dagger(\tau)$ in terms of the Wigner spectrum method, therefore keeping the complete information, details can be found in Chapter 3.

The method we use belongs to the time-frequency analysis. Let $x(t)$ be a quantum variable, e.g., $b(t)$, $b^\dagger(t)$ or $b(t)b^\dagger(t)$, define the two-time autocorrelation function

$$r_x(t,\tau) \triangleq \mathbb{E}_\xi[x(t)x^\dagger(\tau)], \tag{2.22}$$

where the subscript "ξ" indicates that the expectation is taken with respect to the single-photon state $|1_\xi\rangle$. Clearly, by (2.19) we have

$$r_b(t,\tau) = \mathbb{E}_\xi[b(t)b^\dagger(\tau)] = \delta(t-\tau) + \xi(t)\xi^*(\tau). \tag{2.23}$$

Similarly, by normal ordering,

$$r_{b^\dagger}(\tau,t) = \mathbb{E}_\xi[b^\dagger(\tau)b(t)] = \xi(t)\xi^*(\tau) = \mathbb{E}_\xi[:b(t)b^\dagger(\tau):]. \tag{2.24}$$

Applying the Fourier transform to the two-time autocorrelation function $r_x(t,\tau)$ in (2.22) with respect to the time variable τ, yields

$$S_x(t,\omega) = \frac{1}{\sqrt{2\pi}} \int_{-\infty}^{\infty} r_x(t,\tau) e^{-i\omega\tau} d\tau. \tag{2.25}$$

Define

$$W_x(t,\omega) \triangleq \frac{1}{\sqrt{2\pi}} \int_{-\infty}^{\infty} x(t)x^\dagger(\tau) e^{-i\omega\tau} d\tau. \tag{2.26}$$

By (2.22), (2.25), and (2.26) we have

$$S_x(t,\omega) = \mathbb{E}_\xi\left[W_x(t,\omega)\right]. \tag{2.27}$$

In the literature, $W_x(t,\omega)$ is called the *Wigner-Ville distribution function,* or simply *Wigner function*, and accordingly, $S_x(t,\omega)$ the *Wigner spectrum*, [52], [49], [44]. Notice that

$$S_b(t,\omega) = \frac{1}{\sqrt{2\pi}} e^{-i\omega t} + \xi(t)\xi^*[\omega]. \tag{2.28}$$

Comparing (2.23) and (2.28), we see that the Dirac delta function does not appear in the Wigner spectrum $S_b(t, \omega)$. Motivated by this, in Chapter 3 we use the Wigner spectrum to analyze the statistical properties of quantum signals, instead of resorting to the normal ordering.

Chapter 3

Wigner spectrum of continuous-mode single-photon Fock states

The purpose of this chapter is to use Wigner spectrum, the time-frequency variant of the Wigner function, to analyze the covariance functions for continuous-mode single-photon Fock states. In most literature, correlations are calculated for normal ordered (Wick order) operators to avoid the Dirac delta function, see e.g., [20] and Chapter 2.5. With the aid of the Wigner spectrum, such ordering is not necessary. As a result, the whole correlations can be investigated.

3.1 Wigner spectrum for optical cavity

The impulse response function for the optical cavity given in Chapter 2.2 is

$$g_G(t) = \delta(t) - \kappa e^{\left(-\frac{\kappa}{2} - i\omega_0\right)t}, \quad t \geq 0, \tag{3.1}$$

while $g_G(t) \equiv 0$ when $t < 0$. Recall Chapter 2.1, let $|1_\nu\rangle$ be a continuous-mode single-photon Fock state

$$|1_\nu\rangle \equiv \mathbf{B}^\dagger(\nu)|0\rangle := \int_{-\infty}^{\infty} b^\dagger(t)\nu(t)dt|0\rangle \tag{3.2}$$

with an exponentially decaying pulse shape

$$\nu(t) = \begin{cases} \sqrt{2\gamma}e^{-\gamma t}, & t \geq 0, \\ 0, & t < 0. \end{cases} \tag{3.3}$$

The state $|1_\nu\rangle$ can describe a single-photon field emitted from an optical cavity with damping rate $\sqrt{2\gamma}$ [50, 32]. Then, the input covariance function [62, Eq. (35)] is

$$\begin{aligned} R_{\mathrm{in}}(t,r) &\triangleq \mathbb{E}_\nu \begin{bmatrix} b(t)b^\dagger(r) & b(t)b(r) \\ b^\dagger(t)b^\dagger(r) & b^\dagger(t)b(r) \end{bmatrix} \\ &= \begin{bmatrix} \delta(t-r) & 0 \\ 0 & 0 \end{bmatrix} + \begin{bmatrix} \nu^*(r)\nu(t) & 0 \\ 0 & \nu^*(t)\nu(r) \end{bmatrix}. \end{aligned} \tag{3.4}$$

On the other hand, by the steady-state input-output relations [62, Section II-C], the output single-photon state $|1_\eta\rangle$ has the pulse shape

$$\eta(t) = \sqrt{2\gamma}e^{-\gamma t} - \frac{\kappa\sqrt{2\gamma}}{\frac{\kappa}{2} + i\omega_0 - \gamma}\left(e^{-\gamma t} - e^{(-\frac{\kappa}{2} - i\omega_0)t}\right). \tag{3.5}$$

The steady-state output covariance function [62, Section III-D] is

$$\begin{aligned} R_{\mathrm{out}}(t,r) &= \mathbb{E}_\eta \begin{bmatrix} b(t)b^\dagger(r) & b(t)b(r) \\ b^\dagger(t)b^\dagger(r) & b^\dagger(t)b(r) \end{bmatrix} \\ &= \delta(t-r)\begin{bmatrix} 1 & 0 \\ 0 & 0 \end{bmatrix} + \begin{bmatrix} \eta(t)\eta^*(r) & 0 \\ 0 & \eta^*(t)\eta(r) \end{bmatrix}. \end{aligned} \tag{3.6}$$

By (2.25) and (3.4), the Wigner spectrum of the input covariance function can be expressed in terms of both time and frequency

$$S_{\mathrm{in}}(t,\omega) = \frac{1}{\sqrt{2\pi}}\begin{bmatrix} e^{-i\omega t} & 0 \\ 0 & 0 \end{bmatrix} + \frac{1}{\sqrt{2\pi}}\begin{bmatrix} \frac{2\gamma}{\gamma+i\omega}e^{-\gamma t} & 0 \\ 0 & \frac{2\gamma}{\gamma+i\omega}e^{-\gamma t} \end{bmatrix}. \tag{3.7}$$

Similarly, by (2.25) and (3.6), we can get the Wigner spectrum of the output covariance function

$$S_{\mathrm{out}}(t,\omega) = \frac{1}{\sqrt{2\pi}}\begin{bmatrix} e^{-i\omega t} & 0 \\ 0 & 0 \end{bmatrix} + \frac{1}{\sqrt{2\pi}}\begin{bmatrix} \eta(t)S_{11}[\omega] & 0 \\ 0 & \eta^*(t)S_{22}[\omega] \end{bmatrix}, \tag{3.8}$$

where

$$
\begin{aligned}
S_{11}[\omega] &= \int_{-\infty}^{\infty} \eta^*(\tau) e^{-i\omega\tau} d\tau \\
&= \sqrt{2\gamma} \times \frac{-\frac{1}{4}\kappa^2 + \frac{1}{2}\kappa\gamma - \omega_0^2 + \omega\omega_0 + i[\gamma\omega_0 + \frac{1}{2}\omega\kappa - \omega\gamma]}{(\gamma + i\omega)(\frac{\kappa}{2} - i\omega_0 - \gamma)(\frac{\kappa}{2} - i\omega_0 + i\omega)}, \\
S_{22}[\omega] &= \int_{-\infty}^{\infty} \eta(\tau) e^{-i\omega\tau} d\tau \\
&= \sqrt{2\gamma} \times \frac{-\frac{1}{4}\kappa^2 + \frac{1}{2}\kappa\gamma - \omega_0^2 - \omega\omega_0 + i[-\gamma\omega_0 + \frac{1}{2}\omega\kappa - \omega\gamma]}{(\gamma + i\omega)(\frac{\kappa}{2} + i\omega_0 - \gamma)(\frac{\kappa}{2} + i\omega_0 + i\omega)}.
\end{aligned}
$$

If we send decay rate $\kappa \to \infty$, namely the bad cavity case, then the following equation holds

$$
S_{\mathrm{out}}(t, \omega) = S_{\mathrm{in}}(t, \omega). \tag{3.9}
$$

That is, the output single-photon state is identical to the input single-photon state.

It should be noted that, throughout the thesis, the quantities plotted are all *dimensionless*. In the following, we fix damping rate $\gamma = 2$. In Fig. 3.1, (a) and (b) are the diagonal entries of the input Wigner spectrum respectively. It can be seen that both of them are exponentially decaying with respect to time t.

Fig. 3.2, 3.3 and 3.4 are the output Wigner spectra with different decay rates κ and the same de-tuning $\omega_0 = 0$. We can see that: **1**) when $\kappa = 0$, the output Wigner spectrum is the same as the input Wigner spectrum since the output covariance function reduces to the input one, see Fig. 3.2; **2**) compared with the input, the output Wigner spectrum is no longer monotonic in $\omega = 0$ as the decay rate κ becomes larger, see Fig. 3.3; **3**) the output Wigner spectrum is much similar to the input when decay rate κ is sufficiently large, compare Fig. 3.4 and Fig. 3.1.

Fig. 3.5, 3.6 and 3.7 are the output Wigner spectra with the same decay rate $\kappa = 4$ and different de-tunings ω_0. It can be seen that: **1**) in contrast to the case for the decay rate κ, the output Wigner spectrum is much unlike the input Wigner

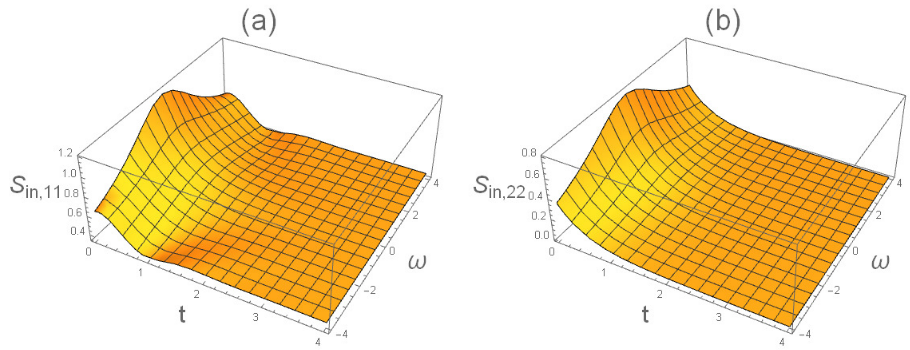

Figure 3.1: (Color online) (a) and (b) are the diagonal entries of the input Wigner spectrum.

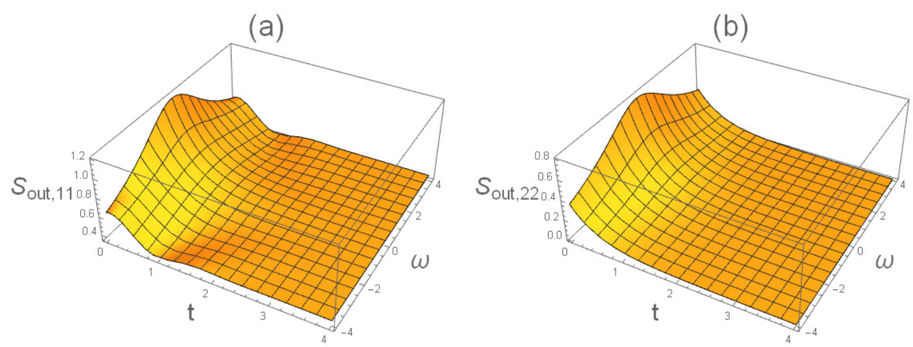

Figure 3.2: (Color online) (a) and (b) are the diagonal entries of the output Wigner spectrum with de-tuning $\omega_0 = 0$ and decay rate $\kappa = 0$.

spectrum even when the de-tuning ω_0 is very small, see Fig. 3.5; **2**) when the de-tuning ω_0 becomes larger, the output Wigner spectrum will tend to be the input one, see Fig. 3.6; **3**) if the de-tuning ω_0 is sufficiently large, the output Wigner spectrum would be close to the input Wigner spectrum, compare Fig. 3.7 and Fig. 3.1.

By comparing these figures, we can see that there exist five cases. **Case 1**: the output Wigner spectrum is close to the input Wigner spectrum when the decay rate κ is very small (compare Fig. 3.1 and Fig. 3.2); this can be explained by comparing (3.7) and (3.8) directly. **Case 2**: the output Wigner spectrum is close to the input Wigner spectrum when the decay rate κ is very large (compare Fig. 3.1 and Fig. 3.4). Since the impulse response function $g_G(t) \to \delta(t)$ when $\kappa \to \infty$, the output

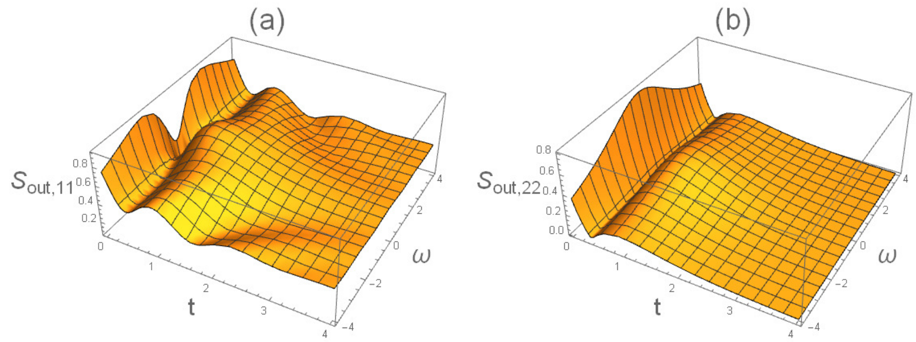

Figure 3.3: (Color online) (a) and (b) are the diagonal entries of the output Wigner spectrum with de-tuning $\omega_0 = 0$ and decay rate $\kappa = 3$.

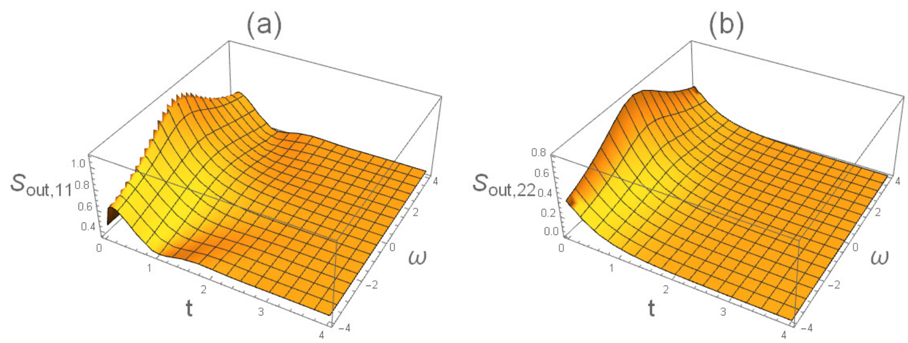

Figure 3.4: (Color online) (a) and (b) are the diagonal entries of the output Wigner spectrum with de-tuning $\omega_0 = 0$ and decay rate $\kappa = 100$.

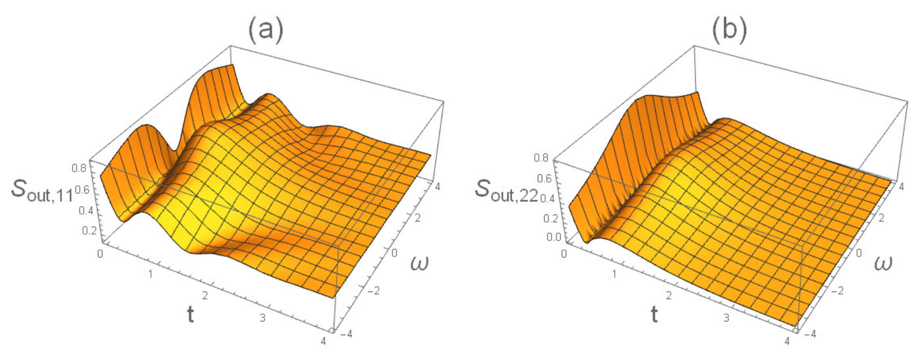

Figure 3.5: (Color online) (a) and (b) are the diagonal entries of the output Wigner spectrum with decay rate $\kappa = 4$ and de-tuning $\omega_0 = 0$.

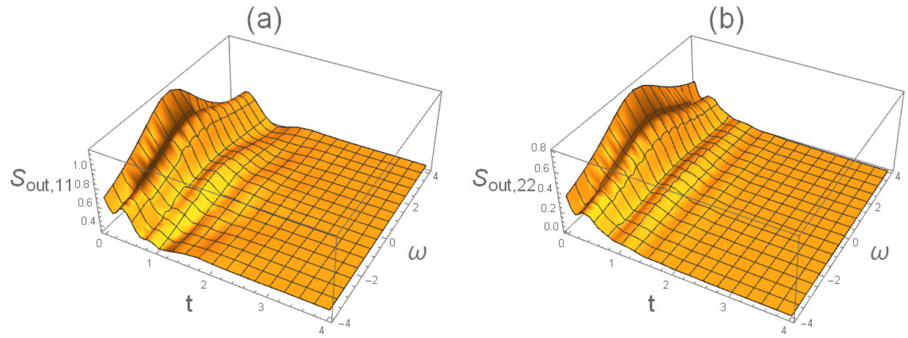

Figure 3.6: (Color online) (a) and (b) are the diagonal entries of the output Wigner spectrum with decay rate $\kappa = 4$ and de-tuning $\omega_0 = 10$.

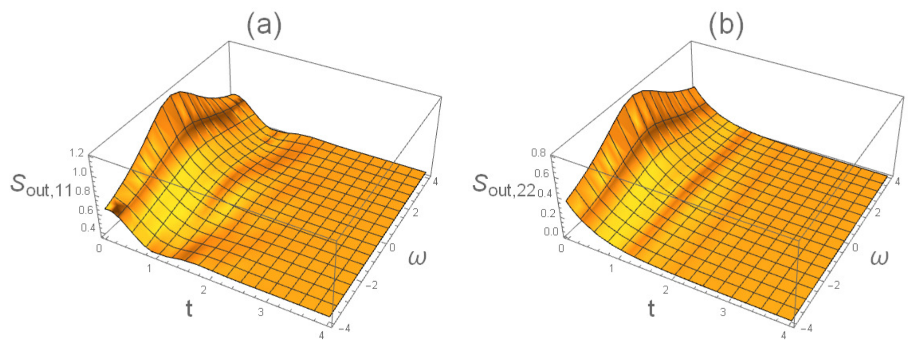

Figure 3.7: (Color online) (a) and (b) are the diagonal entries of the output Wigner spectrum with decay rate $\kappa = 4$ and de-tuning $\omega_0 = 50$.

state will be close to the input state. **Case 3**: the output Wigner spectrum is much similar to the input Wigner spectrum when the de-tuning ω_0 is very large since the optical cavity has little influence on the photons, see Fig. 3.7. **Case 4**: it can be seen from Fig. 3.3 that the output Wigner spectrum is quite different from the input one when κ is not very large or small. Moreover, (a) (for $b_{\rm out}b_{\rm out}^{\dagger}$) and (b) (for $b_{\rm out}^{\dagger}b_{\rm out}$) are quite different. **Case 5**: The output Wigner spectrum would change a lot with a small de-tuning ω_0 since there exists a strong interaction between the photon and system (compare Figs. 3.1 and 3.5).

Therefore, with Wigner spectrum, we are able to observe the changes of the system's response to the input signals in the time and frequency domains simultaneously. To our best knowledge, this has not been done before in the single-photon setting.

3.2 Wigner spectrum for DPA

Recall the quantum stochastic differential equations for a DPA in Fig. 2.2, [20, 62]

$$\begin{aligned} \begin{bmatrix} \dot{a}(t) \\ \dot{a}^\dagger(t) \end{bmatrix} &= -\frac{1}{2}\begin{bmatrix} \kappa & -\epsilon \\ -\epsilon & \kappa \end{bmatrix}\begin{bmatrix} a(t) \\ a^\dagger(t) \end{bmatrix} - \sqrt{\kappa}\begin{bmatrix} b(t) \\ b^\dagger(t) \end{bmatrix}, && (3.10) \\ b_{\rm out}(t) &= \sqrt{\kappa}a(t) + b(t), \quad (0 < \epsilon < \kappa). && (3.11) \end{aligned}$$

The DPA is driven by a single-photon Fock state, but the steady output state is no longer a single-photon state since the DPA has pump designated by ϵ. The steady output state belongs to a class of photon-Gaussian states which is defined in [62]. Let the single-photon input Fock state $|1_\nu\rangle$ be that defined in (3.3). The output covariance function [62, Section III-D] is

$$R_{\rm out}(t,r) = \begin{bmatrix} \chi_{11}(t,r) & \chi_{12}(t,r) \\ \chi_{21}(t,r) & \chi_{22}(t,r) \end{bmatrix} + \Delta(\xi_{\rm out}^-(t), \xi_{\rm out}^+(t))\Delta(\xi_{\rm out}^-(r), \xi_{\rm out}^+(r))^\dagger, \quad (3.12)$$

where

$$\xi_{\rm out}^-(t) = \frac{(\epsilon^2+\kappa^2-4\gamma^2)\sqrt{2\gamma}}{(\kappa+\epsilon-2\gamma)(\epsilon-\kappa+2\gamma)}e^{-\gamma t} + \frac{\kappa\sqrt{2\gamma}}{\kappa+\epsilon-2\gamma}e^{-\frac{\epsilon+\kappa}{2}t} - \frac{\kappa\sqrt{2\gamma}}{\epsilon-\kappa+2\gamma}e^{\frac{\epsilon-\kappa}{2}t},$$

$$\xi_{\rm out}^+(t) = \frac{2\kappa\epsilon\sqrt{2\gamma}}{(\kappa+\epsilon-2\gamma)(\epsilon-\kappa+2\gamma)}e^{-\gamma t} - \frac{\kappa\sqrt{2\gamma}}{\kappa+\epsilon-2\gamma}e^{-\frac{\epsilon+\kappa}{2}t} - \frac{\kappa\sqrt{2\gamma}}{\epsilon-\kappa+2\gamma}e^{\frac{\epsilon-\kappa}{2}t},$$

and

$$\chi_{11}(t,r) = \begin{cases} \dfrac{-\kappa\epsilon}{4(\kappa+\epsilon)} e^{-(\frac{\epsilon+\kappa}{2})(t-r)} + \dfrac{\kappa\epsilon}{4(\kappa-\epsilon)} e^{(\frac{\epsilon-\kappa}{2})(t-r)}, & t > r, \\ \delta(t-r) + \dfrac{3\kappa\epsilon^2 - 2\kappa^3}{2(\kappa^2-\epsilon^2)}, & t = r, \\ \dfrac{-\kappa\epsilon}{4(\kappa+\epsilon)} e^{-(\frac{\epsilon+\kappa}{2})(r-t)} + \dfrac{\kappa\epsilon}{4(\kappa-\epsilon)} e^{(\frac{\epsilon-\kappa}{2})(r-t)}, & t < r, \end{cases}$$

$$\chi_{12}(t,r) = \begin{cases} \dfrac{\kappa\epsilon}{4(\kappa+\epsilon)} e^{-(\frac{\epsilon+\kappa}{2})(t-r)} + \dfrac{\kappa\epsilon}{4(\kappa-\epsilon)} e^{(\frac{\epsilon-\kappa}{2})(t-r)}, & t > r, \\ \dfrac{\kappa^2\epsilon}{2(\kappa^2-\epsilon^2)}, & t = r, \\ \dfrac{\kappa\epsilon}{4(\kappa+\epsilon)} e^{-(\frac{\epsilon+\kappa}{2})(r-t)} + \dfrac{\kappa\epsilon}{4(\kappa-\epsilon)} e^{(\frac{\epsilon-\kappa}{2})(r-t)}, & t < r, \end{cases}$$

$$\chi_{21}(t,r) = \chi_{12}(t,r),$$

$$\chi_{22}(t,r) = \begin{cases} \dfrac{-\kappa\epsilon}{4(\kappa+\epsilon)} e^{-(\frac{\epsilon+\kappa}{2})(t-r)} + \dfrac{\kappa\epsilon}{4(\kappa-\epsilon)} e^{(\frac{\epsilon-\kappa}{2})(t-r)}, & t > r, \\ \dfrac{\kappa\epsilon^2}{2(\kappa^2-\epsilon^2)}, & t = r, \\ \dfrac{-\kappa\epsilon}{4(\kappa+\epsilon)} e^{-(\frac{\epsilon+\kappa}{2})(r-t)} + \dfrac{\kappa\epsilon}{4(\kappa-\epsilon)} e^{(\frac{\epsilon-\kappa}{2})(r-t)}, & t < r. \end{cases}$$

The corresponding Wigner spectrum is

$$S_{\text{out}}(t,\omega) = \begin{bmatrix} S_{\text{out},11}(t,\omega) & S_{\text{out},12}(t,\omega) \\ S_{\text{out},21}(t,\omega) & S_{\text{out},22}(t,\omega) \end{bmatrix}, \tag{3.13}$$

where

$$
\begin{aligned}
S_{\mathrm{out},11}(t,\omega) &= \frac{1}{\sqrt{2\pi}} \times \Big\{ \frac{-\kappa\epsilon}{4(\kappa+\epsilon)(\frac{\kappa}{2}+\frac{\epsilon}{2}-i\omega)} e^{-i\omega t} + \frac{\kappa\epsilon}{4(\kappa-\epsilon)(\frac{\kappa}{2}-\frac{\epsilon}{2}-i\omega)} e^{-i\omega t} \\
&\quad + \frac{-\kappa\epsilon}{4(\kappa+\epsilon)(\frac{\kappa}{2}+\frac{\epsilon}{2}+i\omega)} e^{-i\omega t} + \frac{\kappa\epsilon}{4(\kappa-\epsilon)(\frac{\kappa}{2}-\frac{\epsilon}{2}+i\omega)} e^{-i\omega t} + e^{-i\omega t} \\
&\quad + \xi_{\mathrm{out}}^{-}(t)[\frac{(\epsilon^2+\kappa^2-4\gamma^2)\sqrt{2\gamma}}{(\epsilon+\kappa-2\gamma)(\epsilon-\kappa+2\gamma)(\gamma+i\omega)} + \frac{\kappa\sqrt{2\gamma}}{(\kappa+\epsilon-2\gamma)(\frac{\kappa}{2}+\frac{\epsilon}{2}+i\omega)} \\
&\quad + \frac{\kappa\sqrt{2\gamma}}{(\kappa-\epsilon-2\gamma)(\frac{\kappa}{2}-\frac{\epsilon}{2}+i\omega)}] + \xi_{\mathrm{out}}^{+}(t)[\frac{2\kappa\epsilon\sqrt{2\gamma}}{(\epsilon+\kappa-2\gamma)(\epsilon-\kappa+2\gamma)(\gamma+i\omega)} \\
&\quad - \frac{\kappa\sqrt{2\gamma}}{(\kappa+\epsilon-2\gamma)(\frac{\kappa}{2}+\frac{\epsilon}{2}+i\omega)} + \frac{\kappa\sqrt{2\gamma}}{(\kappa-\epsilon-2\gamma)(\frac{\kappa}{2}-\frac{\epsilon}{2}+i\omega)}]\Big\}, \\
S_{\mathrm{out},12}(t,\omega) &= \frac{1}{\sqrt{2\pi}} \times \Big\{ \frac{\kappa\epsilon}{4(\kappa+\epsilon)(\frac{\epsilon}{2}+\frac{\kappa}{2}-i\omega)} e^{-i\omega t} + \frac{\kappa\epsilon}{4(\kappa-\epsilon)(\frac{\kappa}{2}-\frac{\epsilon}{2}-i\omega)} e^{-i\omega t} \\
&\quad + \frac{\kappa\epsilon}{4(\kappa+\epsilon)(\frac{\kappa}{2}+\frac{\epsilon}{2}+i\omega)} e^{-i\omega t} + \frac{\kappa\epsilon}{4(\kappa-\epsilon)(\frac{\kappa}{2}-\frac{\epsilon}{2}+i\omega)} e^{-i\omega t} \\
&\quad + \xi_{\mathrm{out}}^{-}(t)[\frac{2\kappa\epsilon\sqrt{2\gamma}}{(\epsilon+\kappa-2\gamma)(\epsilon-\kappa+2\gamma)(\gamma+i\omega)} - \frac{\kappa\sqrt{2\gamma}}{(\kappa+\epsilon-2\gamma)(\frac{\kappa}{2}+\frac{\epsilon}{2}+i\omega)} \\
&\quad + \frac{\kappa\sqrt{2\gamma}}{(\kappa-\epsilon-2\gamma)(\frac{\kappa}{2}-\frac{\epsilon}{2}+i\omega)}] + \xi_{\mathrm{out}}^{+}(t)[\frac{(\epsilon^2+\kappa^2-4\gamma^2)\sqrt{2\gamma}}{(\epsilon+\kappa-2\gamma)(\epsilon-\kappa+2\gamma)(\gamma+i\omega)} \\
&\quad + \frac{\kappa\sqrt{2\gamma}}{(\kappa+\epsilon-2\gamma)(\frac{\kappa}{2}+\frac{\epsilon}{2}+i\omega)} + \frac{\kappa\sqrt{2\gamma}}{(\kappa-\epsilon-2\gamma)(\frac{\kappa}{2}-\frac{\epsilon}{2}+i\omega)}]\Big\},
\end{aligned}
$$

$$
S_{\mathrm{out},21}(t,\omega) = S_{\mathrm{out},12}(t,\omega), \quad S_{\mathrm{out},22}(t,\omega) = S_{\mathrm{out},11}(t,\omega) - \frac{1}{\sqrt{2\pi}} e^{-i\omega t}.
$$

Similar to the cavity case, if we let decay rate $\kappa \to \infty$, (3.9) also holds for the DPA case, which is consistent with the simulation result in Fig. 3.10.

In the following, we fix $\epsilon = 1$ and $\gamma = 2$. Because the same single-photon input state $|1_\nu\rangle$ is used, the input Wigner spectrum is the same as the optical cavity case in Fig. 3.1. Figs. 3.8-3.10 are simulation results for the different decay rates κ, where $S_{\mathrm{out},11}(t,\omega)$, $S_{\mathrm{out},12}(t,\omega)$, $S_{\mathrm{out},21}(t,\omega)$, $S_{\mathrm{out},22}(t,\omega)$ are the entries for the output Wigner spectrum in (3.13) respectively. Compared with the cavity case, there exists non-zero off-diagonal entries since DPA is a non-passive system. In Fig. 3.8, compared with the passive system (the optical cavity), the off-diagonal entries are non-zero. The output Wigner spectrum is much different from the cavity case since DPA is an active system. In Fig. 3.9, the output Wigner spectrum becomes non-monotonic with a large decay rate κ. Compared with Fig. 3.5 for the cavity case, it can be seen that the 1-by-1 and 2-by-2 entries converge to 0 more slowly with the same decay rate $\kappa = 4$. Moreover, the off-diagonal entries cannot be ignored since the corresponding amplitudes are close to 0.4. In Fig. 3.10, if we compare the four parts in one figure, it can be seen that the amplitudes in 1-by-2 and 2-by-1 entries are almost 0 (the corresponding amplitudes are less than 0.025). Thus, the output Wigner spectrum is similar to the input Wigner spectrum when the decay rate κ is large enough even though DPA is non-passive. Finally, it can be seen clearly from Figs. 3.8 and 3.9 that the photon-Gaussian state is significantly different from the single-photon state. A photon-Gaussian state is obtained by driving a DPA with a single-photon state, [62]. Intuitively, a photon-Gaussian state is of the form $\mathbf{B}^\dagger(\eta)|\alpha\rangle$ in which η is a pulse shape and $|\alpha\rangle$ is a coherent state. Clearly, when $|\alpha\rangle = |0\rangle$, we get a single-photon Fock state.

An optical cavity is a passive system while a DPA is not. By comparing figures for the cavity case and the DPA case, it can be seen that the Wigner spectrum is able to demonstrate such fundamental difference very clearly in terms of the statistical characterization of the input-output relation.

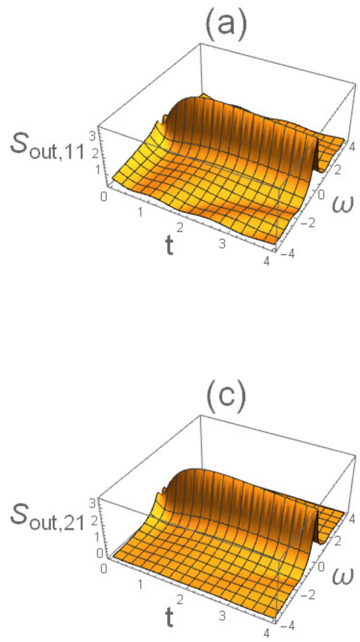

Figure 3.8: (Color online) The Wigner spectrum for the output photon-Gaussian state: $\epsilon = 1$, $\gamma = 2$ and $\kappa = 1.5$.

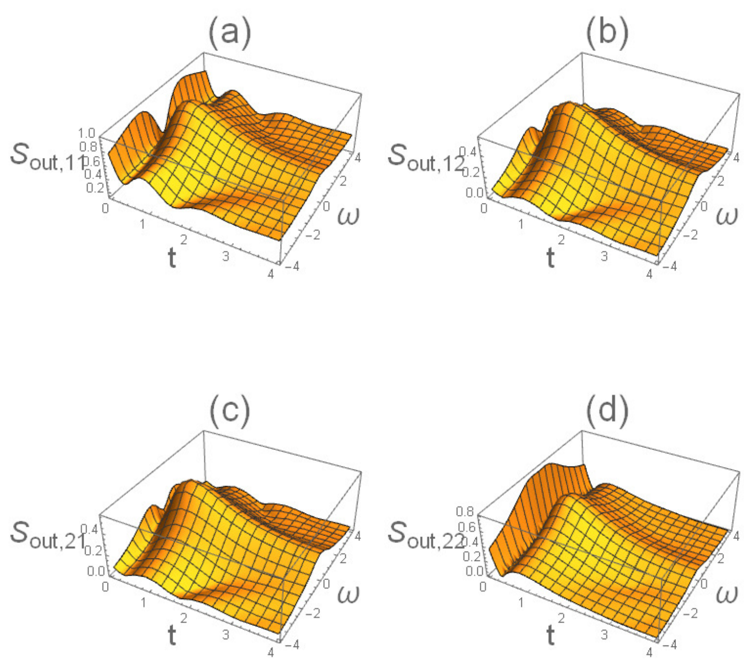

Figure 3.9: (Color online) The Wigner spectrum for the output photon-Gaussian state: $\epsilon = 1$, $\gamma = 2$ and $\kappa = 4$.

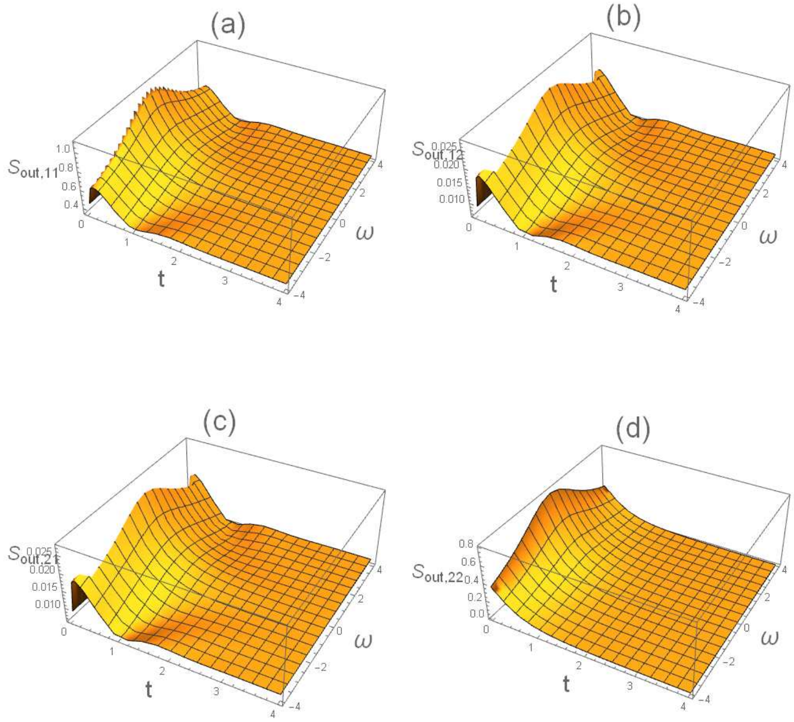

Figure 3.10: (Color online) The Wigner spectrum for the output photon-Gaussian state: $\epsilon = 1$, $\gamma = 2$ and $\kappa = 100$.

3.3 Final remarks

In this chapter, the Wigner spectrum has been used to analyze the statistical properties of continuous-mode single-photon Fock states. The Wigner spectrum is able to show the significant difference between the statistical nature of the output fields of an optical cavity and a degenerate parametric amplifier, driven by a continuous-mode single-photon Fock state.

Chapter 4

Coherent feedback control of continuous-mode single-photon states

In this chapter, we discuss how to engineer pulse shapes of single-photon states by means of coherent feedback control methods, namely direct coupling and coherent feedback.

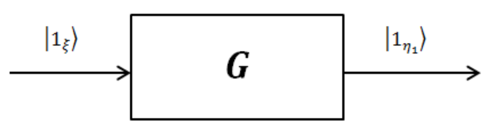

Figure 4.1: The original system G.

As introduced in the Preliminaries, quantum Markovian systems can be conveniently described by the triple (S, L, H) formalism, in which S is the scattering operator matrix, L is the coupling between the system and its environment, and H denotes the initial system Hamiltonian, see [23, 25, 61]. The system G in Fig. 4.1 is an optical cavity with the following parameters,

$$G = (1, \sqrt{\kappa}a_1, \omega_1 a_1^\dagger a_1), \tag{4.1}$$

where κ is the system decay rate and ω_1 denotes the de-tuning for system G. $|1_\xi\rangle$ is the single-photon input Fock state and $|1_{\eta_1}\rangle$ is the output state.

4.1 Direct couplings

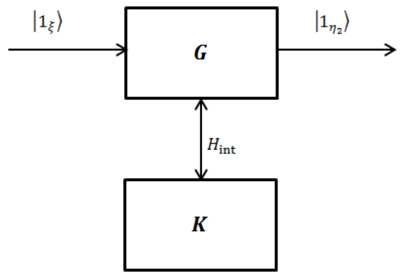

Figure 4.2: Directly coupled system $G \bowtie K$.

In Fig. 4.2, two independent systems G and K may interact by exchanging energy. This energy exchange can be described by an interaction Hamiltonian H_{int} with the form

$$H_{\text{int}} = X_1^\dagger X_2 + X_1 X_2^\dagger, \tag{4.2}$$

where X_1 and X_2 are operators on system G and K respectively. We can denote the directly coupled system by $G \bowtie K$, see [53, 60].

In Fig. 4.2, the system G is directly coupled with another linear quantum system K with parameters

$$K = (-, -, \omega_2 a_2^\dagger a_2), \tag{4.3}$$

where the symbol "$-$" means that there is neither scattering nor coupling, ω_2 and a_2 denote the de-tuning and the annihilation operator for system K, respectively. In this case, the output state is described by $|1_{\eta_2}\rangle$.

Alternatively, we may use a beamsplitter to form a coherent feedback network, see Fig. 4.3. In the following, we derive the explicit forms of output pulse shapes in the frequency domain.

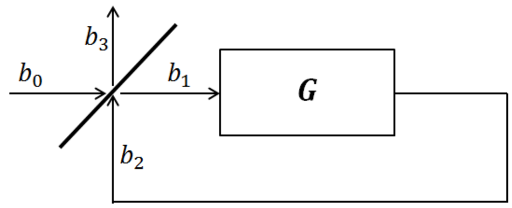

Figure 4.3: A linear quantum feedback network.

4.2 Photon shape synthesis

Let the pulse shape of a single-photon input Fock state $|1_\xi\rangle$ be

$$\xi(t) = \begin{cases} \sqrt{2\beta}e^{-\beta t}, & t \geq 0, \\ 0, & t < 0, \end{cases} \tag{4.4}$$

where β is the damping rate of a single-photon. By the Fourier transform, we can get the input pulse shape in the frequency domain

$$\xi[\omega] = \frac{\sqrt{2\beta}}{i\omega + \beta}. \tag{4.5}$$

The dynamic model for a linear quantum system in Chapter 2.2 is

$$\begin{aligned} \dot{\breve{a}}(t) &= A\breve{a}(t) + B\breve{b}(t), \quad \breve{a}(t_0) = \breve{a}, \\ \breve{b}_{\text{out}} &= C\breve{a}(t) + D\breve{b}(t), \end{aligned}$$

where system matrices can be given in terms of the (S, L, H) formalism,

$$\begin{aligned} D =& \Delta(S, 0), \quad C = \Delta(C_-, C_+), \\ B =& -C^\flat \Delta(S, 0), \quad A = -\frac{1}{2}C^\flat C - iJ_n\Delta(\Omega_-, \Omega_+). \end{aligned}$$

Then by (4.1), the quantum stochastic differential equations for system G in Fig. 4.1 are

$$\begin{aligned} \dot{a}(t) =& \left(-\frac{\kappa}{2} - i\omega_1\right) a(t) - \sqrt{\kappa}b(t), \\ b_{\text{out}}(t) =& \sqrt{\kappa}a(t) + b(t), \end{aligned} \tag{4.6}$$

and the system matrices for system G are

$$A_1 = \begin{bmatrix} -\frac{k}{2} - i\omega_1 & 0 \\ 0 & -\frac{k}{2} + i\omega_1 \end{bmatrix}, \; B_1 = \begin{bmatrix} -\sqrt{k} & 0 \\ 0 & -\sqrt{k} \end{bmatrix},$$

$$C_1 = \begin{bmatrix} \sqrt{k} & 0 \\ 0 & \sqrt{k} \end{bmatrix}, \; D_1 = \begin{bmatrix} 1 & 0 \\ 0 & 1 \end{bmatrix}.$$

The transfer function for system G is given by

$$G_1[\omega] = 1 - \frac{\kappa}{i\omega + i\omega_1 + \frac{\kappa}{2}}, \tag{4.7}$$

and the output pulse shape in the frequency domain is [62, 59]

$$\eta_1[\omega] = G_1[\omega]\xi[\omega]. \tag{4.8}$$

Secondly, for the directly coupled system in Fig. 4.2, we assume that $X_1 = \alpha a_1$, $\alpha \in \mathbb{C}$ and $X_2 = a_2$. The interaction Hamiltonian is given by

$$H_{\text{int}} = \bar{\alpha} a_1^\dagger a_2 + \alpha a_1 a_2^\dagger. \tag{4.9}$$

Then the Hamiltonian for the whole system $G \bowtie K$ is

$$H = H_1 + H_{\text{int}} + H_2, \tag{4.10}$$

where $H_1 = \omega_1 a_1^\dagger a_1$ and $H_2 = \omega_2 a_2^\dagger a_2$.

Similarly, we can get the (S, L, H) parameters for $G \bowtie K$, which is

$$\left(\begin{bmatrix} 1 & 0 \\ 0 & 0 \end{bmatrix}, \begin{bmatrix} \sqrt{\kappa} a_1 \\ 0 \end{bmatrix}, \omega_1 a_1^\dagger a_1 + \bar{\alpha} a_1^\dagger a_2 + \alpha a_1 a_2^\dagger + \omega_2 a_2^\dagger a_2 \right), \tag{4.11}$$

and the quantum stochastic differential equations for $G \bowtie K$ are

$$\begin{aligned} \dot{a}_1(t) =& \left(-\frac{\kappa}{2} - i\omega_1\right) a_1(t) - i\bar{\alpha} a_2(t) - \sqrt{\kappa} b(t), \\ \dot{a}_2(t) =& - i\alpha a_1(t) - i\omega_2 a_2(t), \\ b_{\text{out}}(t) =& \sqrt{\kappa} a_1(t) + b(t). \end{aligned} \tag{4.12}$$

Then we can get the system matrices,

$$A_2 = \begin{bmatrix} -\frac{k}{2} - i\omega_1 & -i\bar{\alpha} & 0 & 0 \\ -i\alpha & -i\omega_2 & 0 & 0 \\ 0 & 0 & -\frac{k}{2} + i\omega_1 & i\alpha \\ 0 & 0 & i\bar{\alpha} & i\omega_2 \end{bmatrix}, \ B_2 = \begin{bmatrix} -\sqrt{k} & 0 & 0 & 0 \\ 0 & 0 & 0 & 0 \\ 0 & 0 & -\sqrt{k} & 0 \\ 0 & 0 & 0 & 0 \end{bmatrix},$$

$$C_2 = \begin{bmatrix} \sqrt{k} & 0 & 0 & 0 \\ 0 & 0 & 0 & 0 \\ 0 & 0 & \sqrt{k} & 0 \\ 0 & 0 & 0 & 0 \end{bmatrix}, \ D_2 = \begin{bmatrix} 1 & 0 & 0 & 0 \\ 0 & 0 & 0 & 0 \\ 0 & 0 & 1 & 0 \\ 0 & 0 & 0 & 0 \end{bmatrix},$$

and the pulse shape of the output single-photon Fock state for the system $G \bowtie K$, which is

$$\eta_2[\omega] = \frac{-\frac{\kappa}{2}(\omega+\omega_2)i - (\omega+\omega_1)(\omega+\omega_2) + |\alpha|^2}{\frac{\kappa}{2}(\omega+\omega_2)i - (\omega+\omega_1)(\omega+\omega_2) + |\alpha|^2}\xi[\omega]. \tag{4.13}$$

Finally, in Fig. 4.3, let the beamsplitter introduced in Chapter 2.2 be

$$S = \begin{bmatrix} \sqrt{\gamma} & \sqrt{1-\gamma} \\ -\sqrt{1-\gamma} & \sqrt{\gamma} \end{bmatrix}, \ 0 < \gamma < 1, \tag{4.14}$$

and the input field b_0 be in the single-photon Fock state $|1_\xi\rangle$.

By $\begin{bmatrix} b_3 \\ b_1 \end{bmatrix} = S \begin{bmatrix} b_0 \\ b_2 \end{bmatrix}$ and $b_0 = \xi[\omega]$, $b_3 = \eta_3[\omega]$, $b_2 = G_1[\omega]b_1$, we can get the pulse shape for the output field b_3 in Fig. 4.3, given by

$$\eta_3[\omega] = \frac{-\frac{1-\sqrt{\gamma}}{1+\sqrt{\gamma}}(\omega+\omega_1)i + \frac{\kappa}{2}}{\frac{1-\sqrt{\gamma}}{1+\sqrt{\gamma}}(\omega+\omega_1)i + \frac{\kappa}{2}}\xi[\omega]. \tag{4.15}$$

4.3 Photon distribution

For the single-photon Fock state we defined before

$$|1_\xi\rangle = \int_{-\infty}^{\infty} b^\dagger(t)\xi(t)dt|0\rangle, \tag{4.16}$$

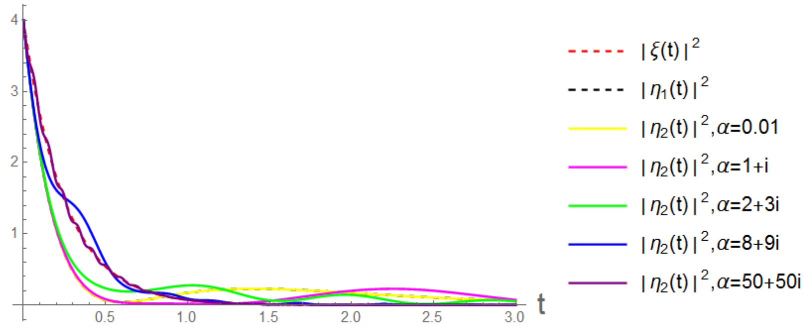

Figure 4.4: (Color online) $|\xi(t)|^2$ denotes the detection probability of input pulse shape, $|\eta_1(t)|^2$ denotes the detection probability of output pulse shape in the case of original system (Fig. 4.1), $|\eta_2(t)|^2$ are the detection probabilities of output pulse shape in the directly coupled system (Fig. 4.2) with different parameters α.

$b^\dagger(t)$ is the creation operator of the input field and the pulse shape $\xi(t)$, which is also known as temporal wave packet, is given by (4.4). $|\xi(t)|^2$ denotes the probability of finding the photon (detection probability) in the interval $[t, t+dt)$. In this section, we will focus on how the system parameters in the control schemes discussed above change the detection probabilities $|\eta_j(t)|^2$, $j = 1, 2, 3$.

By the inverse Fourier transform, we can get the output temporal wave packets

$$\eta_j(t) = \frac{1}{\sqrt{2\pi}} \int_{-\infty}^{\infty} e^{i\omega t} \eta_j[\omega] d\omega, \quad (j = 1, 2, 3) \tag{4.17}$$

where j denotes the j-th case we discussed before.

In what follows, we fix $\beta = 2$, $\kappa = 1$, and $\omega_1 = 1$ for the direct coupling scheme (Fig. 4.2) and the coherent feedback network (Fig. 4.3). Fig. 4.4 and Fig. 4.5 are the detection probabilities for different α and ω_2 respectively. The detection probabilities for different beamsplitter parameter γ are given in Fig. 4.6.

By comparing these three cases, it can be easily seen that the linear quantum feedback network in Fig. 4.3 has much more influence on the detection probability than the directly coupled system. In addition, the changes of output Wigner spectrum with respect to the beamsplitter parameter γ for the quantum feedback network

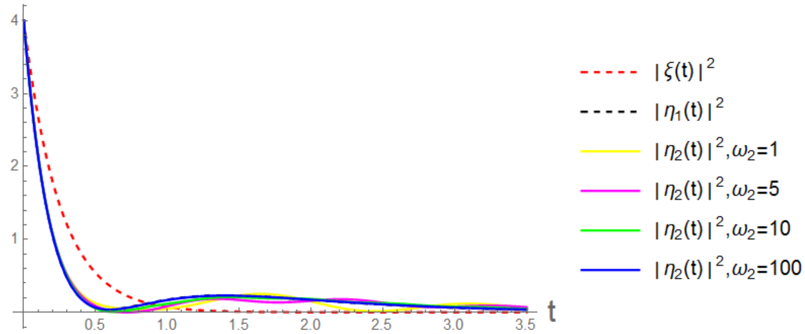

Figure 4.5: (Color online) $|\xi(t)|^2$ denotes the detection probability of input pulse shape, $|\eta_1(t)|^2$ denotes the detection probability of output pulse shape in the case of original system (Fig. 4.1), $|\eta_2(t)|^2$ are the detection probabilities of output pulse shape in the directly coupled system (Fig. 4.2) with different parameters ω_2.

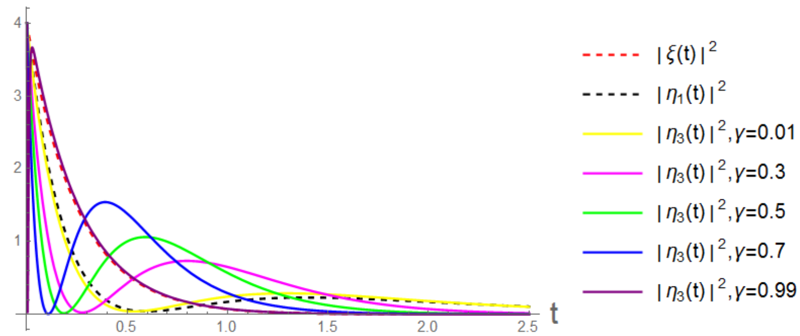

Figure 4.6: (Color online) $|\xi(t)|^2$ denotes the detection probability of input pulse shape, $|\eta_1(t)|^2$ denotes the detection probability of output pulse shape in the case of original system (Fig. 4.1), $|\eta_3(t)|^2$ are the detection probabilities of output pulse shape in the linear quantum feedback network (Fig. 4.3) with different beamsplitter parameters γ.

also have been analyzed. In Figs. 4.7 - 4.9, let the decay rate of the optical cavity be $\kappa = 4$ and damping rate be $\beta = 2$. Specifically, in Fig. 4.7, since $b_3 \to b_2$, $b_1 \to b_0$ when $\gamma \to 0$, the feedback network should reduce to the original system G in Fig. 4.1 without beamsplitter. This can be verified by comparison with Fig. 3.3. In Fig. 4.9, if $\gamma \to 1$, then $b_3 \to b_0$. It means that the output Wigner spectrum will be close to that of the input. It can be verified that those changes are consistent with the photon distributions in Fig. 4.6. Thus, the simulation result should be much similar

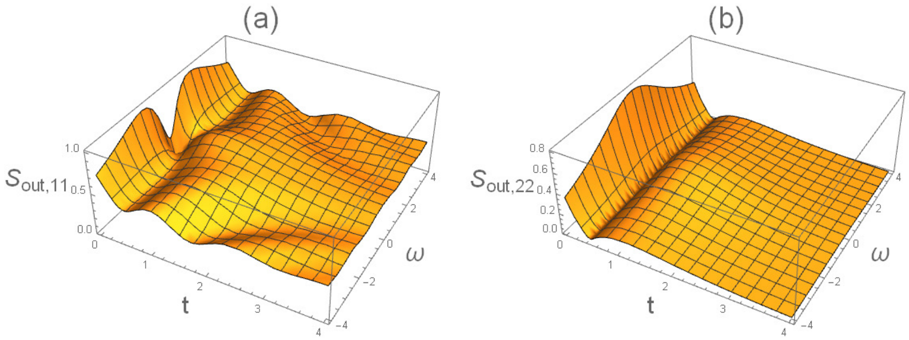

Figure 4.7: (Color online) The output Wigner spectrum for quantum feedback network with beamsplitter parameter $\gamma = 0.01$.

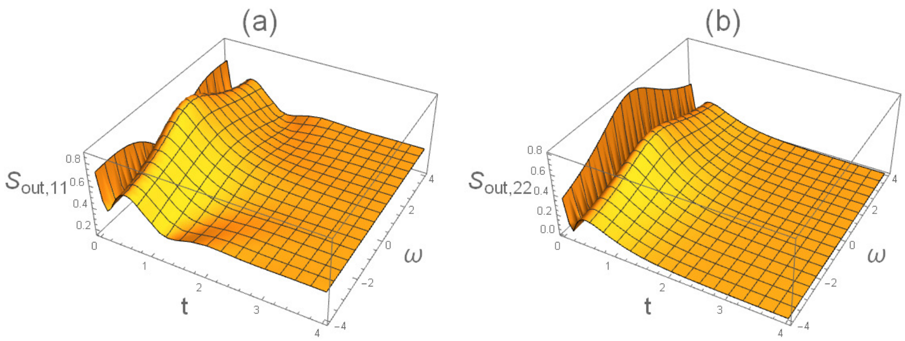

Figure 4.8: (Color online) The output Wigner spectrum for quantum feedback network with beamsplitter parameter $\gamma = 0.5$.

to the input Wigner spectrum in Fig. 3.1.

On the other hand, we assume the system G for the feedback network in Fig. 4.3 is a DPA with the following parameters

$$S_0 = 1, \quad L_0 = \sqrt{\kappa} a, \quad H_0 = \frac{i\epsilon}{4}((a^\dagger)^2 - a^2). \tag{4.18}$$

Then the (S, L, H) formalism of the whole feedback network system in Fig. 4.3 for the DPA case is given by

$$S_1 = -1, \quad L_1 = \sqrt{\frac{1+\sqrt{\gamma}}{1-\sqrt{\gamma}}\kappa} a, \quad H_1 = H_0. \tag{4.19}$$

So the only change between the feedback network and the original system is $\kappa \to$

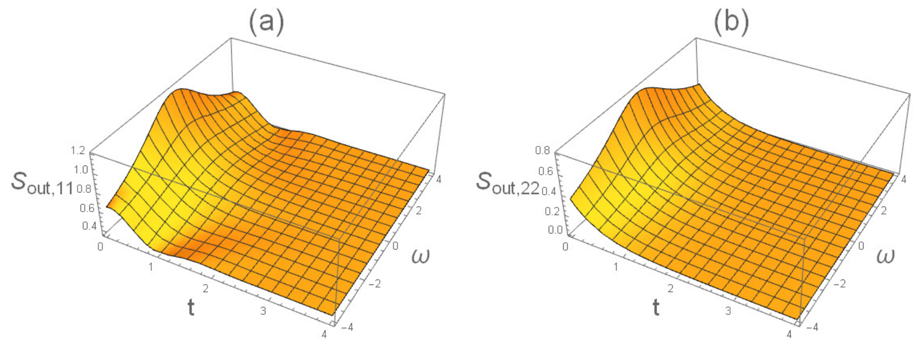

Figure 4.9: (Color online) The output Wigner spectrum for quantum feedback network with beamsplitter parameter $\gamma = 0.99$.

$\dfrac{1+\sqrt{\gamma}}{1-\sqrt{\gamma}}\kappa$. We have the following observations:

1) when $\gamma = 0$, the feedback network reduces to the open-loop system G.

2) when $\gamma = 1$, then $S = 1$, $b_3 = b_0$, there is no interaction between the field and the system.

3) when $0 < \gamma < 1$, $\dfrac{1+\sqrt{\gamma}}{1-\sqrt{\gamma}}\kappa > \kappa$, the decay rate is always enhanced. However, it is clear that

$$\lim_{\gamma\to 0}\frac{1+\sqrt{\gamma}}{1-\sqrt{\gamma}}\kappa = \kappa. \tag{4.20}$$

Therefore, by tuning the beamsplitter, we can get various output single-photon states. It is worth noting that the same feedback scheme Fig. 4.3 has been used for optical squeezing, see theoretical [24] and experimental [29].

4.4 Final remarks

In this chapter, two control schemes have been compared for single-photon pulse-shaping. We have also investigated how to use control methods to engineer photon pulse shapes of the output state of a quantum linear system in response to a single-photon state. It has been demonstrated that the coherent feedback control scheme is the most effective one in terms of single-photon pulse-shaping.

Chapter 5

Quantum filtering with multiple measurements for systems driven by single-photon states

In this chapter, the single-photon filtering framework proposed in [14, 27] are extended by including imperfect measurements. In practice, the detector responds with a quantum efficiency of less than unity since there exists some mode mismatch between the detector and the system [10], and the single-photon signal may be corrupted by quantum white noise [46]. Motivated by this, we study the case when the output light field is corrupted by a vacuum noise. More specifically, we present the

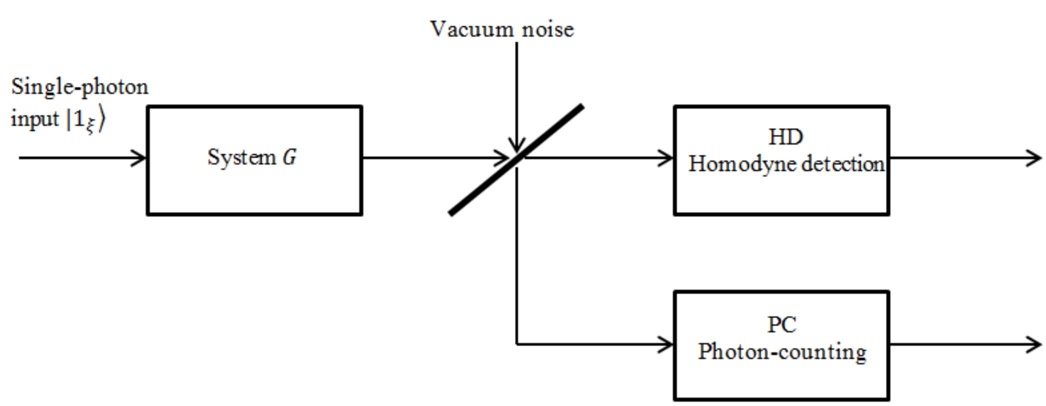

Figure 5.1: Simultaneous homodyne detection and photon-counting detection at the outputs of a beam splitter in a quantum system.

stochastic master equations for a quantum system interacting with a single-photon state, see Fig. 5.1. Quantum filters for the cases of joint homodyne detection and photon-counting detection measurements and both homodyne detection measurements are designed to improve the estimation performance, respectively.

5.1 The extended system

Normally, quantum filtering for a system driven by the vacuum input is easy and convenient to analyze. In this chapter, we use the idea in [27] to construct a quantum signal generating filter $M = (S_M, L_M, H_M)$, which is usually called ancilla. Cascading this ancilla M with the quantum system G, then we get the extended system $G_T = G \lhd M$. Since the extended system G_T is driven by vacuum input, the master equation and quantum filter follow from the known result in [27]. In this chapter, we use a two-level atom as an ancilla. The interaction of the ancilla M with the vacuum input is given by

$$(S_M, L_M, H_M) = (I, \lambda(t)\sigma_-, 0), \tag{5.1}$$

where σ_- is the lowering operator from the upper state $|\uparrow\rangle$ to the ground state $|\downarrow\rangle$, while σ_+ is the rising operator from the ground state $|\downarrow\rangle$ to the upper state $|\uparrow\rangle$. It means that the atom decays into its ground state at some stage, creating a single photon in the output. The ancilla will output the desired single-photon state $|1_\xi\rangle$ since we can choose the coupling strength $\lambda(t)$ to be

$$\lambda(t) = \frac{\xi(t)}{\sqrt{w(t)}}, \tag{5.2}$$

where $w(t) = \int_t^\infty |\xi(s)|^2 ds$.

By using the cascade connection formalism in Chapter 2.3, we have the extended system G_T

$$G_T = \left(S, L + \lambda(t)S\sigma_-, H + \frac{1}{2i}\left(\lambda(t)L^\dagger S\sigma_- - \lambda^*(t)\sigma_+ S^\dagger L\right)\right). \tag{5.3}$$

Let $\tilde{U}(t)$ be the unitary operator for the joint ancilla-system-field system. The following equality can be defined (see [27] for more details)

$$\mathbb{E}_{\eta\xi}[X(t)] = \mathbb{E}_{\uparrow\eta 0}[\tilde{U}^\dagger(t)(I \otimes X \otimes I)\tilde{U}(t)] \tag{5.4}$$

with initial state $|\uparrow\rangle \otimes |\eta\rangle \otimes |0\rangle$ for arbitrary operator $X(t)$ of the system G. Here, $|\uparrow\rangle$ is the upper state of the ancilla, $|\eta\rangle$ is the initial state of the system and $|0\rangle$ denotes the vacuum state of the field.

5.2 Quantum filter with multiple measurements for systems driven by the vacuum input

We will use the following notation to define the conditional expectation

$$\hat{X}_t = \pi_t(X) = \mathbb{E}[j_t(X)|\mathcal{Y}_t],$$

where $\mathcal{Y}_t$ is generated by the observation processes $\{Y(s) : 0 \leq s \leq t\}$. To derive the quantum filter for a system driven by a single-photon input state, we firstly introduce the result of multiple measurements with the vacuum input.

Lemma 5.1. *([18, Theorem 3.2]) Let $\{Y_{i,t}, i = 1, 2, \ldots, N\}$ be a set of N compatible measurement outputs for a quantum system G. With vacuum input state, the corresponding joint measurement quantum filter is given by*

$$d\hat{X}_t = \pi_t[\mathcal{L}_G(\hat{X}_t)]dt + \sum_{i=1}^{N} \beta_{i,t} dW_{i,t}, \tag{5.5}$$

where $dW_{i,t} = dY_{i,t} - \pi_t(dY_{i,t})$ is a martingale process for each measurement output and $\beta_{i,t}$ is the corresponding gain given by

$$\begin{aligned}
\zeta^T &= \pi_t(\hat{X}_t dY_t^T) - \pi_t(\hat{X}_t)\pi_t(dY_t^T) + \pi_t\left([L_t^\dagger, \hat{X}_t]S_t dB dY_t^T\right), \\
\Sigma &= \pi_t(dY_t dY_t^T), \quad \beta = \Sigma^{-1}\zeta,
\end{aligned} \tag{5.6}$$

where Σ is assumed to be non-singular.

Remark 5.1. *The class of measurement outputs is compatible if and only if it satisfies the self-commuting*

$$[Y(t), Y(s)] = 0, \quad s \leqslant t,$$

and non-demolition

$$[X(t), Y(s)] = 0, \quad s \leqslant t,$$

properties.

Remark 5.2. *A general measurement equation, which is a function of annihilation, creation and conservation processes of the output field, is defined as [18]*

$$dY(t) = F^{\#} dB_{\text{out}}^{\#}(t) + F dB_{\text{out}}(t) + G\text{diag}(d\Lambda_{\text{out}}(t)). \tag{5.7}$$

Particularly, a combination of homodyne detection and photon-counting measurement is given by

$$F = \begin{bmatrix} 1 & 0 \\ 0 & 0 \end{bmatrix}, G = \begin{bmatrix} 0 & 0 \\ 0 & 1 \end{bmatrix}.$$

In this case, $[Y_1(t), Y_2(t)] = 0$, it means that the two compatible measurements are independent of each other.

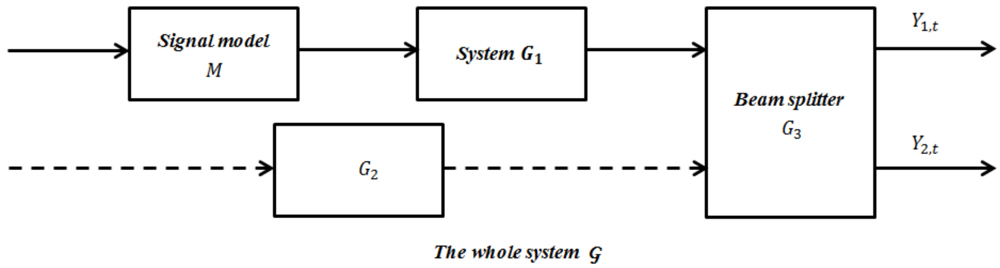

Figure 5.2: Quantum system depiction of Fig. 5.1.

5.3 Quantum filter with joint homodyne and photon-counting detections for systems driven by a single-photon state

Suppose that the system is in an initial state $\rho_0 = |\eta\rangle\langle\eta|$ and the single-photon input state is $|1_\xi\rangle$. For a given system operator X, we define the expectation

$$\omega_t^{jk}(X) = \mathbb{E}_{jk}[j_t(X)] = \langle\eta\phi_j|X(t)|\eta\phi_k\rangle, \quad j,k = 0,1,$$

where $\phi_j = \begin{cases} |0\rangle, & j=0; \\ |1_\xi\rangle, & j=1. \end{cases}$

The quantum filter for the conditional expectation for the system G driven by a single-photon field is given by

$$\pi_t^{11}(X) = \mathbb{E}_{\eta\xi}[X(t)|Y(s), 0 \le s \le t], \tag{5.8}$$

and the quantum filter for the extended system $G_T = G \triangleleft M$ driven by the vacuum input is defined as

$$\tilde{\pi}_t(A \otimes X) = \mathbb{E}_{\uparrow\eta 0}[\tilde{U}^\dagger(t)(A \otimes X)\tilde{U}(t)|I \otimes Y(s), 0 \le s \le t], \tag{5.9}$$

where A is an ancilla operator and X is a system operator.

The whole system $\mathcal{G}$ with the measurements in Fig. 5.1 can be depicted in Fig. 5.2. $G_1 = (S, L, H)$ is the original system G, which has been connected to a signal model (ancilla) $M = (I, \lambda(t)\sigma_-, 0)$. By introducing a second open quantum system $G_2 =$

$(I, 0, 0)$, which is actually an identity operator, we concatenate the vacuum noise into our system. The last open quantum system is a beam splitter $G_3 = (S_b, 0, 0)$, where

$$S_b = \begin{bmatrix} \sqrt{1-r^2}e^{i\theta} & re^{i(\theta+\frac{\pi}{2})} \\ re^{i(\theta+\frac{\pi}{2})} & \sqrt{1-r^2}e^{i\theta} \end{bmatrix}, \quad 0 \leq r \leq 1. \tag{5.10}$$

By the concatenation and series products, the whole system $\mathcal{G}$ is given by

$$\mathcal{G} = G_3 \lhd [(G_1 \lhd M) \boxplus G_2] = (S_t, L_t, H_t), \tag{5.11}$$

where

$$S_t = S_b \begin{bmatrix} S & 0 \\ 0 & 1 \end{bmatrix}, L_t = \begin{bmatrix} L + \lambda(t)S\sigma_- \\ 0 \end{bmatrix}, H_t = H + \frac{1}{2i}\left(\lambda(t)L^\dagger S\sigma_- - \lambda^*(t)\sigma_+ S^\dagger L\right).$$

Furthermore, the Lindblad superoperator $\mathcal{L}_\mathcal{G}(A \otimes X)$ for the whole system $\mathcal{G}$ can be expressed in the following form

$$\begin{aligned} \mathcal{L}_\mathcal{G}(A \otimes X) = & A \otimes \mathcal{L}_G X + (\mathcal{D}_{L_M} A) \otimes X + L_M^\dagger A \otimes S^\dagger[X, L] \\ & + AL_M \otimes [L^\dagger, X]S + L_M^\dagger A L_M \otimes (S^\dagger X S - X), \end{aligned} \tag{5.12}$$

where A is any operator of the ancilla and X is the system operator.

In what follows, we denote by $B_{i,t}$, the vacuum state as the input of signal model M, and $B_{v,t}$ the vacuum noise for system G_2, then the total input, together with gauge process for the whole system $\mathcal{G}$ are given by

$$B_t = \begin{bmatrix} B_{i,t} \\ B_{v,t} \end{bmatrix}, \Lambda_t = \begin{bmatrix} \Lambda_{i,t} & \Lambda_{iv,t} \\ \Lambda_{vi,t} & \Lambda_{v,t} \end{bmatrix},$$

where

$$B_{i,t} = \int_0^t b_i(s)ds, \quad \Lambda_{i,t} = \int_0^t b_i^\dagger(s)b_i(s)ds, \quad \Lambda_{iv,t} = \int_0^t b_i^\dagger(s)b_v(s)ds.$$

By the evolution of output fields (2.6), the measurements stochastic equations are given by

$$\begin{aligned} dY_{1,t} =& \sqrt{1-r^2}\Big\{ \Big[e^{i\theta}(L+SL_M)+e^{-i\theta}(L^\dagger+L_M^\dagger S^\dagger)\Big]\,dt \\ &+e^{i\theta}SdB_{i,t}+e^{-i\theta}S^\dagger dB_{i,t}^\dagger\Big\}+ir\left(e^{i\theta}dB_{v,t}-e^{-i\theta}dB_{v,t}^\dagger\right), \end{aligned} \tag{5.13}$$

and

$$\begin{aligned} dY_{2,t} =& r^2\Big[Sd\Lambda_{i,t}S^\dagger+(L+SL_M)S^\dagger dB_{i,t}^\dagger+S(L^\dagger+L_M^\dagger S^\dagger)dB_{i,t} \\ &+(L^\dagger+L_M^\dagger S^\dagger)(L+SL_M)dt\Big]+(1-r^2)d\Lambda_{v,t} \\ &+ir\sqrt{1-r^2}\Big[Sd\Lambda_{vi,t}-S^\dagger d\Lambda_{iv,t}+(L+SL_M)dB_{v,t}^\dagger \\ &-(L^\dagger+L_M^\dagger S^\dagger)dB_{v,t}\Big], \end{aligned} \tag{5.14}$$

where $dY_{1,t}$ is for the first channel with homodyne detection and $dY_{2,t}$ is for the second channel with photon-counting measurement. Then the expectation and correlation of the measurements can be derived as

$$\begin{aligned} &\tilde{\pi}_t(dY_{1,t}) = \sqrt{1-r^2}\tilde{\pi}_t\left[e^{i\theta}(L+SL_M)+e^{-i\theta}(L^\dagger+L_M^\dagger S^\dagger)\right]dt, \\ &\tilde{\pi}_t(dY_{2,t}) = \tilde{\pi}_t(dY_{2,t}dY_{2,t}) = r^2\tilde{\pi}_t\left[(L^\dagger+L_M^\dagger S^\dagger)(L+SL_M)\right]dt, \\ &\tilde{\pi}_t(dY_{1,t}dY_{1,t}) = dt, \\ &\tilde{\pi}_t(dY_{1,t}dY_{2,t}) = \tilde{\pi}_t(dY_{2,t}dY_{1,t}) = 0. \end{aligned} \tag{5.15}$$

Thus, we have the *non-singular* matrix

$$\Sigma = \begin{bmatrix} dt & 0 \\ 0 & r^2\tilde{\pi}_t\left[(L^\dagger+L_M^\dagger S^\dagger)(L+SL_M)\right]dt \end{bmatrix}, \tag{5.16}$$

and the corresponding gain $\beta = [\beta_1 \ \beta_2]$ can be calculated by (5.6)

$$\begin{aligned}\beta_1 =&\sqrt{1-r^2}e^{i\theta}\tilde{\pi}_t\big(A\otimes XL + AL_M\otimes XS\big)\\&+\sqrt{1-r^2}e^{-i\theta}\tilde{\pi}_t\big(A\otimes L^\dagger X + L_M^\dagger A\otimes S^\dagger X\big)\\&-\sqrt{1-r^2}\tilde{\pi}_t\big(A\otimes X\big)\\&\times\tilde{\pi}_t\left[e^{i\theta}(L+SL_M)+e^{-i\theta}(L^\dagger+L_M^\dagger S^\dagger)\right],\end{aligned}\tag{5.17}$$

$$\begin{aligned}\beta_2 =&\big[\tilde{\pi}_t(L^\dagger L + L_M^\dagger S^\dagger L + L^\dagger S L_M + L_M^\dagger L_M)\big]^{-1}\\&\times\tilde{\pi}_t\big(A\otimes L^\dagger XL + L_M^\dagger A\otimes S^\dagger XL + AL_M\otimes L^\dagger XS\\&+L_M^\dagger AL_M\otimes S^\dagger XS\big)-\tilde{\pi}_t\big(A\otimes X\big),\end{aligned}\tag{5.18}$$

where A is any ancilla operator and X is the system operator.

Finally, by Lemma 5.1, the joint measurement quantum filter for the whole system $\mathcal{G}$ driven by vacuum input state is given by

$$d\tilde{\pi}_t(A\otimes X) =\tilde{\pi}_t(\mathcal{L}_{\mathcal{G}}(A\otimes X))dt + \beta_1\left[dY_{1,t}-\tilde{\pi}_t(dY_{1,t})\right]+\beta_2\left[dY_{2,t}-\tilde{\pi}_t(dY_{2,t})\right],\tag{5.19}$$

where the Lindblad superoperator $\mathcal{L}_{\mathcal{G}}(A\otimes X)$ is defined in (5.12).

If we define [27]

$$\pi_t^{jk}(X) = \frac{\tilde{\pi}_t(Q_{jk}\otimes X)}{w_{jk}}, \quad j,k=0,1,\tag{5.20}$$

where Q_{jk} and w_{jk} are given by

$$Q_{jk} = \begin{bmatrix} Q_{00} & Q_{01}\\ Q_{10} & Q_{11}\end{bmatrix} = \begin{bmatrix}\sigma_+\sigma_- & \sigma_+\\ \sigma_- & I\end{bmatrix},$$

$$w_{jk} = \begin{bmatrix} w_{00} & w_{01}\\ w_{10} & w_{11}\end{bmatrix} = \begin{bmatrix} w(t) & \sqrt{w(t)}\\ \sqrt{w(t)} & 1\end{bmatrix},$$

we obtain the following theorem which presents the quantum filter for the original system G driven by the single-photon state $|1_\xi\rangle$.

$$
\begin{aligned}
d\pi_t^{11}(X) =& \{\pi_t^{11}(\mathcal{L}_G X) + \pi_t^{01}(S^\dagger[X,L])\xi^*(t) + \pi_t^{10}([L^\dagger, X]S)\xi(t) + \pi_t^{00}(S^\dagger XS - X)|\xi(t)|^2\}dt \\
&+ \sqrt{1-r^2}\big[e^{i\theta}\pi_t^{11}(XL) + e^{-i\theta}\pi_t^{11}(L^\dagger X) + e^{-i\theta}\pi_t^{01}(S^\dagger X)\xi^*(t) + e^{i\theta}\pi_t^{10}(XS)\xi(t) - \pi_t^{11}(X)K_t\big]dW(t) \\
&+ \{\nu_t^{-1}[\pi_t^{11}(L^\dagger XL) + \pi_t^{01}(S^\dagger XL)\xi^*(t) + \pi_t^{10}(L^\dagger XS)\xi(t) + \pi_t^{00}(S^\dagger XS)|\xi(t)|^2] - \pi_t^{11}(X)\}dN(t), \\
d\pi_t^{10}(X) =& \Big\{\pi_t^{10}(\mathcal{L}_G X) + \pi_t^{00}(S^\dagger[X,L])\xi^*(t)\Big\}dt \\
&+ \sqrt{1-r^2}\Big[e^{i\theta}\pi_t^{10}(XL) + e^{-i\theta}\pi_t^{10}(L^\dagger X) + e^{-i\theta}\pi_t^{00}(S^\dagger X)\xi^*(t) - \pi_t^{10}(X)K_t\Big]dW(t) \\
&+ \Big\{\nu_t^{-1}\Big[\pi_t^{10}(L^\dagger XL) + \pi_t^{00}(S^\dagger XL)\xi^*(t)\Big] - \pi_t^{10}(X)\Big\}dN(t), \\
d\pi_t^{01}(X) =& \Big\{\pi_t^{01}(\mathcal{L}_G X) + \pi_t^{00}([L^\dagger, X]S)\xi(t)\Big\}dt \\
&+ \sqrt{1-r^2}\Big[e^{i\theta}\pi_t^{01}(XL) + e^{-i\theta}\pi_t^{01}(L^\dagger X) + e^{i\theta}\pi_t^{00}(XS)\xi(t) - \pi_t^{01}(X)K_t\Big]dW(t) \\
&+ \Big\{\nu_t^{-1}\Big[\pi_t^{01}(L^\dagger XL) + \pi_t^{00}(L^\dagger XS)\xi(t)\Big] - \pi_t^{01}(X)\Big\}dN(t), \\
d\pi_t^{00}(X) =& \pi_t^{00}(\mathcal{L}_G X)dt + \sqrt{1-r^2}\Big[e^{i\theta}\pi_t^{00}(XL) + e^{-i\theta}\pi_t^{00}(L^\dagger X) - \pi_t^{00}(X)K_t\Big]dW(t) \\
&+ \Big\{\nu_t^{-1}\Big[\pi_t^{00}(L^\dagger XL)\Big] - \pi_t^{00}(X)\Big\}dN(t).
\end{aligned}
\tag{5.22}
$$

Theorem 5.1. *Let $\{Y_{i,t}, i = 1,2\}$ be a combination of homodyne detection and photon-counting measurement for a quantum system G. With the single-photon input state $|1_\xi\rangle$, the quantum filter for the conditional expectation in the Heisenberg picture is given by* (5.22)*. Here,*

$$
\begin{aligned}
K_t =& e^{i\theta}\pi_t^{11}(L) + e^{-i\theta}\pi_t^{11}(L^\dagger) + e^{-i\theta}\pi_t^{01}(S^\dagger)\xi^*(t) + e^{i\theta}\pi_t^{10}(S)\xi(t), \\
\nu_t =& \pi_t^{11}(L^\dagger L) + \pi_t^{01}(S^\dagger L)\xi^*(t) + \pi_t^{10}(L^\dagger S)\xi(t) + \pi_t^{00}(I)|\xi(t)|^2,
\end{aligned}
\tag{5.23}
$$

the Wiener process $W(t)$ and compensated Poisson process $N(t)$ are given by

$$
dW(t) = dY_{1,t} - \sqrt{1-r^2}K_t dt, \quad dN(t) = dY_{2,t} - r^2\nu_t dt \tag{5.24}
$$

respectively. We have $\pi_t^{10}(X) = \pi_t^{01}(X^\dagger)^\dagger$. The initial conditions are $\pi_0^{11}(X) = \pi_0^{00}(X) = \langle\eta, X\eta\rangle$, $\pi_0^{10}(X) = \pi_0^{01}(X) = 0$.

Proof. We only give the proof of the filtering equation $d\pi_t^{11}(X)$, the other three filtering equations in (5.22) can be derived similarly. Let $j = k = 1$, then

$$
\pi_t^{11}(X) = \frac{\tilde{\pi}_t(Q_{11}\otimes X)}{w_{11}} = \tilde{\pi}_t(I\otimes X).
$$

By (5.19),

$$d\pi_t^{11}(X) = \tilde{\pi}_t(\mathcal{L}_{\mathcal{G}}(I \otimes X))dt + \beta_1 \left[dY_{1,t} - \tilde{\pi}_t(dY_{1,t})\right] + \beta_2 \left[dY_{2,t} - \tilde{\pi}_t(dY_{2,t})\right].$$

Substituting $A = I$ into the corresponding gains (5.17), (5.18) and the Lindblad superoperator (5.12), by the definition (5.20), we can obtain

$$\begin{aligned}
\beta_1 =& \sqrt{1-r^2}\big[e^{i\theta}\pi_t^{11}(XL) + e^{-i\theta}\pi_t^{11}(L^\dagger X) + e^{-i\theta}\pi_t^{01}(S^\dagger X)\xi^*(t) \\
&+ e^{i\theta}\pi_t^{10}(XS)\xi(t) - \pi_t^{11}(X)K_t\big], \\
\beta_2 =& \nu_t^{-1}\big[\pi_t^{11}(L^\dagger XL) + \pi_t^{01}(S^\dagger XL)\xi^*(t) + \pi_t^{10}(L^\dagger XS)\xi(t) \\
&+ \pi_t^{00}(S^\dagger XS)|\xi(t)|^2\big] - \pi_t^{11}(X),
\end{aligned}$$

and the expectation of the Lindblad superoperator is given by

$$\begin{aligned}
\tilde{\pi}_t(\mathcal{L}_{\mathcal{G}}(I \otimes X)) =& \pi_t^{11}(\mathcal{L}_G X) + \pi_t^{01}(S^\dagger[X, L])\xi^*(t) \\
&+ \pi_t^{10}([L^\dagger, X]S)\xi(t) + \pi_t^{00}(S^\dagger XS - X)|\xi(t)|^2.
\end{aligned}$$

Consequently, the explicit form of $d\pi_t^{11}(X)$ is

$$\begin{aligned}
d\pi_t^{11}(X) =& \big\{\pi_t^{11}(\mathcal{L}_G X) + \pi_t^{01}(S^\dagger[X, L])\xi^*(t) + \pi_t^{10}([L^\dagger, X]S)\xi(t) \\
&+ \pi_t^{00}(S^\dagger XS - X)|\xi(t)|^2\big\}dt \\
&+ \sqrt{1-r^2}\big[e^{i\theta}\pi_t^{11}(XL) + e^{-i\theta}\pi_t^{11}(L^\dagger X) + e^{-i\theta}\pi_t^{01}(S^\dagger X)\xi^*(t) \\
&+ e^{i\theta}\pi_t^{10}(XS)\xi(t) - \pi_t^{11}(X)K_t\big]dW(t) \\
&+ \big\{\nu_t^{-1}\big[\pi_t^{11}(L^\dagger XL) + \pi_t^{01}(S^\dagger XL)\xi^*(t) + \pi_t^{10}(L^\dagger XS)\xi(t) \\
&+ \pi_t^{00}(S^\dagger XS)|\xi(t)|^2\big] - \pi_t^{11}(X)\big\}dN(t),
\end{aligned}$$

where $dW(t)$ and $dN(t)$ are given by (5.24). □

Remark 5.3. *If we let $r = 0$, $\theta = 0$, the filter equations reduce to an estimation problem with a single homodyne detection. It can be verified that* (5.22) *would be in*

$$
\begin{aligned}
d\rho^{11}(t) =& \Big\{\mathcal{L}_G^\star \rho^{11}(t) + [S\rho^{01}(t), L^\dagger]\xi(t) + [L, \rho^{10}(t)S^\dagger]\xi^*(t) + [S\rho^{00}(t)S^\dagger - \rho^{00}(t)]|\xi(t)|^2\Big\}\, dt \\
&+ \sqrt{1-r^2}\left[e^{-i\theta}\rho^{11}(t)L^\dagger + e^{i\theta}L\rho^{11}(t) + e^{i\theta}S\rho^{01}(t)\xi(t) + e^{-i\theta}\rho^{10}(t)S^\dagger\xi^*(t) - K_t\rho^{11}(t)\right] dW(t) \\
&+ \Big\{\nu_t^{-1}\left[L\rho^{11}(t)L^\dagger + S\rho^{01}(t)L^\dagger\xi(t) + L\rho^{10}(t)S^\dagger\xi^*(t) + S\rho^{00}(t)S^\dagger|\xi(t)|^2\right] - \rho^{11}(t)\Big\}\, dN(t), \\
d\rho^{10}(t) =& \Big\{\mathcal{L}_G^\star \rho^{10}(t) + [S\rho^{00}(t), L^\dagger]\xi(t)\Big\}\, dt \\
&+ \sqrt{1-r^2}\left[e^{-i\theta}\rho^{10}(t)L^\dagger + e^{i\theta}L\rho^{10}(t) + e^{i\theta}S\rho^{00}(t)\xi(t) - K_t\rho^{10}(t)\right] dW(t) \\
&+ \Big\{\nu_t^{-1}[L\rho^{10}(t)L^\dagger + S\rho^{00}(t)L^\dagger\xi(t)] - \rho^{10}(t)\Big\}\, dN(t), \\
d\rho^{01}(t) =& \Big\{\mathcal{L}_G^\star \rho^{01}(t) + [L, \rho^{00}(t)S^\dagger]\xi^*(t)\Big\}\, dt \\
&+ \sqrt{1-r^2}\left[e^{-i\theta}\rho^{01}(t)L^\dagger + e^{i\theta}L\rho^{01}(t) + e^{-i\theta}\rho^{00}(t)S^\dagger\xi^*(t) - K_t\rho^{01}(t)\right] dW(t) \\
&+ \Big\{\nu_t^{-1}[L\rho^{01}(t)L^\dagger + L\rho^{00}(t)S^\dagger\xi^*(t)] - \rho^{01}(t)\Big\}\, dN(t), \\
d\rho^{00}(t) =& \mathcal{L}_G^\star \rho^{00}(t)dt + \sqrt{1-r^2}\left[e^{-i\theta}\rho^{00}(t)L^\dagger + e^{i\theta}L\rho^{00}(t) - K_t\rho^{00}(t)\right] dW(t) \\
&+ \Big\{\nu_t^{-1}[L\rho^{00}(t)L^\dagger] - \rho^{00}(t)\Big\}\, dN(t).
\end{aligned}
\tag{5.25}
$$

---

the same form as in [27]. On the other hand, if we let $r = 1$, $\theta = -\frac{\pi}{2}$, *the filter equations reduce to an estimation problem with a single photon-counting measurement. It also can be checked that* (5.22) *would reduce to the corresponding case in [27].*

If we write $\pi_t^{jk}(X) = \mathrm{Tr}[(\rho^{jk}(t))^\dagger X]$, by the quantum filter (5.22), we can get the following stochastic master equations for the evolution of conditional density operator $\rho^{jk}(t)$.

Corollary 5.1. *With a combination of homodyne detection and photon-counting measurement, the quantum filter for the system G driven by the single-photon input state $|1_\xi\rangle$ in the Schrödinger picture is given by* (5.25). *Here,*

$$
\begin{aligned}
K_t =& e^{-i\theta}\mathrm{Tr}[L^\dagger\rho^{11}(t)] + e^{i\theta}\mathrm{Tr}[L\rho^{11}(t)] + e^{i\theta}\mathrm{Tr}[S\rho^{01}(t)]\xi(t) + e^{-i\theta}\mathrm{Tr}[S^\dagger\rho^{10}(t)]\xi^*(t), \\
\nu_t =& \mathrm{Tr}[L^\dagger L\rho^{11}(t)] + \mathrm{Tr}[L^\dagger S\rho^{01}(t)]\xi(t) + \mathrm{Tr}[S^\dagger L\rho^{10}(t)]\xi^*(t) + \mathrm{Tr}[\rho^{00}(t)]|\xi(t)|^2,
\end{aligned}
\tag{5.26}
$$

and the initial conditions are $\rho^{11}(0) = \rho^{00}(0) = |\eta\rangle\langle\eta|, \quad \rho^{10}(0) = \rho^{01}(0) = 0.$

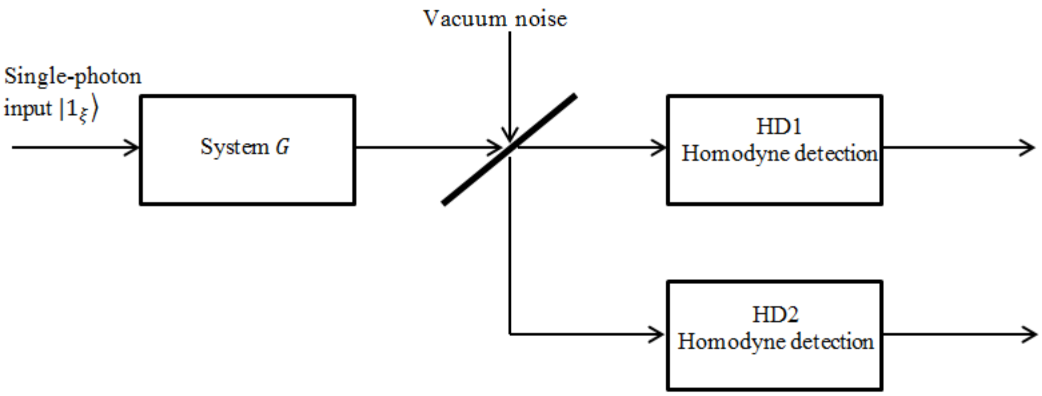

Figure 5.3: Both homodyne detection measurements at the outputs of a beam splitter in a quantum system.

5.4 Quantum filter for both homodyne detection measurements

In this section, we will derive the filter equations for the case of joint homodyne-homodyne measurements, see Fig. 5.3. Here, by the general measurement equation (5.7), we choose

$$F = I, \quad G = 0.$$

Then, the measurements stochastic equations are given by (5.13) and

$$\begin{aligned} dY_{2,t} =& \sqrt{1-r^2}\big(e^{i\theta}dB_{v,t} + e^{-i\theta}dB_{v,t}^\dagger\big) \\ &+ ir\big\{\big[e^{i\theta}(L+SL_M) - e^{-i\theta}(L^\dagger + L_M^\dagger S^\dagger)\big]dt \\ &+ e^{i\theta}SdB_{i,t} - e^{-i\theta}S^\dagger dB_{i,t}^\dagger\big\}, \end{aligned} \tag{5.27}$$

where $dY_{2,t}$ is for the second channel with homodyne detection measurement. Thus, the corresponding gain β can also be calculated by (5.6), where β_1 is given by (5.17) and β_2 is given by

$$\begin{aligned} \beta_2 =& ire^{i\theta}\tilde{\pi}_t(A\otimes XL + AL_M\otimes XS) - ire^{-i\theta}\tilde{\pi}_t(A\otimes L^\dagger X + L_M^\dagger A\otimes S^\dagger X) \\ &- ir\tilde{\pi}_t(A\otimes X)\tilde{\pi}_t[e^{i\theta}(L+SL_M) - e^{-i\theta}(L^\dagger + L_M^\dagger S^\dagger)]. \end{aligned} \tag{5.28}$$

$$
\begin{aligned}
d\pi_t^{11}(X) =& \left\{\pi_t^{11}(\mathcal{L}_G X) + \pi_t^{01}(S^\dagger[X,L])\xi^*(t) + \pi_t^{10}([L^\dagger, X]S)\xi(t) + \pi_t^{00}(S^\dagger XS - X)|\xi(t)|^2\right\} dt \\
&+ \sqrt{1-r^2}\left[e^{i\theta}\pi_t^{11}(XL) + e^{-i\theta}\pi_t^{11}(L^\dagger X) + e^{-i\theta}\pi_t^{01}(S^\dagger X)\xi^*(t) + e^{i\theta}\pi_t^{10}(XS)\xi(t) - \pi_t^{11}(X)K_{1,t}\right] dW_1(t) \\
&+ ir\left[e^{i\theta}\pi_t^{11}(XL) - e^{-i\theta}\pi_t^{11}(L^\dagger X) - e^{-i\theta}\pi_t^{01}(S^\dagger X)\xi^*(t) + e^{i\theta}\pi_t^{10}(XS)\xi(t) - \pi_t^{11}(X)K_{2,t}\right] dW_2(t), \\
d\pi_t^{10}(X) =& \left\{\pi_t^{10}(\mathcal{L}_G X) + \pi_t^{00}(S^\dagger[X,L])\xi^*(t)\right\} dt \\
&+ \sqrt{1-r^2}\left[e^{i\theta}\pi_t^{10}(XL) + e^{-i\theta}\pi_t^{10}(L^\dagger X) + e^{-i\theta}\pi_t^{00}(S^\dagger X)\xi^*(t) - \pi_t^{10}(X)K_{1,t}\right] dW_1(t) \\
&+ ir\left[e^{i\theta}\pi_t^{10}(XL) - e^{-i\theta}\pi_t^{10}(L^\dagger X) - e^{-i\theta}\pi_t^{00}(S^\dagger X)\xi^*(t) - \pi_t^{10}(X)K_{2,t}\right] dW_2(t), \\
d\pi_t^{01}(X) =& \left\{\pi_t^{01}(\mathcal{L}_G X) + \pi_t^{00}([L^\dagger, X]S)\xi(t)\right\} dt \\
&+ \sqrt{1-r^2}\left[e^{i\theta}\pi_t^{01}(XL) + e^{-i\theta}\pi_t^{01}(L^\dagger X) + e^{i\theta}\pi_t^{00}(XS)\xi(t) - \pi_t^{01}(X)K_{1,t}\right] dW_1(t) \\
&+ ir\left[e^{i\theta}\pi_t^{01}(XL) - e^{-i\theta}\pi_t^{01}(L^\dagger X) + e^{i\theta}\pi_t^{00}(XS)\xi(t) - \pi_t^{01}(X)K_{2,t}\right] dW_2(t), \\
d\pi_t^{00}(X) =& \pi_t^{00}(\mathcal{L}_G X)dt + \sqrt{1-r^2}\left[e^{i\theta}\pi_t^{00}(XL) + e^{-i\theta}\pi_t^{00}(L^\dagger X) - \pi_t^{00}(X)K_{1,t}\right] dW_1(t) \\
&+ ir\left[e^{i\theta}\pi_t^{00}(XL) - e^{-i\theta}\pi_t^{00}(L^\dagger X) - \pi_t^{00}(X)K_{2,t}\right] dW_2(t).
\end{aligned}
\tag{5.29}
$$

Then, in the case of both channels are under homodyne detection measurements, we have the filter equations which are given by the following theorem.

Theorem 5.2. *Let $\{Y_{i,t}, i = 1, 2\}$ be the two homodyne detection measurements for a quantum system G. With the single-photon input state $|1_\xi\rangle$, the quantum filter for the conditional expectation in the Heisenberg picture is given by* (5.29)*. Here,*

$$
\begin{aligned}
K_{1,t} =& e^{i\theta}\pi_t^{11}(L) + e^{-i\theta}\pi_t^{11}(L^\dagger) + e^{-i\theta}\pi_t^{01}(S^\dagger)\xi^*(t) + e^{i\theta}\pi_t^{10}(S)\xi(t), \\
K_{2,t} =& e^{i\theta}\pi_t^{11}(L) - e^{-i\theta}\pi_t^{11}(L^\dagger) - e^{-i\theta}\pi_t^{01}(S^\dagger)\xi^*(t) + e^{i\theta}\pi_t^{10}(S)\xi(t),
\end{aligned}
\tag{5.30}
$$

the Wiener processes $W_1(t)$ and $W_2(t)$ are given by

$$
dW_1(t) = dY_{1,t} - \sqrt{1-r^2}K_{1,t}dt, \quad dW_2(t) = dY_{2,t} - irK_{2,t}dt, \tag{5.31}
$$

respectively. We have $\pi_t^{10}(X) = \pi_t^{01}(X^\dagger)^\dagger$. The initial conditions are $\pi_0^{11}(X) = \pi_0^{00}(X) = \langle\eta, X\eta\rangle$, $\pi_0^{10}(X) = \pi_0^{01}(X) = 0$.

By the filter equations (5.29) and $\pi_t^{jk}(X) = \mathrm{Tr}[(\rho^{jk}(t))^\dagger X]$, we also have the quantum filter in the Schrödinger picture.

$$
\begin{aligned}
d\rho^{11}(t) =& \Big\{\mathcal{L}_G^\star\rho^{11}(t) + [S\rho^{01}(t), L^\dagger]\xi(t) + [L, \rho^{10}(t)S^\dagger]\xi^*(t) + [S\rho^{00}(t)S^\dagger - \rho^{00}(t)]|\xi(t)|^2\Big\}\, dt \\
&+ \sqrt{1-r^2}\Big[e^{-i\theta}\rho^{11}(t)L^\dagger + e^{i\theta}L\rho^{11}(t) + e^{i\theta}S\rho^{01}(t)\xi(t) + e^{-i\theta}\rho^{10}(t)S^\dagger\xi^*(t) - K_{1,t}\rho^{11}(t)\Big]\, dW_1(t) \\
&- ir\Big[e^{-i\theta}\rho^{11}(t)L^\dagger - e^{i\theta}L\rho^{11}(t) - e^{i\theta}S\rho^{01}(t)\xi(t) + e^{-i\theta}\rho^{10}(t)S^\dagger\xi^*(t) + K_{2,t}\rho^{11}(t)\Big]\, dW_2(t), \\
d\rho^{10}(t) =& \Big\{\mathcal{L}_G^\star\rho^{10}(t) + [S\rho^{00}(t), L^\dagger]\xi(t)\Big\}\, dt \\
&+ \sqrt{1-r^2}\Big[e^{-i\theta}\rho^{10}(t)L^\dagger + e^{i\theta}L\rho^{10}(t) + e^{i\theta}S\rho^{00}(t)\xi(t) - K_{1,t}\rho^{10}(t)\Big]\, dW_1(t) \\
&- ir\Big[e^{-i\theta}\rho^{10}(t)L^\dagger - e^{i\theta}L\rho^{10}(t) - e^{i\theta}S\rho^{00}(t)\xi(t) + K_{2,t}\rho^{10}(t)\Big]\, dW_2(t), \\
d\rho^{01}(t) =& \Big\{\mathcal{L}_G^\star\rho^{01}(t) + [L, \rho^{00}(t)S^\dagger]\xi^*(t)\Big\}\, dt \\
&+ \sqrt{1-r^2}\Big[e^{-i\theta}\rho^{01}(t)L^\dagger + e^{i\theta}L\rho^{01}(t) + e^{-i\theta}\rho^{00}(t)S^\dagger\xi^*(t) - K_{1,t}\rho^{01}(t)\Big]\, dW_1(t) \\
&- ir\Big[e^{-i\theta}\rho^{01}(t)L^\dagger - e^{i\theta}L\rho^{01}(t) + e^{-i\theta}\rho^{00}(t)S^\dagger\xi^*(t) + K_{2,t}\rho^{01}(t)\Big]\, dW_2(t), \\
d\rho^{00}(t) =& \mathcal{L}_G^\star\rho^{00}(t)dt + \sqrt{1-r^2}\Big[e^{-i\theta}\rho^{00}(t)L^\dagger + e^{i\theta}L\rho^{00}(t) - K_{1,t}\rho^{00}(t)\Big]\, dW_1(t) \\
&- ir\Big[e^{-i\theta}\rho^{00}(t)L^\dagger - e^{i\theta}L\rho^{00}(t) + K_{2,t}\rho^{00}(t)\Big]\, dW_2(t).
\end{aligned}
\tag{5.32}
$$

Corollary 5.2. *With the two homodyne detection measurements, the quantum filter for the system G driven by the single-photon input state $|1_\xi\rangle$ in the Schrödinger picture is given by* (5.32)*. Here,*

$$
\begin{aligned}
K_{1,t} =& e^{-i\theta}\mathrm{Tr}[L^\dagger\rho^{11}(t)] + e^{i\theta}\mathrm{Tr}[L\rho^{11}(t)] + e^{i\theta}\mathrm{Tr}[S\rho^{01}(t)]\xi(t) + e^{-i\theta}\mathrm{Tr}[S^\dagger\rho^{10}(t)]\xi^*(t), \\
K_{2,t} =& e^{-i\theta}\mathrm{Tr}[L^\dagger\rho^{11}(t)] - e^{i\theta}\mathrm{Tr}[L\rho^{11}(t)] - e^{i\theta}\mathrm{Tr}[S\rho^{01}(t)]\xi(t) + e^{-i\theta}\mathrm{Tr}[S^\dagger\rho^{10}(t)]\xi^*(t),
\end{aligned}
\tag{5.33}
$$

and the initial conditions are $\rho^{11}(0) = \rho^{00}(0) = |\eta\rangle\langle\eta|$, $\rho^{10}(0) = \rho^{01}(0) = 0$.

5.5 Simulation results

In this section, we apply the filter equations derived in section 5.4 to the problem of exciting a two-level atom with a continuous-mode single-photon field, [27]. This system can be parameterized as follows. The scattering is $S = I$, the coupling operator is $L = \kappa\sigma_-$ with the coupling strength $\kappa = 1$. The atom is taken to be in the ground state initially $|g\rangle\langle g|$ with the Hamiltonian $H = 0$. The wave packet $\xi(t)$

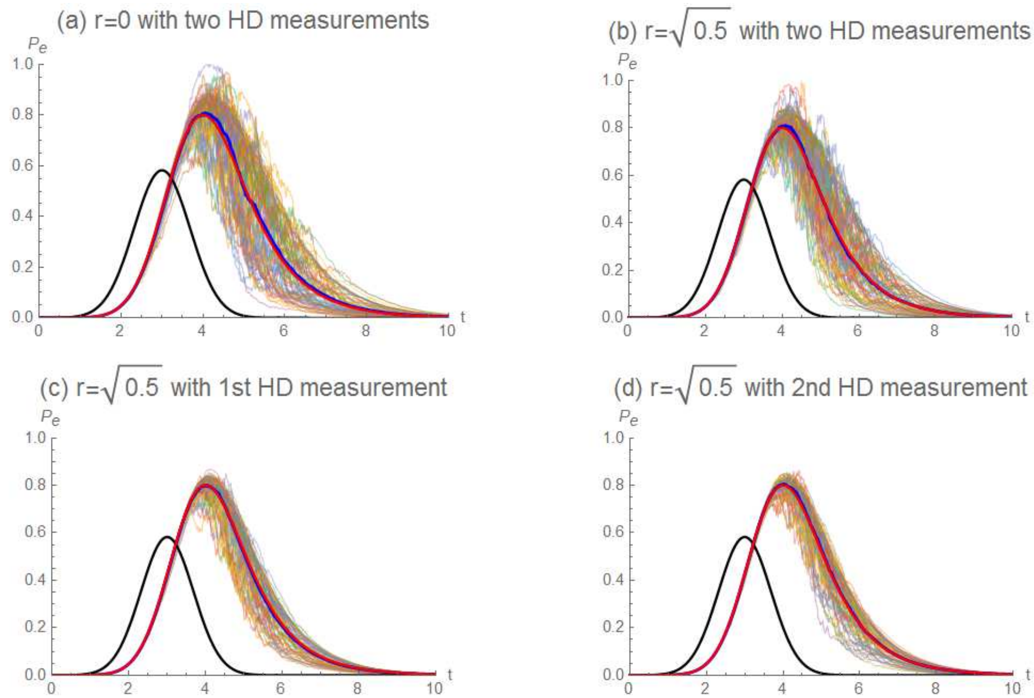

Figure 5.4: (Color online) The excitation probability for a two-level system interacting with one photon in a Gaussian pulse shape with different beam splitter parameters. The black line is the wave packet $|\xi(t)|^2$, the red line is $P_e(t)$ given by the master equation, the colored lines are the trajectories $P_e^c(t)$ and the blue line denotes the average of these trajectories.

for the single-photon is given by

$$\xi(t) = \left(\frac{\Omega^2}{2\pi}\right)^{1/4} \exp\left[-\frac{\Omega^2}{4}(t-t_0)^2\right], \tag{5.34}$$

where t_0 is the peak arrival time and Ω is the frequency bandwidth of the wave packet.

Now we choose $\Omega = 1.46$ and wish to calculate the excitation probability for the atom as a function of time. The excitation probability for quantum filtering equations is given by

$$P_e^c(t) = \mathrm{Tr}[\rho^{11}(t)|e\rangle\langle e|], \tag{5.35}$$

where $\rho^{11}(t)$ is the solution to (5.32) and $|e\rangle$ means the excited state.

In Fig. 5.4, 72 stochastic trajectories are presented as colored lines in each case given by (5.35). Fig. 5.4(a) ($r = 0$) denotes the ideal case which is equivalent to the single measurement (HD1) without any additional noise, [27]. For $r = 1$, the case will be similar to Fig. 5.4(a) since the single measurement becomes HD2. We can see that many of the stochastic trajectories begin to decay after the bulk of the wave packet, i.e., $t = 4$. Meanwhile, some trajectories continue to rise towards $P_e^c(t) = 1$, it means that the atom may be fully excited. In Fig. 5.4(b), $r = \sqrt{0.5}$, that is, the output field is contaminated by the vacuum noise. Nevertheless, it can be seen that by means of joint measurement the estimation performance is close to those for the ideal case. The excitation probabilities become bad if we only use single measurement, see Fig. 5.4(c) and (d). By comparing Fig. 5.4(b), (c) and (d), it is clear that the multiple measurement scheme is able to improve the estimation performance.

5.6 Final remarks

In this chapter, we have derived the quantum filter for a quantum system driven by the single-photon input state with multiple compatible measurements. Particularly, the explicit forms of stochastic master equations with two homodyne detection measurements and a combination of homodyne detection and photon-counting measurements have been presented. A numerical study of a two-level system driven by a single-photon state has demonstrated the advantage of filtering design based on multiple measurements when the output filed is contaminated by quantum vacuum noise.

Chapter 6

Quantum filtering with multiple measurements for systems driven by two single-photon states

In this chapter, we study quantum filtering for a two-level system G which is driven by two single-photon states $|1_{\xi_1}\rangle$ and $|1_{\xi_2}\rangle$, see Fig. 6.1. Initially, each channel contains one photon and they are independent of each other. Then the two photons interact with the system and excite the atom simultaneously. The filtering equations with two homodyne detection measurements are derived explicitly. In addition, numerical simulations for master equations with various pulse shape parameters are also presented and compared.

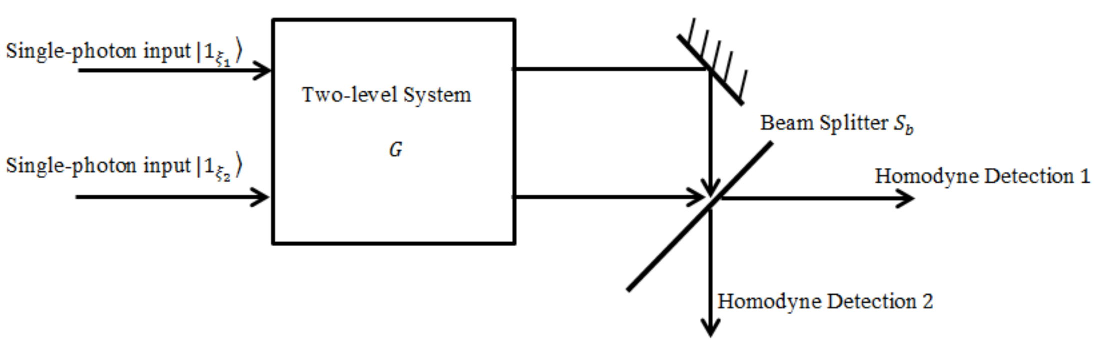

Figure 6.1: Quantum system description.

6.1 System description

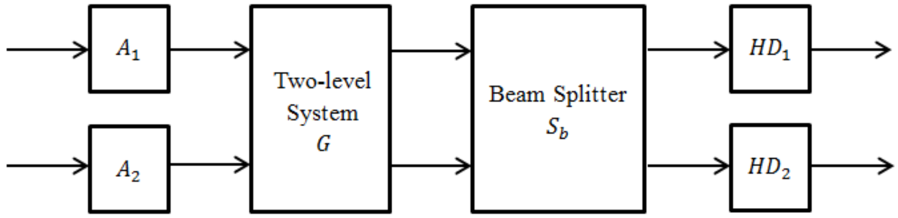

Figure 6.2: Quantum system depiction of Fig. 6.1.

In Fig. 6.2, A_1, A_2 and G are two-level systems with the following (S, L, H) formalism:

$$A_1 = (I, L_1, 0), \quad A_2 = (I, L_2, 0), \quad G = (I_2, L, 0),$$

where $L_1 = \lambda_1(t)\sigma_{-1}$, $L_2 = \lambda_2(t)\sigma_{-2}$ and $L = \begin{bmatrix} \sqrt{\kappa_1}\sigma_- \\ \sqrt{\kappa_2}\sigma_- \end{bmatrix}$. Here, σ_{-1}, σ_{-2} and σ_- are lowering operators and $\lambda_1(t)$, $\lambda_2(t)$ are given by

$$\lambda_1(t) = \frac{\xi_1(t)}{\sqrt{w_1(t)}}, \quad \lambda_2(t) = \frac{\xi_2(t)}{\sqrt{w_2(t)}},$$

where $w_1(t) = \int_t^\infty |\xi_1(s)|^2 ds$, $w_2(t) = \int_t^\infty |\xi_2(s)|^2 ds$ and $\xi_1(t)$, $\xi_2(t)$ are the input pulse shapes in the first and second channels respectively. As introduced in Chapter 5, we usually call A_1 and A_2 ancilla. With the aid of A_1 and A_2, single-photon states with desired pulse shapes can be generated. Moreover, after cascading them with the two-level atom G, we can obtain the extended system which is driven by the vacuum state. Hence, the master equations and stochastic master equations for this extended system can be derived [27, 18].

By adding a beam splitter $S_b = (S_b, 0, 0)$ with parameter

$$S_b = \begin{bmatrix} \sqrt{1-r^2} & ir \\ ir & \sqrt{1-r^2} \end{bmatrix}, 0 \leqslant r \leqslant 1$$

and the concatenation and series products [23], we can derive the whole system

$$(A_1 \boxplus A_2) \triangleright G \triangleright S_b = (S_t, L_t, H_t), \tag{6.1}$$

where

$$\begin{aligned}
S_t &= \begin{bmatrix} \sqrt{1-r^2} & ir \\ ir & \sqrt{1-r^2} \end{bmatrix}, \\
L_t &= \begin{bmatrix} \sqrt{1-r^2}(L_1+\sqrt{\kappa_1}\sigma_-)+ir(L_2+\sqrt{\kappa_2}\sigma_-) \\ ir(L_1+\sqrt{\kappa_1}\sigma_-)+\sqrt{1-r^2}(L_2+\sqrt{\kappa_2}\sigma_-) \end{bmatrix}, \\
H_t &= \frac{\sqrt{\kappa_1}\sigma_+L_1+\sqrt{\kappa_2}\sigma_+L_2-\sqrt{\kappa_1}L_1^\dagger\sigma_- - \sqrt{\kappa_2}L_2^\dagger\sigma_-}{2i}.
\end{aligned} \tag{6.2}$$

By Itō calculus, the evolution of output fields

$$dB_{\text{out}}(t) = S_t dB_t + L_t dt,$$

and the general measurement equation

$$dY(t) = F^{\#}dB_{\text{out}}^{\#}(t) + FdB_{\text{out}}(t) + G\text{diag}(d\Lambda_{\text{out}}(t)),$$

with $F = I$, $G = 0$, which means that both channels are under homodyne detection measurements, we can get the measurement stochastic equations

$$\begin{aligned}
dY_{1,t} =& \sqrt{1-r^2}\Big[dB_1(t)+dB_1^\dagger(t)+(L_1+\sqrt{\kappa_1}\sigma_-)dt+(L_1^\dagger+\sqrt{\kappa_1}\sigma_+)dt\Big] \\
&+ir\Big[dB_2(t)-dB_2^\dagger(t)+(L_2+\sqrt{\kappa_2}\sigma_-)dt-(L_2^\dagger+\sqrt{\kappa_2}\sigma_+)dt\Big], \\
dY_{2,t} =& ir\Big[dB_1(t)-dB_1^\dagger(t)+(L_1+\sqrt{\kappa_1}\sigma_-)dt-(L_1^\dagger+\sqrt{\kappa_1}\sigma_+)dt\Big] \\
&+\sqrt{1-r^2}\Big[dB_2(t)+dB_2^\dagger(t)+(L_2+\sqrt{\kappa_2}\sigma_-)dt+(L_2^\dagger+\sqrt{\kappa_2}\sigma_+)dt\Big],
\end{aligned} \tag{6.3}$$

where $dY_{1,t}$ and $dY_{2,t}$ are the homodyne detection measurements in the first and second channels, respectively.

By Itō calculus, it is easy to show that

$$dY_{1,t}dY_{1,t} = dt,\ dY_{1,t}dY_{2,t} = 0,$$
$$dY_{2,t}dY_{1,t} = 0,\ dY_{2,t}dY_{2,t} = dt.$$

Let us denote by $\tilde{\pi}_t$ the conditional expectation for the extended system $(A_1 \boxplus A_2) \rhd G \rhd S_b$ driven by the vacuum input on the ancilla-system Hilbert space. Then, the expectation and correlation of the measurements can be derived as

$$\begin{aligned}\tilde{\pi}_t(dY_{1,t}) =& \sqrt{1-r^2}\tilde{\pi}_t(L_1 + L_1^\dagger + \sqrt{\kappa_1}\sigma_- + \sqrt{\kappa_1}\sigma_+)dt \\ &+ ir\tilde{\pi}_t(L_2 - L_2^\dagger + \sqrt{\kappa_2}\sigma_- - \sqrt{\kappa_2}\sigma_+)dt, \\ \tilde{\pi}_t(dY_{2,t}) =& \sqrt{1-r^2}\tilde{\pi}_t(L_2 + L_2^\dagger + \sqrt{\kappa_2}\sigma_- + \sqrt{\kappa_2}\sigma_+)dt \\ &+ ir\tilde{\pi}_t(L_1 - L_1^\dagger + \sqrt{\kappa_1}\sigma_- - \sqrt{\kappa_1}\sigma_+)dt,\end{aligned} \tag{6.4}$$

and the non-singular matrix Σ is given by

$$\Sigma = \begin{bmatrix} \tilde{\pi}_t(dY_{1,t}dY_{1,t}) & \tilde{\pi}_t(dY_{1,t}dY_{2,t}) \\ \tilde{\pi}_t(dY_{2,t}dY_{1,t}) & \tilde{\pi}_t(dY_{2,t}dY_{2,t}) \end{bmatrix} = \begin{bmatrix} dt & 0 \\ 0 & dt \end{bmatrix}. \tag{6.5}$$

The Lindblad superoperator for the whole system may be expressed in the form

$$\begin{aligned}\mathcal{L}_{L_t}(A_1 \otimes A_2 \otimes X) =& \mathcal{D}_{L_1}A_1 \otimes A_2 \otimes X + A_1 \otimes \mathcal{D}_{L_2}A_2 \otimes X \\ &+ (\kappa_1 + \kappa_2)A_1 \otimes A_2 \otimes \mathcal{D}_{\sigma_-}X \\ &+ \sqrt{\kappa_1}L_1^\dagger A_1 \otimes A_2 \otimes [X, \sigma_-] + \sqrt{\kappa_1}A_1L_1 \otimes A_2 \otimes [\sigma_+, X] \\ &+ \sqrt{\kappa_2}A_1 \otimes L_2^\dagger A_2 \otimes [X, \sigma_-] + \sqrt{\kappa_2}A_1 \otimes A_2L_2 \otimes [\sigma_+, X],\end{aligned}$$

for any ancilla operators A_1, A_2 and system operator X.

Using Theorem 3.2 in [18], we can derive the following result directly.

Theorem 6.1. *Let $\{Y_{i,t}, i = 1, 2, \ldots, N\}$ be a set of N compatible measurement outputs for a quantum system G. With the vacuum initial state, the corresponding* *joint measurement quantum filter is given by*

$$d\tilde{\pi}_t(A_1 \otimes A_2 \otimes X) = \tilde{\pi}_t(\mathcal{L}_{L_t}(A_1 \otimes A_2 \otimes X))dt + \beta_t^T \left[dY_t - \tilde{\pi}_t(dY_t)\right], \tag{6.6}$$

where $dW_{i,t} = dY_{i,t} - \tilde{\pi}_t(dY_{i,t})$ *is a martingale process for each measurement output and* β *is the corresponding gain which given by*

$$\begin{aligned}\beta_t^T = &\frac{1}{\tilde{\pi}_t(dY_t dY_t^T)}\Big\{\tilde{\pi}_t(A_1 \otimes A_2 \otimes X dY_t^T) - \tilde{\pi}_t(A_1 \otimes A_2 \otimes X)\tilde{\pi}_t(dY_t^T) \\ &+ \tilde{\pi}_t\Big([L_t^\dagger, A_1 \otimes A_2 \otimes X]S_t dB_t dY_t^T\Big)\Big\}.\end{aligned} \tag{6.7}$$

In Fig. 6.2, the corresponding gain $\beta = \begin{bmatrix} \beta_1 & \beta_2 \end{bmatrix}$ can be calculated by (6.4) and (6.5), given by

$$\begin{aligned}\beta_1 = &\sqrt{1-r^2}\tilde{\pi}_t\Big[A_1 L_1 \otimes A_2 \otimes X + L_1^\dagger A_1 \otimes A_2 \otimes X + \sqrt{\kappa_1} A_1 \otimes A_2 \otimes X\sigma_- + \sqrt{\kappa_1} A_1 \otimes A_2 \otimes \sigma_+ X\Big] \\ &+ ir\tilde{\pi}_t\Big[A_1 \otimes A_2 L_2 \otimes X - A_1 \otimes L_2^\dagger A_2 \otimes X + \sqrt{\kappa_2} A_1 \otimes A_2 \otimes X\sigma_- - \sqrt{\kappa_2} A_1 \otimes A_2 \otimes \sigma_+ X\Big] \\ &- \tilde{\pi}_t(A_1 \otimes A_2 \otimes X)\left[\sqrt{1-r^2}k_{11}(t) + irk_{12}(t)\right], \\ \beta_2 = &ir\tilde{\pi}_t\Big[A_1 L_1 \otimes A_2 \otimes X - L_1^\dagger A_1 \otimes A_2 \otimes X + \sqrt{\kappa_1} A_1 \otimes A_2 \otimes X\sigma_- - \sqrt{\kappa_1} A_1 \otimes A_2 \otimes \sigma_+ X\Big] \\ &+ \sqrt{1-r^2}\tilde{\pi}_t\Big[A_1 \otimes A_2 L_2 \otimes X + A_1 \otimes L_2^\dagger A_2 \otimes X + \sqrt{\kappa_2} A_1 \otimes A_2 \otimes X\sigma_- + \sqrt{\kappa_2} A_1 \otimes A_2 \otimes \sigma_+ X\Big] \\ &- \tilde{\pi}_t(A_1 \otimes A_2 \otimes X)\left[irk_{21}(t) + \sqrt{1-r^2}k_{22}(t)\right],\end{aligned} \tag{6.8}$$

where

$$k_{11}(t) = \tilde{\pi}_t(L_1 + L_1^\dagger + \sqrt{\kappa_1}\sigma_- + \sqrt{\kappa_1}\sigma_+)dt,$$

$$k_{12}(t) = \tilde{\pi}_t(L_2 - L_2^\dagger + \sqrt{\kappa_2}\sigma_- - \sqrt{\kappa_2}\sigma_+)dt,$$

$$k_{21}(t) = \tilde{\pi}_t(L_1 - L_1^\dagger + \sqrt{\kappa_1}\sigma_- - \sqrt{\kappa_1}\sigma_+)dt,$$

$$k_{22}(t) = \tilde{\pi}_t(L_2 + L_2^\dagger + \sqrt{\kappa_2}\sigma_- + \sqrt{\kappa_2}\sigma_+)dt.$$

Remark 6.1. *Compared with the theorems given in [18] and Chapter 5, the extended system operator* $A \otimes X$ *has been replaced by* $A_1 \otimes A_2 \otimes X$ *in this chapter. Moreover,* *when a quantum system is driven by n single-photon states $|1_{\xi_1}\rangle$, $|1_{\xi_2}\rangle$, ... $|1_{\xi_n}\rangle$, the theorem in terms of quantum filter can be generalized by introducing a corresponding extended system operator $A_1 \otimes A_2 \otimes \cdots \otimes A_n \otimes X$.*

6.2 Master equations

In this section, we present the master equations for the quantum system G driven by two photons, one in each input channel. In what follows, write

$$\pi_t^{jk;mn}(X) = \mathbb{E}_{jk;mn}\left[j_t(X)\right] = \langle \eta\phi_j\phi_m | j_t(X) | \eta\phi_k\phi_n \rangle,$$

where X is any system operator and

$$\phi_j = \begin{cases} |1_\xi\rangle & j = 1; \\ |0\rangle & j = 0. \end{cases}$$

Here, the notation "j, k, m, n" is used to indicate that the input field in each channel is in a single-photon state or vacuum state. For example,

$$\pi_t^{11;11}(X) = \langle \eta 1_{\xi_1} 1_{\xi_2} | j_t(X) | \eta 1_{\xi_1} 1_{\xi_2} \rangle.$$

Define

$$\pi_t^{jk;mn}(X) = \mathrm{Tr}\left\{(\rho^{jk;mn}(t))^\dagger X\right\}, \quad j,k,m,n = 0,1,$$

where $\rho^{jk;mn}(t)$ is the density operator and we only present master equations in the Schrödinger picture for simplicity, and set

$$\mathcal{D}^\star_{\sigma_-}\rho = \sigma_-\rho\sigma_+ - \frac{1}{2}\sigma_+\sigma_-\rho - \frac{1}{2}\rho\sigma_+\sigma_-.$$

The master equations are given by (6.9) with initial conditions:

$$\rho^{11;11}(0) = \rho^{00;11}(0) = \rho^{11;00}(0) = \rho^{00;00}(0) = |\eta\rangle\langle\eta|.$$

Remark 6.2. *It can be easily verified that*

$$\rho^{jk;mn}(t) = (\rho^{kj;nm}(t))^\dagger, \quad j,k,m,n = 0,1.$$

$$
\begin{aligned}
\dot{\rho}^{11;11}(t) =&(k_1+k_2)\mathcal{D}^{\star}_{\sigma_-}\rho^{11;11}(t) + \sqrt{k_1}\xi_1(t)[\rho^{01;11}(t),\sigma_+] + \sqrt{k_1}\xi_1^*(t)[\sigma_-,\rho^{10;11}(t)]\\
&+ \sqrt{k_2}\xi_2(t)[\rho^{11;01}(t),\sigma_+] + \sqrt{k_2}\xi_2^*(t)[\sigma_-,\rho^{11;10}(t)],\\
\dot{\rho}^{10;11}(t) =&(k_1+k_2)\mathcal{D}^{\star}_{\sigma_-}\rho^{10;11}(t) + \sqrt{k_1}\xi_1(t)[\rho^{00;11}(t),\sigma_+] + \sqrt{k_2}\xi_2(t)[\rho^{10;01}(t),\sigma_+] + \sqrt{k_2}\xi_2^*(t)[\sigma_-,\rho^{10;10}(t)],\\
\dot{\rho}^{01;11}(t) =&(k_1+k_2)\mathcal{D}^{\star}_{\sigma_-}\rho^{01;11}(t) + \sqrt{k_1}\xi_1^*(t)[\sigma_-,\rho^{00;11}(t)] + \sqrt{k_2}\xi_2(t)[\rho^{01;01}(t),\sigma_+] + \sqrt{k_2}\xi_2^*(t)[\sigma_-,\rho^{01;10}(t)],\\
\dot{\rho}^{00;11}(t) =&(k_1+k_2)\mathcal{D}^{\star}_{\sigma_-}\rho^{00;11}(t) + \sqrt{k_2}\xi_2(t)[\rho^{00;01}(t),\sigma_+] + \sqrt{k_2}\xi_2^*(t)[\sigma_-,\rho^{00;10}(t)];\\
\dot{\rho}^{11;10}(t) =&(k_1+k_2)\mathcal{D}^{\star}_{\sigma_-}\rho^{11;10}(t) + \sqrt{k_1}\xi_1(t)[\rho^{01;10}(t),\sigma_+] + \sqrt{k_1}\xi_1^*(t)[\sigma_-,\rho^{10;10}(t)] + \sqrt{k_2}\xi_2(t)[\rho^{11;00}(t),\sigma_+],\\
\dot{\rho}^{10;10}(t) =&(k_1+k_2)\mathcal{D}^{\star}_{\sigma_-}\rho^{10;10}(t) + \sqrt{k_1}\xi_1(t)[\rho^{00;10}(t),\sigma_+] + \sqrt{k_2}\xi_2(t)[\rho^{10;00}(t),\sigma_+],\\
\dot{\rho}^{01;10}(t) =&(k_1+k_2)\mathcal{D}^{\star}_{\sigma_-}\rho^{01;10}(t) + \sqrt{k_1}\xi_1^*(t)[\sigma_-,\rho^{00;10}(t)] + \sqrt{k_2}\xi_2(t)[\rho^{01;00}(t),\sigma_+],\\
\dot{\rho}^{00;10}(t) =&(k_1+k_2)\mathcal{D}^{\star}_{\sigma_-}\rho^{00;10}(t) + \sqrt{k_2}\xi_2(t)[\rho^{00;00}(t),\sigma_+];\\
\dot{\rho}^{11;01}(t) =&(k_1+k_2)\mathcal{D}^{\star}_{\sigma_-}\rho^{11;01}(t) + \sqrt{k_1}\xi_1(t)[\rho^{01;01}(t),\sigma_+] + \sqrt{k_1}\xi_1^*(t)[\sigma_-,\rho^{10;01}(t)] + \sqrt{k_2}\xi_2^*(t)[\sigma_-,\rho^{11;00}(t)],\\
\dot{\rho}^{10;01}(t) =&(k_1+k_2)\mathcal{D}^{\star}_{\sigma_-}\rho^{10;01}(t) + \sqrt{k_1}\xi_1(t)[\rho^{00;01}(t),\sigma_+] + \sqrt{k_2}\xi_2^*(t)[\sigma_-,\rho^{10;00}(t)],\\
\dot{\rho}^{01;01}(t) =&(k_1+k_2)\mathcal{D}^{\star}_{\sigma_-}\rho^{01;01}(t) + \sqrt{k_1}\xi_1^*(t)[\sigma_-,\rho^{00;01}(t)] + \sqrt{k_2}\xi_2^*(t)[\sigma_-,\rho^{01;00}(t)],\\
\dot{\rho}^{00;01}(t) =&(k_1+k_2)\mathcal{D}^{\star}_{\sigma_-}\rho^{00;01}(t) + \sqrt{k_2}\xi_2^*(t)[\sigma_-,\rho^{00;00}(t)];\\
\dot{\rho}^{11;00}(t) =&(k_1+k_2)\mathcal{D}^{\star}_{\sigma_-}\rho^{11;00}(t) + \sqrt{k_1}\xi_1(t)[\rho^{01;00}(t),\sigma_+] + \sqrt{k_1}\xi_1^*(t)[\sigma_-,\rho^{10;00}(t)],\\
\dot{\rho}^{10;00}(t) =&(k_1+k_2)\mathcal{D}^{\star}_{\sigma_-}\rho^{10;00}(t) + \sqrt{k_1}\xi_1(t)[\rho^{00;00}(t),\sigma_+],\\
\dot{\rho}^{01;00}(t) =&(k_1+k_2)\mathcal{D}^{\star}_{\sigma_-}\rho^{01;00}(t) + \sqrt{k_1}\xi_1^*(t)[\sigma_-,\rho^{00;00}(t)],\\
\dot{\rho}^{00;00}(t) =&(k_1+k_2)\mathcal{D}^{\star}_{\sigma_-}\rho^{00;00}(t),
\end{aligned}
\tag{6.9}
$$

6.3 Quantum filtering equations

In this section, under two homodyne detection measurements, the filtering equations for the quantum system G driven by two single-photon input states are derived explicitly.

We define

$$
\pi_t^{jk;mn}(X) = \frac{\tilde{\pi}_t(Q_1^{jk}\otimes Q_2^{mn}\otimes X)}{w_1^{jk}(t)w_2^{mn}(t)}, \quad j,k=0,1,
$$

where Q_1^{jk}, Q_2^{mn} are operators for ancilla A_1 and A_2 respectively, with

$$
Q_i^{jk} = \begin{bmatrix} Q_i^{00} & Q_i^{01} \\ Q_i^{10} & Q_i^{11} \end{bmatrix} = \begin{bmatrix} \sigma_{+i}\sigma_{-i} & \sigma_{+i} \\ \sigma_{-i} & I \end{bmatrix}, \quad i=1,2.
$$

and w_1^{jk}, w_2^{mn} are given by

$$
w_i^{jk} = \begin{bmatrix} w_i^{00} & w_i^{01} \\ w_i^{10} & w_i^{11} \end{bmatrix} = \begin{bmatrix} w_i(t) & \sqrt{w_i(t)} \\ \sqrt{w_i(t)} & 1 \end{bmatrix}, \quad i=1,2.
$$

Here, σ_{-i} denotes the lowering operator and σ_{+i} is the rising operator for ancilla A_i.

For simplicity, the following theorem only presents the quantum filter in the Heisenberg picture for the two-level system G, and we give the form of $d\pi_t^{11;11}(X)$ explicitly.

Theorem 6.2. *Let $\{Y_{i,t}, i = 1, 2\}$ be the two homodyne detection measurements for a quantum system G. With single-photon input states $|1_{\xi_1}\rangle$ and $|1_{\xi_2}\rangle$, one for each input channel, the quantum filter for the conditional expectation in the Heisenberg picture is given by* (6.10) - (6.25).

$$\begin{aligned}
d\pi_t^{11;11}(X) =&\Big\{(\kappa_1+\kappa_2)\pi_t^{11;11}(\mathcal{D}_{\sigma_-}X) + \sqrt{\kappa_1}\xi_1^*(t)\pi_t^{01;11}([X,\sigma_-]) + \sqrt{\kappa_1}\xi_1(t)\pi_t^{10;11}([\sigma_+,X]) \\
&+ \sqrt{\kappa_2}\xi_2^*(t)\pi_t^{11;01}([X,\sigma_-]) + \sqrt{\kappa_2}\xi_2(t)\pi_t^{11;10}([\sigma_+,X])\Big\}dt \\
&+ \Big\{\sqrt{1-r^2}\Big[\xi_1(t)\pi_t^{10;11}(X) + \xi_1^*(t)\pi_t^{01;11}(X) + \sqrt{\kappa_1}\pi_t^{11;11}(X\sigma_-) + \sqrt{\kappa_1}\pi_t^{11;11}(\sigma_+X)\Big] \\
&+ ir\Big[\xi_2(t)\pi_t^{11;10}(X) - \xi_2^*(t)\pi_t^{11;01}(X) + \sqrt{\kappa_2}\pi_t^{11;11}(X\sigma_-) - \sqrt{\kappa_2}\pi_t^{11;11}(\sigma_+X)\Big] \\
&- \pi_t^{11;11}(X)\Big[\sqrt{1-r^2}k_{11}(t) + irk_{12}(t)\Big]\Big\}dW_1(t) \\
&+ \Big\{ir\Big[\xi_1(t)\pi_t^{10;11}(X) - \xi_1^*(t)\pi_t^{01;11}(X) + \sqrt{\kappa_1}\pi_t^{11;11}(X\sigma_-) - \sqrt{\kappa_1}\pi_t^{11;11}(\sigma_+X)\Big] \\
&+ \sqrt{1-r^2}\Big[\xi_2(t)\pi_t^{11;10}(X) + \xi_2^*(t)\pi_t^{11;01}(X) + \sqrt{\kappa_2}\pi_t^{11;11}(X\sigma_-) + \sqrt{\kappa_2}\pi_t^{11;11}(\sigma_+X)\Big] \\
&- \pi_t^{11;11}(X)\Big[irk_{21}(t) + \sqrt{1-r^2}k_{22}(t)\Big]\Big\}dW_2(t);
\end{aligned} \tag{6.10}$$

$$\begin{aligned}
d\pi_t^{10;11}(X) =&\Big\{(\kappa_1+\kappa_2)\pi_t^{10;11}(\mathcal{D}_{\sigma_-}X) + \sqrt{\kappa_1}\xi_1^*(t)\pi_t^{00;11}([X,\sigma_-]) \\
&+ \sqrt{\kappa_2}\xi_2^*(t)\pi_t^{10;01}([X,\sigma_-]) + \sqrt{\kappa_2}\xi_2(t)\pi_t^{10;10}([\sigma_+,X])\Big\}dt \\
&+ \Big\{\sqrt{1-r^2}\Big[\xi_1^*(t)\pi_t^{00;11}(X) + \sqrt{\kappa_1}\pi_t^{10;11}(X\sigma_-) + \sqrt{\kappa_1}\pi_t^{10;11}(\sigma_+X)\Big] \\
&+ ir\Big[\xi_2(t)\pi_t^{10;10}(X) - \xi_2^*(t)\pi_t^{10;01}(X) + \sqrt{\kappa_2}\pi_t^{10;11}(X\sigma_-) - \sqrt{\kappa_2}\pi_t^{10;11}(\sigma_+X)\Big] \\
&- \pi_t^{10;11}(X)\Big[\sqrt{1-r^2}k_{11}(t) + irk_{12}(t)\Big]\Big\}dW_1(t) \\
&+ \Big\{ir\Big[-\xi_1^*(t)\pi_t^{00;11}(X) + \sqrt{\kappa_1}\pi_t^{10;11}(X\sigma_-) - \sqrt{\kappa_1}\pi_t^{10;11}(\sigma_+X)\Big] \\
&+ \sqrt{1-r^2}\Big[\xi_2(t)\pi_t^{10;10}(X) + \xi_2^*(t)\pi_t^{10;01}(X) + \sqrt{\kappa_2}\pi_t^{10;11}(X\sigma_-) + \sqrt{\kappa_2}\pi_t^{10;11}(\sigma_+X)\Big] \\
&- \pi_t^{10;11}(X)\Big[irk_{21}(t) + \sqrt{1-r^2}k_{22}(t)\Big]\Big\}dW_2(t);
\end{aligned} \tag{6.11}$$

$$
\begin{aligned}
d\pi_t^{01;11}(X) =& \Big\{(\kappa_1+\kappa_2)\pi_t^{01;11}(\mathcal{D}_{\sigma_-}X) + \sqrt{\kappa_1}\xi_1(t)\pi_t^{00;11}([\sigma_+,X]) \\
&+ \sqrt{\kappa_2}\xi_2^*(t)\pi_t^{01;01}([X,\sigma_-]) + \sqrt{\kappa_2}\xi_2(t)\pi_t^{01;10}([\sigma_+,X])\Big\}dt \\
&+ \Big\{\sqrt{1-r^2}\Big[\xi_1(t)\pi_t^{00;11}(X) + \sqrt{\kappa_1}\pi_t^{01;11}(X\sigma_-) + \sqrt{\kappa_1}\pi_t^{01;11}(\sigma_+X)\Big] \\
&+ ir\Big[\xi_2(t)\pi_t^{01;10}(X) - \xi_2^*(t)\pi_t^{01;01}(X) + \sqrt{\kappa_2}\pi_t^{01;11}(X\sigma_-) - \sqrt{\kappa_2}\pi_t^{01;11}(\sigma_+X)\Big] \\
&- \pi_t^{01;11}(X)\Big[\sqrt{1-r^2}k_{11}(t) + irk_{12}(t)\Big]\Big\}dW_1(t) \\
&+ \Big\{ir\Big[\xi_1(t)\pi_t^{00;11}(X) + \sqrt{\kappa_1}\pi_t^{01;11}(X\sigma_-) - \sqrt{\kappa_1}\pi_t^{01;11}(\sigma_+X)\Big] \\
&+ \sqrt{1-r^2}\Big[\xi_2(t)\pi_t^{01;10}(X) + \xi_2^*(t)\pi_t^{01;01}(X) + \sqrt{\kappa_2}\pi_t^{01;11}(X\sigma_-) + \sqrt{\kappa_2}\pi_t^{01;11}(\sigma_+X)\Big] \\
&- \pi_t^{01;11}(X)\Big[irk_{21}(t) + \sqrt{1-r^2}k_{22}(t)\Big]\Big\}dW_2(t);
\end{aligned} \tag{6.12}
$$

$$
\begin{aligned}
d\pi_t^{00;11}(X) =& \Big\{(\kappa_1+\kappa_2)\pi_t^{00;11}(\mathcal{D}_{\sigma_-}X) + \sqrt{\kappa_2}\xi_2^*(t)\pi_t^{00;01}([X,\sigma_-]) + \sqrt{\kappa_2}\xi_2(t)\pi_t^{00;10}([\sigma_+,X])\Big\}dt \\
&+ \Big\{\sqrt{1-r^2}\Big[\sqrt{\kappa_1}\pi_t^{00;11}(X\sigma_-) + \sqrt{\kappa_1}\pi_t^{00;11}(\sigma_+X)\Big] \\
&+ ir\Big[\xi_2(t)\pi_t^{00;10}(X) - \xi_2^*(t)\pi_t^{00;01}(X) + \sqrt{\kappa_2}\pi_t^{00;11}(X\sigma_-) - \sqrt{\kappa_2}\pi_t^{00;11}(\sigma_+X)\Big] \\
&- \pi_t^{00;11}(X)\Big[\sqrt{1-r^2}k_{11}(t) + irk_{12}(t)\Big]\Big\}dW_1(t) \\
&+ \Big\{ir\Big[\sqrt{\kappa_1}\pi_t^{00;11}(X\sigma_-) - \sqrt{\kappa_1}\pi_t^{00;11}(\sigma_+X)\Big] \\
&+ \sqrt{1-r^2}\Big[\xi_2(t)\pi_t^{00;10}(X) + \xi_2^*(t)\pi_t^{00;01}(X) + \sqrt{\kappa_2}\pi_t^{00;11}(X\sigma_-) + \sqrt{\kappa_2}\pi_t^{00;11}(\sigma_+X)\Big] \\
&- \pi_t^{00;11}(X)\Big[irk_{21}(t) + \sqrt{1-r^2}k_{22}(t)\Big]\Big\}dW_2(t);
\end{aligned} \tag{6.13}
$$

$$
\begin{aligned}
d\pi_t^{11;10}(X) =& \Big\{(\kappa_1+\kappa_2)\pi_t^{11;10}(\mathcal{D}_{\sigma_-}X) + \sqrt{\kappa_1}\xi_1^*(t)\pi_t^{01;10}([X,\sigma_-]) + \sqrt{\kappa_1}\xi_1(t)\pi_t^{10;10}([\sigma_+,X]) \\
&+ \sqrt{\kappa_2}\xi_2^*(t)\pi_t^{11;00}([X,\sigma_-])\Big\}dt \\
&+ \Big\{\sqrt{1-r^2}\Big[\xi_1(t)\pi_t^{10;10}(X) + \xi_1^*(t)\pi_t^{01;10}(X) + \sqrt{\kappa_1}\pi_t^{11;10}(X\sigma_-) + \sqrt{\kappa_1}\pi_t^{11;10}(\sigma_+X)\Big] \\
&+ ir\Big[-\xi_2^*(t)\pi_t^{11;00}(X) + \sqrt{\kappa_2}\pi_t^{11;10}(X\sigma_-) - \sqrt{\kappa_2}\pi_t^{11;10}(\sigma_+X)\Big] \\
&- \pi_t^{11;10}(X)\Big[\sqrt{1-r^2}k_{11}(t) + irk_{12}(t)\Big]\Big\}dW_1(t) \\
&+ \Big\{ir\Big[\xi_1(t)\pi_t^{10;10}(X) - \xi_1^*(t)\pi_t^{01;10}(X) + \sqrt{\kappa_1}\pi_t^{11;10}(X\sigma_-) - \sqrt{\kappa_1}\pi_t^{11;10}(\sigma_+X)\Big] \\
&+ \sqrt{1-r^2}\Big[\xi_2^*(t)\pi_t^{11;00}(X) + \sqrt{\kappa_2}\pi_t^{11;10}(X\sigma_-) + \sqrt{\kappa_2}\pi_t^{11;10}(\sigma_+X)\Big] \\
&- \pi_t^{11;10}(X)\Big[irk_{21}(t) + \sqrt{1-r^2}k_{22}(t)\Big]\Big\}dW_2(t);
\end{aligned} \tag{6.14}
$$

$$
\begin{aligned}
d\pi_t^{10;10}(X) =& \Big\{(\kappa_1+\kappa_2)\pi_t^{10;10}(\mathcal{D}_{\sigma_-}X) + \sqrt{\kappa_1}\xi_1^*(t)\pi_t^{00;10}([X,\sigma_-]) + \sqrt{\kappa_2}\xi_2^*(t)\pi_t^{10;00}([X,\sigma_-])\Big\}dt \\
&+ \Big\{\sqrt{1-r^2}\Big[\xi_1^*(t)\pi_t^{00;10}(X) + \sqrt{\kappa_1}\pi_t^{10;10}(X\sigma_-) + \sqrt{\kappa_1}\pi_t^{10;10}(\sigma_+X)\Big] \\
&+ ir\Big[-\xi_2^*(t)\pi_t^{10;00}(X) + \sqrt{\kappa_2}\pi_t^{10;10}(X\sigma_-) - \sqrt{\kappa_2}\pi_t^{10;10}(\sigma_+X)\Big] \\
&- \pi_t^{10;10}(X)\Big[\sqrt{1-r^2}k_{11}(t) + irk_{12}(t)\Big]\Big\}dW_1(t) \\
&+ \Big\{ir\Big[-\xi_1^*(t)\pi_t^{00;10}(X) + \sqrt{\kappa_1}\pi_t^{10;10}(X\sigma_-) - \sqrt{\kappa_1}\pi_t^{10;10}(\sigma_+X)\Big] \\
&+ \sqrt{1-r^2}\Big[\xi_2^*(t)\pi_t^{10;00}(X) + \sqrt{\kappa_2}\pi_t^{10;10}(X\sigma_-) + \sqrt{\kappa_2}\pi_t^{10;10}(\sigma_+X)\Big] \\
&- \pi_t^{10;10}(X)\Big[irk_{21}(t) + \sqrt{1-r^2}k_{22}(t)\Big]\Big\}dW_2(t);
\end{aligned}
\tag{6.15}
$$

$$
\begin{aligned}
d\pi_t^{01;10}(X) =& \Big\{(\kappa_1+\kappa_2)\pi_t^{01;10}(\mathcal{D}_{\sigma_-}X) + \sqrt{\kappa_1}\xi_1(t)\pi_t^{00;10}([\sigma_+,X]) + \sqrt{\kappa_2}\xi_2^*(t)\pi_t^{01;00}([X,\sigma_-])\Big\}dt \\
&+ \Big\{\sqrt{1-r^2}\Big[\xi_1(t)\pi_t^{00;10}(X) + \sqrt{\kappa_1}\pi_t^{01;10}(X\sigma_-) + \sqrt{\kappa_1}\pi_t^{01;10}(\sigma_+X)\Big] \\
&+ ir\Big[-\xi_2^*(t)\pi_t^{01;00}(X) + \sqrt{\kappa_2}\pi_t^{01;10}(X\sigma_-) - \sqrt{\kappa_2}\pi_t^{01;10}(\sigma_+X)\Big] \\
&- \pi_t^{01;10}(X)\Big[\sqrt{1-r^2}k_{11}(t) + irk_{12}(t)\Big]\Big\}dW_1(t) \\
&+ \Big\{ir\Big[\xi_1(t)\pi_t^{00;10}(X) + \sqrt{\kappa_1}\pi_t^{01;10}(X\sigma_-) - \sqrt{\kappa_1}\pi_t^{01;10}(\sigma_+X)\Big] \\
&+ \sqrt{1-r^2}\Big[\xi_2^*(t)\pi_t^{01;00}(X) + \sqrt{\kappa_2}\pi_t^{01;10}(X\sigma_-) + \sqrt{\kappa_2}\pi_t^{01;10}(\sigma_+X)\Big] \\
&- \pi_t^{01;10}(X)\Big[irk_{21}(t) + \sqrt{1-r^2}k_{22}(t)\Big]\Big\}dW_2(t);
\end{aligned}
\tag{6.16}
$$

Here,

$$
\begin{aligned}
k_{11}(t) =& \xi_1(t)\pi_t^{10;11}(I) + \xi_1^*(t)\pi_t^{01;11}(I) + \sqrt{\kappa_1}\pi_t^{11;11}(\sigma_- + \sigma_+), \\
k_{12}(t) =& \xi_2(t)\pi_t^{11;10}(I) - \xi_2^*(t)\pi_t^{11;01}(I) + \sqrt{\kappa_2}\pi_t^{11;11}(\sigma_- - \sigma_+), \\
k_{21}(t) =& \xi_1(t)\pi_t^{10;11}(I) - \xi_1^*(t)\pi_t^{01;11}(I) + \sqrt{\kappa_1}\pi_t^{11;11}(\sigma_- - \sigma_+), \\
k_{22}(t) =& \xi_2(t)\pi_t^{11;10}(I) + \xi_2^*(t)\pi_t^{11;01}(I) + \sqrt{\kappa_2}\pi_t^{11;11}(\sigma_- + \sigma_+).
\end{aligned}
$$

The innovation processes $W_1(t)$ and $W_2(t)$ are given by

$$
dW_1(t) = dY_{1,t} - \Big[\sqrt{1-r^2}k_{11}(t) + irk_{12}(t)\Big]\,dt,
$$

$$
dW_2(t) = dY_{2,t} - \Big[irk_{21}(t) + \sqrt{1-r^2}k_{22}(t)\Big]\,dt,
$$

respectively. We have $\pi_t^{jk;mn}(X) = (\pi_t^{kj;nm}(X^\dagger))^\dagger$. The initial conditions are

$$
\pi_t^{jk;mn}(X) = \begin{cases} \langle\eta|X|\eta\rangle, & j=k \text{ and } m=n, \\ 0, & \text{otherwise.} \end{cases}
$$

$$
\begin{aligned}
d\pi_t^{00;10}(X) =& \Big\{(\kappa_1+\kappa_2)\pi_t^{00;10}(\mathcal{D}_{\sigma_-}X) + \sqrt{\kappa_2}\xi_2^*(t)\pi_t^{00;00}([X,\sigma_-])\Big\}dt \\
&+ \Big\{\sqrt{1-r^2}\Big[\sqrt{\kappa_1}\pi_t^{00;10}(X\sigma_-) + \sqrt{\kappa_1}\pi_t^{00;10}(\sigma_+X)\Big] \\
&+ ir\Big[-\xi_2^*(t)\pi_t^{00;00}(X) + \sqrt{\kappa_2}\pi_t^{00;10}(X\sigma_-) - \sqrt{\kappa_2}\pi_t^{00;10}(\sigma_+X)\Big] \\
&- \pi_t^{00;10}(X)\Big[\sqrt{1-r^2}k_{11}(t) + irk_{12}(t)\Big]\Big\}dW_1(t) \\
&+ \Big\{ir\Big[\sqrt{\kappa_1}\pi_t^{00;10}(X\sigma_-) - \sqrt{\kappa_1}\pi_t^{00;10}(\sigma_+X)\Big] \\
&+ \sqrt{1-r^2}\Big[\xi_2^*(t)\pi_t^{00;00}(X) + \sqrt{\kappa_2}\pi_t^{00;10}(X\sigma_-) + \sqrt{\kappa_2}\pi_t^{00;10}(\sigma_+X)\Big] \\
&- \pi_t^{00;10}(X)\Big[irk_{21}(t) + \sqrt{1-r^2}k_{22}(t)\Big]\Big\}dW_2(t);
\end{aligned}
\tag{6.17}
$$

$$
\begin{aligned}
d\pi_t^{11;01}(X) =& \Big\{(\kappa_1+\kappa_2)\pi_t^{11;01}(\mathcal{D}_{\sigma_-}X) + \sqrt{\kappa_1}\xi_1^*(t)\pi_t^{01;01}([X,\sigma_-]) + \sqrt{\kappa_1}\xi_1(t)\pi_t^{10;01}([\sigma_+,X]) \\
&+ \sqrt{\kappa_2}\xi_2(t)\pi_t^{11;00}([\sigma_+,X])\Big\}dt \\
&+ \Big\{\sqrt{1-r^2}\Big[\xi_1(t)\pi_t^{10;01}(X) + \xi_1^*(t)\pi_t^{01;01}(X) + \sqrt{\kappa_1}\pi_t^{11;01}(X\sigma_-) + \sqrt{\kappa_1}\pi_t^{11;01}(\sigma_+X)\Big] \\
&+ ir\Big[\xi_2(t)\pi_t^{11;00}(X) + \sqrt{\kappa_2}\pi_t^{11;01}(X\sigma_-) - \sqrt{\kappa_2}\pi_t^{11;01}(\sigma_+X)\Big] \\
&- \pi_t^{11;01}(X)\Big[\sqrt{1-r^2}k_{11}(t) + irk_{12}(t)\Big]\Big\}dW_1(t) \\
&+ \Big\{ir\Big[\xi_1(t)\pi_t^{10;01}(X) - \xi_1^*(t)\pi_t^{01;01}(X) + \sqrt{\kappa_1}\pi_t^{11;01}(X\sigma_-) - \sqrt{\kappa_1}\pi_t^{11;01}(\sigma_+X)\Big] \\
&+ \sqrt{1-r^2}\Big[\xi_2(t)\pi_t^{11;00}(X) + \sqrt{\kappa_2}\pi_t^{11;01}(X\sigma_-) + \sqrt{\kappa_2}\pi_t^{11;01}(\sigma_+X)\Big] \\
&- \pi_t^{11;01}(X)\Big[irk_{21}(t) + \sqrt{1-r^2}k_{22}(t)\Big]\Big\}dW_2(t);
\end{aligned}
\tag{6.18}
$$

6.4 Simulation results

In this section, we apply the master equations derived in section 6.2 to the problem of exciting a two-level atom with two continuous-mode single-photon fields. Assume the atom is initially in the ground state, i.e., $|\eta\rangle = |g\rangle$. The annihilation operator is $\sigma_- = |g\rangle\langle e|$, and the creation operator is $\sigma_+ = |e\rangle\langle g|$. The pulse shapes of the two photons are given by

$$
\xi_i(t) = \left(\frac{\Omega_i^2}{2\pi}\right)^{\frac{1}{4}} \exp\left[-\frac{\Omega_i^2}{4}(t-t_i)^2\right], \quad i = 1, 2. \tag{6.26}
$$

The excitation probability, i.e., the conditional excited-state population, is defined as

$$
P_e(t) = \mathrm{Tr}\left\{\rho^{11;11}(t)|e\rangle\langle e|\right\} = \langle e|\rho^{11;11}(t)|e\rangle, \tag{6.27}
$$

$$
\begin{aligned}
d\pi_t^{10;01}(X) =& \Big\{(\kappa_1+\kappa_2)\pi_t^{10;01}(\mathcal{D}_{\sigma_-}X) + \sqrt{\kappa_1}\xi_1^*(t)\pi_t^{00;01}([X,\sigma_-]) + \sqrt{\kappa_2}\xi_2(t)\pi_t^{10;00}([\sigma_+,X])\Big\}dt \\
&+ \Big\{\sqrt{1-r^2}\Big[\xi_1^*(t)\pi_t^{00;01}(X) + \sqrt{\kappa_1}\pi_t^{10;01}(X\sigma_-) + \sqrt{\kappa_1}\pi_t^{10;01}(\sigma_+X)\Big] \\
&+ ir\Big[\xi_2(t)\pi_t^{10;00}(X) + \sqrt{\kappa_2}\pi_t^{10;01}(X\sigma_-) - \sqrt{\kappa_2}\pi_t^{10;01}(\sigma_+X)\Big] \\
&- \pi_t^{10;01}(X)\Big[\sqrt{1-r^2}k_{11}(t) + irk_{12}(t)\Big]\Big\}dW_1(t) \\
&+ \Big\{ir\Big[-\xi_1^*(t)\pi_t^{00;01}(X) + \sqrt{\kappa_1}\pi_t^{10;01}(X\sigma_-) - \sqrt{\kappa_1}\pi_t^{10;01}(\sigma_+X)\Big] \\
&+ \sqrt{1-r^2}\Big[\xi_2(t)\pi_t^{10;00}(X) + \sqrt{\kappa_2}\pi_t^{10;01}(X\sigma_-) + \sqrt{\kappa_2}\pi_t^{10;01}(\sigma_+X)\Big] \\
&- \pi_t^{10;01}(X)\Big[irk_{21}(t) + \sqrt{1-r^2}k_{22}(t)\Big]\Big\}dW_2(t);
\end{aligned}
\tag{6.19}
$$

$$
\begin{aligned}
d\pi_t^{01;01}(X) =& \Big\{(\kappa_1+\kappa_2)\pi_t^{01;01}(\mathcal{D}_{\sigma_-}X) + \sqrt{\kappa_1}\xi_1(t)\pi_t^{00;01}([\sigma_+,X]) + \sqrt{\kappa_2}\xi_2(t)\pi_t^{01;00}([\sigma_+,X])\Big\}dt \\
&+ \Big\{\sqrt{1-r^2}\Big[\xi_1(t)\pi_t^{00;01}(X) + \sqrt{\kappa_1}\pi_t^{01;01}(X\sigma_-) + \sqrt{\kappa_1}\pi_t^{01;01}(\sigma_+X)\Big] \\
&+ ir\Big[\xi_2(t)\pi_t^{01;00}(X) + \sqrt{\kappa_2}\pi_t^{01;01}(X\sigma_-) - \sqrt{\kappa_2}\pi_t^{01;01}(\sigma_+X)\Big] \\
&- \pi_t^{01;01}(X)\Big[\sqrt{1-r^2}k_{11}(t) + irk_{12}(t)\Big]\Big\}dW_1(t) \\
&+ \Big\{ir\Big[\xi_1(t)\pi_t^{00;01}(X) + \sqrt{\kappa_1}\pi_t^{01;01}(X\sigma_-) - \sqrt{\kappa_1}\pi_t^{01;01}(\sigma_+X)\Big] \\
&+ \sqrt{1-r^2}\Big[\xi_2(t)\pi_t^{01;00}(X) + \sqrt{\kappa_2}\pi_t^{01;01}(X\sigma_-) + \sqrt{\kappa_2}\pi_t^{01;01}(\sigma_+X)\Big] \\
&- \pi_t^{01;01}(X)\Big[irk_{21}(t) + \sqrt{1-r^2}k_{22}(t)\Big]\Big\}dW_2(t);
\end{aligned}
\tag{6.20}
$$

where $\rho^{11;11}(t)$ is the solution to (6.9).

In Fig. 6.3, the master equations for the two-level system are simulated. Particularly, the red line denotes the case that the two photons have the same peak arrival time $t_1 = t_2 = 3$ and the same ratio for their decay rates $\Omega_1 = 5.84\kappa_1$, $\Omega_2 = 5.84\kappa_2$, and we can get the maximum value of excitation probability $P_e = 0.44$. When we let $\kappa_2 = 0$, it means that the system has only one input channel. Then the problem reduces to quantum filtering for a two-level system driven by a single-photon state, which has been considered in [27] and Chapter 5. Meanwhile, let $\Omega_1 = 1.46\kappa_1$, the maximum value of excitation probability $P_e = 0.8$ (black line), which is consistent with the simulation result in [27] and Chapter 5. Moreover, we also considered the case of two pulse shapes with different peak arrival times, see the green line. In this case, the maximum excitation probability $P_e = 0.36$ can be attained at two time instants.

$$
\begin{aligned}
d\pi_t^{00;01}(X) =& \Big\{(\kappa_1+\kappa_2)\pi_t^{00;01}(\mathcal{D}_{\sigma_-}X) + \sqrt{\kappa_2}\xi_2(t)\pi_t^{00;00}([\sigma_+, X])\Big\}dt \\
&+ \Big\{\sqrt{1-r^2}\Big[\sqrt{\kappa_1}\pi_t^{00;01}(X\sigma_-) + \sqrt{\kappa_1}\pi_t^{00;01}(\sigma_+X)\Big] \\
&+ ir\Big[\xi_2(t)\pi_t^{00;00}(X) + \sqrt{\kappa_2}\pi_t^{00;01}(X\sigma_-) - \sqrt{\kappa_2}\pi_t^{00;01}(\sigma_+X)\Big] \\
&- \pi_t^{00;01}(X)\Big[\sqrt{1-r^2}k_{11}(t) + irk_{12}(t)\Big]\Big\}dW_1(t) \qquad (6.21)\\
&+ \Big\{ir\Big[\sqrt{\kappa_1}\pi_t^{00;01}(X\sigma_-) - \sqrt{\kappa_1}\pi_t^{00;01}(\sigma_+X)\Big] \\
&+ \sqrt{1-r^2}\Big[\xi_2(t)\pi_t^{00;00}(X) + \sqrt{\kappa_2}\pi_t^{00;01}(X\sigma_-) + \sqrt{\kappa_2}\pi_t^{00;01}(\sigma_+X)\Big] \\
&- \pi_t^{00;01}(X)\Big[irk_{21}(t) + \sqrt{1-r^2}k_{22}(t)\Big]\Big\}dW_2(t);
\end{aligned}
$$

$$
\begin{aligned}
d\pi_t^{11;00}(X) =& \Big\{(\kappa_1+\kappa_2)\pi_t^{11;00}(\mathcal{D}_{\sigma_-}X) + \sqrt{\kappa_1}\xi_1^*(t)\pi_t^{01;00}([X,\sigma_-]) + \sqrt{\kappa_1}\xi_1(t)\pi_t^{10;00}([\sigma_+, X])\Big\}dt \\
&+ \Big\{\sqrt{1-r^2}\Big[\xi_1(t)\pi_t^{10;00}(X) + \xi_1^*(t)\pi_t^{01;00}(X) + \sqrt{\kappa_1}\pi_t^{11;00}(X\sigma_-) + \sqrt{\kappa_1}\pi_t^{11;00}(\sigma_+X)\Big] \\
&+ ir\Big[\sqrt{\kappa_2}\pi_t^{11;00}(X\sigma_-) - \sqrt{\kappa_2}\pi_t^{11;00}(\sigma_+X)\Big] \\
&- \pi_t^{11;00}(X)\Big[\sqrt{1-r^2}k_{11}(t) + irk_{12}(t)\Big]\Big\}dW_1(t) \qquad (6.22)\\
&+ \Big\{ir\Big[\xi_1(t)\pi_t^{10;00}(X) - \xi_1^*(t)\pi_t^{01;00}(X) + \sqrt{\kappa_1}\pi_t^{11;00}(X\sigma_-) - \sqrt{\kappa_1}\pi_t^{11;00}(\sigma_+X)\Big] \\
&+ \sqrt{1-r^2}\Big[\sqrt{\kappa_2}\pi_t^{11;00}(X\sigma_-) + \sqrt{\kappa_2}\pi_t^{11;00}(\sigma_+X)\Big] \\
&- \pi_t^{11;00}(X)\Big[irk_{21}(t) + \sqrt{1-r^2}k_{22}(t)\Big]\Big\}dW_2(t);
\end{aligned}
$$

6.5 Final remarks

In this chapter, we have derived the master equations and filtering equations for a two-level system driven by two single-photon states. Particularly, two homodyne detection measurements are applied and the influence of photon pulse shape parameters on the excitation probability have been shown with numerical simulation results. By simulation, it seems that the maximum of excitation probability can be achieved with the same peak arrival time and the same ratio for bandwidth of the two photons, i.e., $\Omega = 5.84\kappa$.

$$
\begin{aligned}
d\pi_t^{10;00}(X) =& \Big\{(\kappa_1+\kappa_2)\pi_t^{10;00}(\mathcal{D}_{\sigma_-}X) + \sqrt{\kappa_1}\xi_1^*(t)\pi_t^{00;00}([X,\sigma_-])\Big\}dt \\
&+ \Big\{\sqrt{1-r^2}\Big[\xi_1^*(t)\pi_t^{00;00}(X) + \sqrt{\kappa_1}\pi_t^{10;00}(X\sigma_-) + \sqrt{\kappa_1}\pi_t^{10;00}(\sigma_+X)\Big] \\
&+ ir\Big[\sqrt{\kappa_2}\pi_t^{10;00}(X\sigma_-) - \sqrt{\kappa_2}\pi_t^{10;00}(\sigma_+X)\Big] \\
&- \pi_t^{10;00}(X)\Big[\sqrt{1-r^2}k_{11}(t) + irk_{12}(t)\Big]\Big\}dW_1(t) \\
&+ \Big\{ir\Big[-\xi_1^*(t)\pi_t^{00;00}(X) + \sqrt{\kappa_1}\pi_t^{10;00}(X\sigma_-) - \sqrt{\kappa_1}\pi_t^{10;00}(\sigma_+X)\Big] \\
&+ \sqrt{1-r^2}\Big[\sqrt{\kappa_2}\pi_t^{10;00}(X\sigma_-) + \sqrt{\kappa_2}\pi_t^{10;00}(\sigma_+X)\Big] \\
&- \pi_t^{10;00}(X)\Big[irk_{21}(t) + \sqrt{1-r^2}k_{22}(t)\Big]\Big\}dW_2(t);
\end{aligned}
\tag{6.23}
$$

$$
\begin{aligned}
d\pi_t^{01;00}(X) =& \Big\{(\kappa_1+\kappa_2)\pi_t^{01;00}(\mathcal{D}_{\sigma_-}X) + \sqrt{\kappa_1}\xi_1(t)\pi_t^{00;00}([\sigma_+,X])\Big\}dt \\
&+ \Big\{\sqrt{1-r^2}\Big[\xi_1(t)\pi_t^{00;00}(X) + \sqrt{\kappa_1}\pi_t^{01;00}(X\sigma_-) + \sqrt{\kappa_1}\pi_t^{01;00}(\sigma_+X)\Big] \\
&+ ir\Big[\sqrt{\kappa_2}\pi_t^{01;00}(X\sigma_-) - \sqrt{\kappa_2}\pi_t^{01;00}(\sigma_+X)\Big] \\
&- \pi_t^{01;00}(X)\Big[\sqrt{1-r^2}k_{11}(t) + irk_{12}(t)\Big]\Big\}dW_1(t) \\
&+ \Big\{ir\Big[\xi_1(t)\pi_t^{00;00}(X) + \sqrt{\kappa_1}\pi_t^{01;00}(X\sigma_-) - \sqrt{\kappa_1}\pi_t^{01;00}(\sigma_+X)\Big] \\
&+ \sqrt{1-r^2}\Big[\sqrt{\kappa_2}\pi_t^{01;00}(X\sigma_-) + \sqrt{\kappa_2}\pi_t^{01;00}(\sigma_+X)\Big] \\
&- \pi_t^{01;00}(X)\Big[irk_{21}(t) + \sqrt{1-r^2}k_{22}(t)\Big]\Big\}dW_2(t);
\end{aligned}
\tag{6.24}
$$

$$
\begin{aligned}
d\pi_t^{00;00}(X) =& (\kappa_1+\kappa_2)\pi_t^{00;00}(\mathcal{D}_{\sigma_-}X)dt \\
&+ \Big\{\sqrt{1-r^2}\Big[\sqrt{\kappa_1}\pi_t^{00;00}(X\sigma_-) + \sqrt{\kappa_1}\pi_t^{00;00}(\sigma_+X)\Big] + ir\Big[\sqrt{\kappa_2}\pi_t^{00;00}(X\sigma_-) - \sqrt{\kappa_2}\pi_t^{00;00}(\sigma_+X)\Big] \\
&- \pi_t^{00;00}(X)\Big[\sqrt{1-r^2}k_{11}(t) + irk_{12}(t)\Big]\Big\}dW_1(t) \\
&+ \Big\{ir\Big[\sqrt{\kappa_1}\pi_t^{00;00}(X\sigma_-) - \sqrt{\kappa_1}\pi_t^{00;00}(\sigma_+X)\Big] + \sqrt{1-r^2}\Big[\sqrt{\kappa_2}\pi_t^{00;00}(X\sigma_-) + \sqrt{\kappa_2}\pi_t^{00;00}(\sigma_+X)\Big] \\
&- \pi_t^{00;00}(X)\Big[irk_{21}(t) + \sqrt{1-r^2}k_{22}(t)\Big]\Big\}dW_2(t).
\end{aligned}
\tag{6.25}
$$

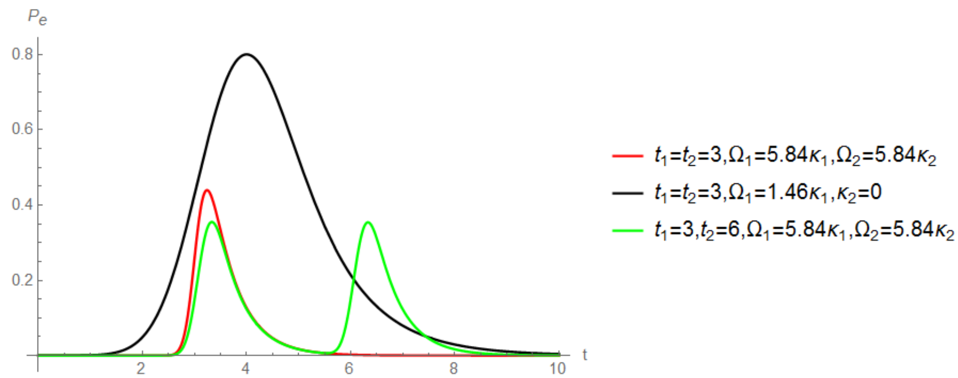

Figure 6.3: (Color online) The excitation probability for the two-level system driven by two single-photon states.

Chapter 7

Conclusions and future work

This chapter draws conclusions on the thesis, and points out some possible future research directions related to the work done in this thesis.

7.1 Conclusions

The focus of the thesis has been placed on the characterization of continuous-mode single-photon Fock states. Specifically, four research problems have been investigated in detail.

1. Wigner distribution and Wigner spectrum have been used in Chapter 3 to analyze the response of quantum linear systems to single-photon input states. In most literature, correlations are calculated for normally ordered (Wick order) operators by ignoring the Dirac delta function. For example, let $b(t)$ be a boson annihilation operator of a travelling field, the normal ordering of the product $b(t)b^\dagger(r)$ is $: b(t)b^\dagger(r) := b^\dagger(r)b(t)$. That is, the Dirac delta function $\delta(t-r)$ has been thrown away. As a result, partial information has been lost in the procedure of normal ordering. In contrast to normal ordering, Wigner spectrum is able to provide full information of the quantum states. We showed that the Wigner spectrum could handle the Dirac delta function naturally, thus no information was abandoned. Moreover, the Wigner spectrum allows us

to visualize continuous-mode single-photon Fock states and photon-Gaussian states in both the time domain and the frequency domain simultaneously.

2. In the input-output formalism, the problem of pulse-shaping of continuous-mode single-photon Fock states has been investigated. In Chapter 4, we demonstrated how various control methods (direct coupling and coherent feedback control) could be used for pulse-shaping of continuous-mode single-photon Fock states. In addition, the effect of control techniques on pulse-shaping was visualized by the Wigner spectrum of the output single-photon states. Several control schemes were compared for photon pulse-shaping. It was demonstrated that the coherent feedback control scheme is the most effective one for single-photon pulse-shaping.

3. The single-photon filtering framework in [14, 27] has been extended in Chapter 5 by taking into account imperfect measurements. More specifically, we studied the case when the output light field is corrupted by a vacuum noise. We showed how to design filters based on multiple measurements to achieve desired estimation performance. Two scenarios have been studied: 1) homodyne plus homodyne detection, and 2) homodyne plus photon-counting detection. The explicit forms of stochastic master equations for a quantum system driven by single-photon input state with multiple measurements have been given. A numerical study of a two-level system driven by a single-photon state demonstrated the advantage of filtering design based on multiple measurement when the output filed is contaminated by quantum vacuum noise.

4. The system we considered in Chapter 6 is a two-level atom driven by two single-photon states. Initially, each channel contains one photon and they are independent of each other. Then the two photons interact with the atom and

excite it simultaneously. The filtering equations with two homodyne detection measurements have been derived explicitly and numerical results of master equations for the system have been given. By simulation, it seems that the maximum of excitation probability can be achieved with the same peak arrival time and the same ratio for bandwidth of the two photons, i.e., $\Omega = 5.84\kappa$.

7.2 Future work

Related topics for the future research work are listed below.

1. Wigner spectrum has been used to describe the statistical feature of a single-channel single-photon state. More specifically, Wigner distribution and Wigner spectrum are used to analyze the response of quantum linear systems to single-photon input states in Chapter 3. On the other hand, the degree of second-order coherence and Mandel's Q parameter are widely used to analyze the statistical properties of correlation functions. One possible research direction is to compare our results with the degree of second-order coherence and Mandel's Q parameter for quantum correlation functions and verify their consistency.

2. Quantum filtering with multiple measurements for quantum systems driven by single-photon states have been investigated in Chapter 5 and Chapter 6. In the future, we will consider the stability of single photon filtering. Our approach is based on applying the method proposed in [3]. As a further direction, we can study the filtering problem when we consider the multi-photon input state [47]. Also, we may take into account imperfections in measurements. Moreover, showing the stability of multi-photon filtering is in the perspective of our research.

Bibliography

[1] Aghamalyan, D. and Malakyan, Y. (2011), "Quantum repeaters based on deterministic storage of a single photon in distant atomic ensembles," *Physical Review A*, 84, 042305.

[2] Amini, H., Somaraju, R. A., Dotsenko, I., Sayrin, C., Mirrahimi, M., and Rouchon, P. (2013), "Feedback stabilization of discrete-time quantum systems subject to non-demolition measurements with imperfections and delays," *Automatica*, 49, 2683–2692.

[3] Amini, H., Pellegrini, C., and Rouchon, P. (2014), "Stability of continuous-time quantum filters with measurement imperfections," *Russian Journal of Mathematical Physics*, 21, 297–315.

[4] Bachor, H.-A. and Ralph, T. C. (2004), *A guide to experiments in quantum optics*, Wiley.

[5] Baragiola, B. Q., Cook, R. L., Brańczyk, A. M., and Combes, J. (2012), "N-photon wave packets interacting with an arbitrary quantum system," *Physical Review A*, 86, 013811.

[6] Barzanjeh, S., Abdi, M., Milburn, G., Tombesi, P., and Vitali, D. (2012), "Reversible optical-to-microwave quantum interface," *Physical review letters*, 109, 130503.

[7] Belavkin, V. P. (1989), "Nondemolition measurements, nonlinear filtering and dynamic programming of quantum stochastic processes," in *Modeling and Control of Systems*, pp. 245–265, Springer.

[8] Belavkin, V. P. (1995), "Quantum filtering of Markov signals with white quantum noise," in *Quantum communications and measurement*, pp. 381–391, Springer.

[9] Beveratos, A., Brouri, R., Gacoin, T., Villing, A., Poizat, J.-P., and Grangier, P. (2002), "Single photon quantum cryptography," *Physical Review Letters*, 89, 187901.

[10] Blow, K., Loudon, R., Phoenix, S. J., and Shepherd, T. (1990), "Continuum fields in quantum optics," *Physical Review A*, 42, 4102.

[11] Braunstein, S. L. and Van Loock, P. (2005), "Quantum information with continuous variables," *Reviews of Modern Physics*, 77, 513.

[12] Brecht, B., Reddy, D. V., Silberhorn, C., and Raymer, M. G. (2015), "Photon temporal modes: a complete framework for quantum information science," *Physical Review X*, 5, 041017.

[13] Carmichael, H. (2009), *An open systems approach to quantum optics: lectures presented at the Université Libre de Bruxelles, October 28 to November 4, 1991*, vol. 18, Springer Science & Business Media.

[14] Carvalho, A., Hush, M., and James, M. (2012), "Cavity driven by a single photon: Conditional dynamics and nonlinear phase shift," *Physical Review A*, 86, 023806.

[15] Chia, A. and Wiseman, H. M. (2011), "Quantum theory of multiple-input–multiple-output Markovian feedback with diffusive measurements," *Physical Review A*, 84, 012120.

[16] Dum, R., Parkins, A., Zoller, P., and Gardiner, C. (1992), "Monte Carlo simulation of master equations in quantum optics for vacuum, thermal, and squeezed reservoirs," *Physical Review A*, 46, 4382.

[17] Eichler, C., Bozyigit, D., Lang, C., Steffen, L., Fink, J., and Wallraff, A. (2011), "Experimental state tomography of itinerant single microwave photons," *Physical Review Letters*, 106, 220503.

[18] Emzir, M. F., Woolley, M. J., and Petersen, I. R. (2015), "Quantum filtering for multiple diffusive and Poissonian measurements," *Journal of Physics A: Mathematical and Theoretical*, 48, 385302.

[19] Furusawa, A. and Van Loock, P. (2011), *Quantum teleportation and entanglement: a hybrid approach to optical quantum information processing*, John Wiley & Sons.

[20] Gardiner, C. and Zoller, P. (2004), *Quantum noise: a handbook of Markovian and non-Markovian quantum stochastic methods with applications to quantum optics*, vol. 56, Springer Science & Business Media.

[21] Gheri, K. M., Ellinger, K., Pellizari, T., and Zoller, P. (1998), "Photon-wavepackets as flying quantum bits," *Fortschritte der Physik*, 46, 401–416.

[22] Giovannetti, V., Lloyd, S., and Maccone, L. (2011), "Advances in quantum metrology," *Nature Photonics*, 5, 222.

[23] Gough, J. and James, M. R. (2009), "The series product and its application to quantum feedforward and feedback networks," *Automatic Control, IEEE Transactions on*, 54, 2530.

[24] Gough, J. E. and Wildfeuer, S. (2009), "Enhancement of field squeezing using coherent feedback," *Physical Review A*, 80, 042107.

[25] Gough, J. E., James, M., and Nurdin, H. (2010), "Squeezing components in linear quantum feedback networks," *Physical Review A*, 81, 023804.

[26] Gough, J. E., James, M. R., and Nurdin, H. I. (2011), "Quantum master equation and filter for systems driven by fields in a single photon state," *50th IEEE Conference on Decision and Control and European Control Conference*, pp. 5570–5576.

[27] Gough, J. E., James, M. R., Nurdin, H. I., and Combes, J. (2012), "Quantum filtering for systems driven by fields in single-photon states or superposition of coherent states," *Physical Review A*, 86, 043819.

[28] Gough, J. E., James, M. R., and Nurdin, H. I. (2013), "Quantum filtering for systems driven by fields in single photon states and superposition of coherent states using non-Markovian embeddings," *Quantum information processing*, 12, 1469.

[29] Iida, S., Yukawa, M., Yonezawa, H., Yamamoto, N., and Furusawa, A. (2012)*Automatic Control, IEEE Transactions on*, 57, 2045.

[30] Kimble, H. J. (2008), "The quantum internet," *Nature*, 453, 1023.

[31] Leroux, I. D., Schleier-Smith, M. H., Zhang, H., and Vuletić, V. (2012), "Unitary cavity spin squeezing by quantum erasure," *Physical Review A*, 85, 013803.

[32] Loudon, R. (2000), *The quantum theory of light*, Oxford university press.

[33] Lvovsky, A. I., Hansen, H., Aichele, T., Benson, O., Mlynek, J., and Schiller, S. (2001), "Quantum state reconstruction of the single-photon Fock state," *Physical Review Letters*, 87, 050402.

[34] Mandel, L. and Wolf, E. (1995), *Optical coherence and quantum optics*, Cambridge university press.

[35] McKeever, J., Boca, A., Boozer, A., Miller, R., Buck, J., Kuzmich, A., and Kimble, H. (2004), "Deterministic generation of single photons from one atom trapped in a cavity," *Science*, 303, 1992–1994.

[36] Milburn, G. (2008), "Coherent control of single photon states," *The European Physical Journal Special Topics*, 159, 113.

[37] Moehring, D., Maunz, P., Olmschenk, S., Younge, K., Matsukevich, D., Duan, L.-M., and Monroe, C. (2007), "Entanglement of single-atom quantum bits at a distance," *Nature*, 449, 68.

[38] Nurdin, H. I. (2014), "Quantum filtering for multiple input multiple output systems driven by arbitrary zero-mean jointly Gaussian input fields," *Russian Journal of Mathematical Physics*, 21, 386–398.

[39] Nurdin, H. I., James, M. R., and Doherty, A. C. (2009), "Network synthesis of linear dynamical quantum stochastic systems," *SIAM Journal on Control and Optimization*, 48, 2686–2718.

[40] Ogawa, H., Ohdan, H., Miyata, K., Taguchi, M., Makino, K., Yonezawa, H., Yoshikawa, J.-i., and Furusawa, A. (2016), "Real-Time Quadrature Measurement of a Single-Photon Wave Packet with Continuous Temporal-Mode Matching," *Physical Review Letters*, 116, 233602.

[41] Pan, Y., Zhang, G., and James, M. R. (2016), "Analysis and control of quantum finite-level systems driven by single-photon input states," *Automatica*, 69, 18–23.

[42] Parthasarathy, K. R. (2012), *An introduction to quantum stochastic calculus*, Springer Science & Business Media.

[43] Qin, Z., Prasad, A. S., Brannan, T., MacRae, A., Lezama, A., and Lvovsky, A. (2015), "Complete temporal characterization of a single photon," *Light: Science & Applications*, 4, e298.

[44] Sandsten, M. (2013), *Time-Frequency Analysis of Non-Stationary Processes*, Lund University, Centre for Mathematical Sciences.

[45] Sayrin, C., Dotsenko, I., Zhou, X., Peaudecerf, B., Rybarczyk, T., Gleyzes, S., Rouchon, P., Mirrahimi, M., Amini, H., Brune, M., et al. (2011), "Real-time quantum feedback prepares and stabilizes photon number states," *Nature*, 477, 73–77.

[46] Song, H., Kuntz, K. B., and Huntington, E. H. (2013), "Limitations on the quantum non-Gaussian characteristic of Schrödinger kitten state generation," *New Journal of Physics*, 15, 023042.

[47] Song, H., Zhang, G., and Xi, Z. (2016), "Continuous-Mode MultiPhoton Filtering," *SIAM Journal on Control and Optimization*, 54, 1602–1632.

[48] Tezak, N., Niederberger, A., Pavlichin, D. S., Sarma, G., and Mabuchi, H. (2012), "Specification of photonic circuits using quantum hardware description language," *Philosophical Transactions of the Royal Society of London A: Mathematical, Physical and Engineering Sciences*, 370, 5270–5290.

[49] Ville, J. d. et al. (1948), "Théorie et applications de la notion de signal analytique," *Cables et transmission*, 2, 61–74.

[50] Walls, D. F. and Milburn, G. J. (2007), *Quantum optics*, Springer Science & Business Media.

[51] Wang, Y., Minář, J., Sheridan, L., and Scarani, V. (2011), "Efficient excitation of a two-level atom by a single photon in a propagating mode," *Physical Review A*, 83, 063842.

[52] Wigner, E. (1932), "On the quantum correction for thermodynamic equilibrium," *Physical Review*, 40, 749.

[53] Wiseman, H. M. and Milburn, G. J. (1994), "All-optical versus electro-optical quantum-limited feedback," *Physical review A*, 49, 4110.

[54] Wiseman, H. M. and Milburn, G. J. (2009), *Quantum measurement and control*, Cambridge University Press.

[55] Yamamoto, N. and James, M. R. (2014), "Zero-dynamics principle for perfect quantum memory in linear networks," *New Journal of Physics*, 16, 073032.

[56] Yanagisawa, M. and Kimura, H. (2003), "Transfer function approach to quantum control-part I: Dynamics of quantum feedback systems," *IEEE Transactions on Automatic control*, 48, 2107–2120.

[57] Yuan, Z., Kardynal, B. E., Stevenson, R. M., Shields, A. J., Lobo, C. J., Cooper, K., Beattie, N. S., Ritchie, D. A., and Pepper, M. (2002), "Electrically driven single-photon source," *Science*, 295, 102–105.

[58] Yukawa, M., Miyata, K., Mizuta, T., Yonezawa, H., Marek, P., Filip, R., and Furusawa, A. (2013), "Generating superposition of up-to three photons for continuous variable quantum information processing," *Optics express*, 21, 5529.

[59] Zhang, G. (2014), "Analysis of quantum linear systems response to multi-photon states," *Automatica*, 50, 442.

[60] Zhang, G. and James, M. R. (2011), "Direct and indirect couplings in coherent feedback control of linear quantum systems," *Automatic Control, IEEE Transactions on*, 56, 1535.

[61] Zhang, G. and James, M. R. (2012), "Quantum feedback networks and control: a brief survey," *Chinese Science Bulletin*, 57, 2200.

[62] Zhang, G. and James, M. R. (2013), "On the response of quantum linear systems to single photon input fields," *Automatic Control, IEEE Transactions on*, 58, 1221.